# INFORMATION TO USERS

This manuscript has been reproduced from the microfilm master. UMI films the text directly from the original or copy submitted. Thus, some thesis and dissertation copies are in typewriter face, while others may be from any type of computer printer.

**The quality of this reproduction is dependent upon the quality of the copy submitted.** Broken or indistinct print, colored or poor quality illustrations and photographs, print bleedthrough, substandard margins, and improper alignment can adversely affect reproduction.

In the unlikely event that the author did not send UMI a complete manuscript and there are missing pages, these will be noted. Also, if unauthorized copyright material had to be removed, a note will indicate the deletion.

Oversize materials (e.g., maps, drawings, charts) are reproduced by sectioning the original, beginning at the upper left-hand corner and continuing from left to right in equal sections with small overlaps.

Photographs included in the original manuscript have been reproduced xerographically in this copy. Higher quality 6" x 9" black and white photographic prints are available for any photographs or illustrations appearing in this copy for an additional charge. Contact UMI directly to order.

Bell & Howell Information and Learning
300 North Zeeb Road, Ann Arbor, MI 48106-1346 USA
800-521-0600

# Surface and Interfacial Tension Measurements of Polymer Melts with Pendant Drop Apparatus:

## Effect of Structural and Material Properties on the Surface Tension of LLDPE

## An Improved Experimental Method

**Kevin Alam**

**A thesis submitted to the Faculty of Graduate Studies and Research in partial fulfillment of the requirements of the degree of Master of Engineering.**

**May 1999**

**Department of Chemical Engineering**
**McGill University**
**Montreal, Quebec, Canada**

# ABSTRACT

The pendant drop apparatus is the most reliable and accurate method of measuring the interfacial tension of polymer melts. In spite of its widespread use, a detailed experimental procedure has yet to be published. This study examined all practical aspects of pendant drop experiments with viscous polymer melts and establishes procedures for material preparation, syringe diameter selection, experimental protocol, determination of equilibrium, and the most accurate measurement of interfacial tension. In addition, the effects of both drop volume and unstable drops on interfacial tension measurements are discussed. Comparing the surface tension and interfacial tension values for several polyethylene (PE) and polystyrene (PS) resins to literature data tested the effectiveness of the experimental procedure.

The values of surface tension of several experimental linear low-density polyethylene (LLDPE) resins were determined and related to the copolymer structural and material properties. It was determined that the surface tension of the LLDPE hexene copolymers is primarily a function of the chain branching density rather than number average molecular weight. This occurs because the properties of a branched end are believed to be similar to those of a chain end. Therefore, bulk polymer properties of a branched polymer should depend primarily on the concentration of branched ends. Studying the relationship between the surface tension and the free volume of the LLDPE copolymers corroborated the relationship between the surface tension and the branching density. The values of surface tension and surface tension temperature coefficients of the LLDPE copolymers were found to be similar to literature values of linear polyethylene of equal effective molecular weight. However, the findings are inconclusive due to inconsistencies in the literature data. Also, the effects of polydispersity were believed to have caused a significant surface tension reduction and increased the value of the surface tension temperature coefficient in one of the samples.

# ABSTRAIT

La machine pendentif goutte est la meileure methode pour mesurer la tension interfaciale des polymères. Mais, actuellement, il n'existe pas aucune procédure détailée. Cette étude cocnerne touts les aspects expérimentaux de machine pendentif goutte et elle il établit des procédures pour la préparation des matériaux, la sélection du diamètre de la seringue, le protocol expérimental, la détermination de l'équilibre et la mésure la plus précise de la tension interfaciale. De plus, les effets du volume de la goutte et de l'instabilté des gouttes sur les mesures de la tension interfaciale sont discutés. Les valeurs de la tension de surface et interfaciale pour plusieurs résines polyethylene et polystyrène sont comparés aux valeurs de la littérature a fin de vérifier l'efficacité de la nouvelle methode.

Les valeurs de tensions de surface de plusieurs résines LLDPE sont mesurées et reliées aux propriétes structurals et physique. On s'aperçoit alors que la tension de surface des résines LLDPE est un fonction de la densité de chaines, puis que les propriétes en fin de chaines sont similaires à celle des chaines primaire.

# ACKNOWLEDGEMENTS

I would like to express my sincere gratitude and thanks to my research director, Dr. Musa Kamal, for his support and guidance throughout my research and studies.

I would also like to thank:

Dr. Martin Weber, for taking the time to discuss many an issue which was of great help to my research.

Charles, for making all the equipment needed for the pendant drop experiments.

# TABLE OF CONTENTS


1. INTRODUCTION 1

2. OBJECTIVES 3

PART 1: SURFACE TENSION OF LLDPE

3. BACKGROUND: SURFACE TENSION OF LIQUIDS 4

3.1. INTRODUCTION 4

3.1.1. ENTHALPY OF SURFACE FORMATION 6

3.1.2. ENTROPY OF SURFACE FORMATION 7

3.2. POLYMER LIQUIDS AND MELTS 7

3.3. INTERFACIAL TENSION 8

3.4. VARIABLES AFFECTING SURFACE TENSION 9

3.4.1. CHEMICAL COMPOSITION 9

3.4.2. MOLECULAR WEIGHT 9

3.4.2.1. Low Molecular Weight Polymers 11

3.4.3. TEMPERATURE 12

3.4.3.1. Effect of Molecular Weight on $d\gamma/dT$ 12

3.4.3.2. Entropy of Surface Formation and $d\gamma/dT$ 13

3.4.3.3. Interfacial Tension Temperature Coefficient 13

3.4.4. POLYDISPERSITY 14

3.4.4.1. Interfacial Tension 14

3.4.4.2. Surface Tension 14

3.4.4.3. Comparison between Surface and Interfacial Tension 15

3.4.5. CHAIN BRANCHING 15

3.5. THE PRINCIPLE OF CORRESPONDING STATES 16

4. RESULTS & DISCUSSION 19

4.1. DENSITY 19

4.2. MOLECULAR WEIGHT AND CHAIN BRANCHING 23

4.3. POLYDISPERSITY 26

4.4. SURFACE TENSION OF BUTENE AND OCTENE COPOLYMERS 28
4.5. EFFECT OF α-OLEFIN LENGTH 29
4.6. FREE VOLUME 32
4.7. COMPARING VALUES OF SURFACE TENSION W/ LITERATURE 34
4.8 SURFACE TENSION TEMPERATURE COEFFICIENTS 37
4.9. COMPARING VALUES OF SURFACE TENSION TEMPERATURE COEFFICIENTS W/ LITERATURE 37
4.10. INTERFACIAL TENSION & INTERFACIAL TENSION TEMPERATURE COEFFICIENTS 41

PART 2: PENDANT DROP METHOD

5. BACKGROUND 42
5.1. METHODS OF MEASURING INTERFACIAL TENSION 42
5.2. PENDANT DROP THEORY 43
5.3. EVOLUTION OF PENDANT DROP METHOD 46
5.4. DYNAMIC ASPECTS OF PENDANT DROP EXPERIMENTS 49
5.4.1. EQUILIBRATION TIME 49
5.4.2. NECKING AND CAPILLARY EFFECTS 50
5.5. EFFECT OF DROP VOLUME ON INTERFACIAL TENSION MEASUREMENTS 52
5.5.1. WORK OF JENNINGS AND PALLAS 53
5.5.2. WORK OF LIN ET AL. 54
5.6. EFFECT OF SYRINGE DIAMETER ON INTERFACIAL TENSION MEASUREMENTS 58
5.6.1. WORK OF STAUFFER 58
5.6.2. WORK OF JENNINGS AND PALLAS 58
5.6.3. WORK OF LIN ET AL. 58

**6. MATERIALS & METHODS** 61

**6.1. PENDANT DROP APPARATUS** 61

**6.1.1. OPTICAL SYSTEM** 62

**6.1.2. EXPERIMENTAL CELL** 62

**6.1.3. DROP INSERTION DEVICE** 64

**6.2. EXPERIMENTAL PROCEDURES** 66

**6.2.1. SELECTION OF SYRINGE DIAMETER** 66

**6.2.2. SAMPLE PREPARATION** 67

6.2.2.1. Denser Polymer with Capillary Rheometer 67

6.2.2.2. Less Dense Polymer with Compression Mold 70

**6.2.3. PENDANT DROP EXPERIMENTS** 70

6.2.3.1. Pendant Drop Apparatus Alignment 70

6.2.3.2. Sample Preparation 71

6.2.3.3. Establishing an Inert Atmosphere 71

6.2.3.4. Interfacial Tension Experiment 72

6.2.3.5. Optical Correction Factor 73

6.2.3.6. Surface Tension Experiment 73

6.2.3.7. Recording Pendant Drop Images 73

6.2.3.8. Critical Drop Volume 74

6.2.3.9. Terminating Pendant Drop Experiment 75

**6.3. ANALYZING PENDANT DROP PROFILES** 76

**6.3.1. PENDANT DROP EQUILIBRIUM** 76

**6.3.2. EQUILIBRIUM VALUE OF INTERFACIAL TENSION** 77

**6.3.3. DROP VOLUME** 77

**6.3.4. INTERFACIAL TENSION** 78

**6.3.5. ERROR ANALYSIS** 78

6.3.5.1. Error in $B$ and $a$ 78

6.3.5.2. Error in $\Delta\rho$ 79

6.3.5.3. Error in $M$ 79

6.3.5.4. Error in $n$ 79

6.3.5.5. Procedural Errors 80

6.3.5.6. Total error in determining interfacial tension 80

**6.4. COMPUTER PROGRAMS** 82

**6.4.1. AUTOMATED RECORDING OF DROP IMAGES** 82

**6.4.2. DROP PROFILE ANALYSIS PROGRAM** 84

6.4.2.1. Edge Detection 84

6.4.2.2. Profile Smoothing 84

6.4.2.3. Shape Comparison 84

6.4.3. RADIUS OF CURVATURE 85
6.5. MATERIALS 85

7. RESULTS & DISCUSSION 86

7.1. DETERMINATION OF EQUILIBRIUM STATE 86
7.1.1. DROP DIMENSIONS 86
7.1.2. INTERFACIAL TENSION 88
7.2. SURFACE TENSION MEASUREMENTS 91
7.2.1. ACCURACY 91
7.2.2. STANDARD DEVIATION 92
7.3. EFFECT OF DROP VOLUME ON SURFACE TENSION MEASUREMENTS 93
7.3.1. SURFACE TENSION OF HEPTANE 93
7.3.1.1. 1.8 mm Diameter Syringe 93
7.3.1.2. 4.0 mm Diameter Syringe 94
7.3.2. SURFACE TENSION OF LLDPE E 95
7.3.2.1. 1.8 mm Syringe Diameter 96
7.3.2.2. 4.0 mm Syringe Diameter 97
7.4. EFFECT OF SYRINGE DIAMETER 98

8. CONCLUSION 101

7. REFERENCES 105

APPENDIX

A.1) MOLECULAR STRUCTURE OF LLDPE A1
A.2) EFFECT OF CATALYST ON LLDPE STRUCTURE A1
A.2.1) ZIEGLER-NATTA CATALYSTS A2
A.2.2) METALLOCENE CATALYSTS A2
A.3) FREE VOLUME A2
A.3.1) FREE VOLUME OF POLYMERS A3
A.4) SPINNING DROP METHOD A4
A.4.1) EVOLUTION OF THE SPINNING DROP METHOD A4
A.5) DROP PROFILE ANALYSIS PROGRAM A6

A.6) RADIUS OF CURVATURE A7
A.7) AUTOMATED RECORDING OF DROP IMAGES A8
A.8) PROGRAM CODE A9
A.8.1) AUTOMATED RECORDING OF IMAGES A9
A.8.2) RADIUS OF CURVARTURE PROGRAM A10

# List of Figures


Fig. 3.1: Schematic diagram of cell model of a liquid system. 5

Fig. 3.2: Plot of reduced surface tension vs. αT. 18

Fig. 4.1: Surface Tension vs. density for LLDPE hexene copolymer series. 20

Fig. 4.2: Surface tension vs. number average molecular weight for LLDPE hexene copolymer series. 23

Fig. 4.3: Surface Tension as function of the inverse of number average molecular weight for LLDPE hexene copolymer series. 25

Fig. 4.4: Surface Tension as a function of the effective molecular weight for LLDPE hexene copolymer series. 26

Fig. 4.5: Surface tension vs. polydispersity index of LLDPE hexene copolymer series. 27

Fig. 4.6: Surface Tension vs. effective molecular weight for LLDPE α-olefin copolymer resins. 31

Fig. 4.7: Surface Tension vs. inverse of effective molecular weight for LLDPE α-olefin copolymer resins. 31

Fig. 4.8: Surface tension of LLDPE resins as function of thermal expansion coefficient. 33

Fig. 4.9: Surface tension temperature coefficients ($-dy/dT$) of linear PE as a function of the inverse of number average molecular weight. 39

Fig. 5.1: Pendant drop geometry. 44

Fig. 5.2: Measurements defining the pendant drop diameter ratio. 47

Fig. 5.3: Necking Pendant Drop. 50

Fig. 5.4: Retracting Pendant Drop. 51

Fig. 5.5: Surface tension of water for different drop volumes. 55

Fig. 5.6: Profiles of air drops in water with syringe diameter, d = 0.4 mm. 56

Fig. 5.7: Enlarged rectangular region from Fig 2.6. 56

Fig. 5.8: Surface tension of water vs. drop volume for 2 syringe diameters. 59

Fig. 5.9: Drop profiles of air drop in water w/ syringe inner diameter = 1.2 mm. 60

Fig. 6.1: Pendant Drop Apparatus 61

Fig. 6.2: Experimental Cell 63

Fig. 6.3: Drop Plunger in Syringe 65

Fig. 6.4: Iterative action plan to manipulate diameter of filaments of denser polymer phase using capillary rheometer 69

Fig. 7.1: Drop Length Ratio ($L/L_o$) as a function of time for LLDPE A/PS 71 87
Fig. 7.2: Drop Diameter Ratio ($D/D_o$) as a function of time for LLDPE A/PS 88
Fig. 7.3: Apparent interfacial tension as a function of time for LLDPE A/PS. 91
Fig. 7.4: Surface Tension as function of drop volume for heptane with syringe diameter 1.8 mm. 94
Fig. 7.5: Surface Tension as function of drop volume for heptane with syringe diameter 4 mm. 95
Fig. 7.6: Surface Tension of LLDPE E as a function of drop volume with syringe diameter 1.8 mm. 96
Fig. 7.7: Surface Tension of LLDPE E as a function of drop volume with syringe diameter 4 mm. 97
Fig. 7.8: Gravitational to surface force ratio for 3 syringe diameters and 3 fluids 100

# List of Tables


Table 3.1: Values of surface tension determined by Dettre and Johnson[63] for several branched PE resins 15

Table 4.1: Material properties of the LLDPE resins. 21

Table 4.2: Relevant LLDPE resin properties. 22

Table 4.3: PVT properties of LLDPE resins at 160 °C 22

Table 4.4: Table of constants k and $\gamma_\infty$ used to fit the effective molecular weights and surface tensions to the relation $\gamma=\gamma_\infty-k/(M_n)_{eff}$. 32

Table 4.5: Comparison of experimental values of surface tension of LLDPE to the surface tension of linear PE of equal number average molecular weight and equal effective molecular weight. 36

Table 4.6: Comparison of experimental values of surface tension temperature coefficient of LLDPE to the surface tension temperature coefficients of linear PE of equal number average molecular weight and equal effective molecular weight. 40

Table 4.7: Values of interfacial tension and interfacial tension temperature coefficients. 41

Table 6.1: Percent errors for surface tension experiment with 4.0 mm diameter syringe. 81

Table 6.1: Percent errors for interfacial tension experiments with 1.8 mm diameter syringe. 82

Table 7.1: Experimentally determined values of surface tension for water and ethylene glycol compared to literature values. 92

Table 7.2: Standard deviation of surface tension measurements from several LLDPE resins with the 1.8 mm diameter syringe. 93

Table 7.3: Comparing results for heptane and LLDPE for two syringe diameters: 1.8 and 4.0 mm. 98

# List of Variables

$\gamma$: Interfacial / Surface Tension

$A$: Unit area

$R$: Syringe radius

$W$: Pendant drop weight

$W_{max}$: Maximum stable drop weight

$\Delta P$: Pressure difference

$\Delta P_o$: Pressure difference at drop apex, position coordinate (0,0)

$(x,z)$: Position coordinates of pendant drop profile

$R_1(x,z)$, $R_2(x,z)$: mutually perpendicular radii of curvature at position $(x,z)$ on pendant drop profile

$\phi(x,z)$: Angel between horizontal axis and tangent to pendant drop profile at position $(x,z)$

$a$: Radius of curvature at drop apex

$B$: Dimensionless shape factor

$g$: Gravitational constant

$\rho$: Density

$\Delta\rho$: Density difference between immiscible liquid phases

$S$: Diameter ratio of pendant drop

$H$: Correction factor related to $S$

$V_c$: Critical drop volume / Maximum stable drop volume

$R_d$: dimensionless syringe radius

$\varepsilon_{min}$: Drop weight to surface force ratio of smallest drop volume which yields literature or maximum value of interfacial tension

$V_\gamma$: Smallest drop volume which yields literature or maximum value of interfacial tension

$S_D$: Linear measurement of drop size

$D$: Syringe diameter

$\gamma^*$: Dimensionless surface tension, ratio of experimental surface tension to literature or maximum value

$V^*$: Reduced drop volume, ratio of drop volume to critical drop volume

$n$: Optical correction factor

$M$: Magnification factor

$\gamma_{12}$: Interfacial tension

$\gamma_1$: Surface tension

$W_a$: Work of adhesion

$^d$: Dispersive (non-polar) component

$^{P}$: Polar component

$_{lit}$: literature value

$_{max}$: maximum value

DICM: Discrete interface cell model.

$\Gamma_i$: Surface concentration of species $i$.

$h_s$: Surface enthalpy per unit area

$s_s$: Surface entropy per unit area

$\overline{h_i}$ : Partial molar enthalpy of the species $i$ in the bulk phase

$\overline{s_i}$ : Partial molar entropy of the species $i$ in the bulk phase

$\Delta e$: Characteristic molecular binding energy

$\Delta E$: Molar binding energy

$m$: Fraction of missing bonds of surface molecule

$V$: Cell volume

$v$: Molar volume

$CED$: Cohesive energy density, ratio of the binding energy to the volume, $\Delta E/V$

$v_{sf}$: Surface free volume

$v_{sb}$: Bulk free volume

$DP$: Degree of polymerization

$N_o$: Avogadro's number

$\theta$ : Free volume per end group

$M_n$: Number average molecular weight

$(M_n)_{eff}$: Effective (number average) molecular weight

$M_w$: Weight average molecular weight

$X$: Polymer property at any molecular weight

$X_\infty$: Polymer property at infinite molecular weight

$k$: Constant for molecular weight expression for a homologous series

$\gamma_\infty$: Surface tension at infinite molecular weight

$\gamma_e$: Surface tension of the end group

$v_e$: Molar volume of the end group

$m_r$: Molecular weight of the repeat unit

$v_r$: Molar volume of the repeat unit

$d\gamma/dT$: Surface tension temperature coefficient

$n$: Number of chain branches per molecule

$\varepsilon$: Well depth of molecular potential curve between two similar molecules

$r$: Hard core molecular radius

$\tilde{P}$: Reduced Pressure

$\tilde{V}$: Reduced Volume

$\tilde{T}$: Reduced Temperature

$\tilde{\gamma}$: Reduced surface tension, $\gamma/\gamma^*$

$\gamma^*$: Surface tension Reduction variable

$v^*$: Hardcore molar volume of the spherical molecule (Volume reduction variable)

$\beta$: Isothermal compressibility factor

$\alpha$: Isobaric thermal expansion coefficient

$k$: Boltzmann's constant

$c$: Degrees of freedom of molecule

$q$: number of external contacts of molecule

$c/q$: Prigogine structural free volume parameter

# 1) INTRODUCTION

Interfacial tension plays a crucial role in the design, processing, performance and durability of polymeric systems intended for a variety of applications. The most important example is in the field of polymer blends, where the interfacial tension of a polymer-polymer melt is an indirect measure of miscibility, and as such, it determines the morphology and mechanical performance of the blend[1].

The most reliable technique of measuring the interfacial tension of polymer melts is the pendant drop method. It is based on equations derived by Bashforth and Adams[2] in 1882, and its accuracy has steadily improved over the years, most recently with the incorporation of computerized drop profile analysis[3-5]. The polymer engineering group at McGill University built a pendant drop apparatus to study the surface and interfacial tension of polymer melts (Demarquette et Kamal[5]). The modified design improved drop stability and allowed for on-line measurements of the interfacial tension. The interfacial tension is calculated by analyzing the drop profile with a computer program based on shape comparison routines developed by Anastasiadis[3].

In spite of the widespread use of the pendant drop method, a detailed experimental procedure has yet to be published. The majority of papers measuring the surface and interfacial tension of polymer melts quote Wu[6-10] and Roe[11-15] for their experimental method, but these references are lacking in procedural detail. Specifically, the effects of drop volume, syringe diameter and unstable drops on interfacial tension measurements of polymer melts are not addressed in sufficient detail. In addition, the standard criterion established by Wu[6] and Roe[11] to determine equilibrium is not compatible with the computerized methods currently used to calculate the interfacial tension. A detailed experimental procedure will be developed to address the aforementioned issues and improve the accuracy of experimental results.

The surface and interfacial tensions of several polyethylene and polystyrene resins will be determined experimentally and compared to literature values to test the improved experimental procedure. In addition, several experimental linear low-density polyethylene

(LLDPE) resins have been well characterized in terms of molecular weight, chain branching, polydispersity and density. The effects of these factors on the surface tension of the LLDPE copolymers will be discussed and compared to data available in the literature.

## 2) OBJECTIVES

1) To develop a definitive experimental procedure for the measurement of the interfacial tension of polymer melts with the pendant drop apparatus.

2) To clarify the issue of the dependence of interfacial tension on drop size, for polymer melts.

3) To determine the experimental values of surface and interfacial tension for several polymer resins and compare the data with literature values..

4) To relate the values of surface tension of several experimental linear low-density polyethylene (LLDPE) resins to their material and structural properties.

# PART 1

# THE EFFECT OF STRUCTURAL AND MATERIAL PROPERTIES ON THE SURFACE TENSION OF LLDPE

# 3) BACKGROUND: SURFACE TENSION OF LIQUIDS

## 3.1) INTRODUCTION

The interfacial tension, as defined by Adamson[21], is the reversible work required to create a unit of interfacial area at constant temperature $T$, pressure $P$ and number of molecules, $n$.

$$\gamma = \left(\frac{\partial G}{\partial A}\right)_{T,P,n} \qquad (3\text{-}1)$$

where $G$ is the Gibb's free energy of the total system and $A$ is the interfacial area. Therefore, the interfacial tension is usually referred to as an energy per unit area, but it can also be viewed as a force per unit length. It is worth noting that interfacial tension ($\gamma_{12}$) is associated with an interface between any two phases. Surface tension ($\gamma_1$) is only a special case of interfacial tension, where one of the phases is air or an inert gas.

The term surface tension is often used without understanding its true physical meaning and what are the forces which lead to this phenomenon. The following discussion explains the concept of surface tension and its causes with a simple model.

The discrete interface cell model (DICM) (Fig. 3.1) represents a two dimensional slice through a liquid consisting of an array of spherical molecules in a condensed state. Each molecule is confined to wander within a cell of defined volume. Molecules at the free surface are indicated by the lighter shaded spheres and are contained within a cell volume that is larger than that found in the bulk of the liquid. The sudden increase in volume at the surface indicates that the density decreases rapidly over the length scale of a single molecule when moving from the liquid to the vapor phase.

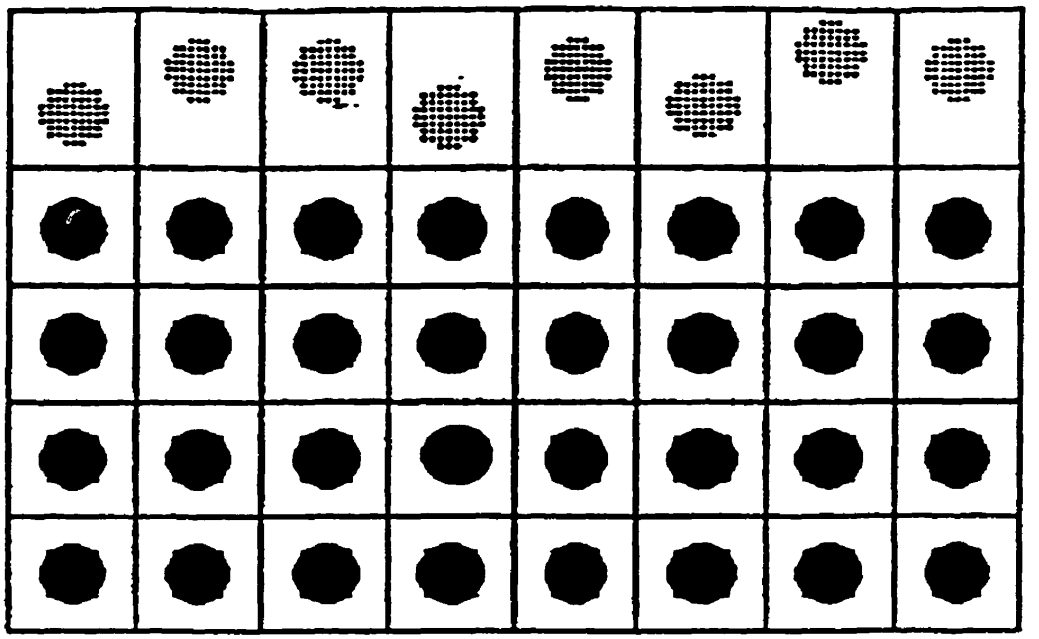

Fig. 3.1: Schematic diagram of cell model of a liquid system with the free surface denoted by lightly shaded spheres.

The surface tension is a function of the enthalpy and entropy of interfacial formation per unit surface area, $\Delta h_s$ and $\Delta s_s$ respectively:

$$\gamma = \Delta h_s - T\Delta s_s \tag{3-2}$$

$$\Delta h_s = h_s - \Gamma_1 \overline{h_1} - \Gamma_2 \overline{h_2} \tag{3-3}$$

$$\Delta s_s = s_s - \Gamma_1 \overline{s_1} - \Gamma_2 \overline{s_2} \tag{3-4}$$

where $\Gamma_i$ is the surface concentration of species $i$, $h_s$ and $s_s$ are the surface enthalpy and surface entropy per unit area and $\overline{h_i}$ and $\overline{s_i}$ are the partial molar enthalpy and partial molar entropy of the species $i$ in the bulk phase. There is a difference in enthalpy and entropy between the surface and the bulk liquid regions. Both the enthalpy and entropy of surface formation contribute to a free energy difference between molecules in the bulk and at the surface. Thus, the surface tension represents an imbalance of forces acting on the molecules occupying the free surface. The next few paragraphs will explain qualitatively how the enthalpy of surface formation, $\Delta h_s$, and the entropy of surface formation, $\Delta s_s$, affect the surface tension.

### 3.1.1) ENTHALPY OF SURFACE FORMATION

The molecules in the bulk are held together by interactions with their nearest neighbours and each molecule is bound with a characteristic binding energy, $\Delta e$, which for small molecules is measured by the energy of vaporization. Molecular interactions are strongly related to the density of the fluid, $\rho$. The closer are the molecules to one another, the stronger is the resulting molecular interaction. Molecules at the surface are in contact with both liquid and vapor molecules. The molecular interactions with the vapor phase are negligible because of the lower density of the gas phase. Therefore, molecules at the surface have fewer neighbours with significant binding potential and their binding energy is reduced by a factor proportional to the fraction, $m$, of missing bonds. Thus, molecules at the surface have an excess surface enthalpy (energy) which is equal to the number of missing bonds multiplied by the binding energy per bond, $m\Delta e$. The excess surface enthalpy per unit area, $\Delta h_s$, is obtained by dividing the excess surface enthalpy by a characteristic area occupied by a molecule at the surface, which is proportional to $V^{\frac{2}{3}}$, where $V$ is the cell volume occupied by a molecule in the bulk. Therefore, the excess surface enthalpy per unit area, $\Delta h_s$, can be expressed as:

$$\Delta h_s = \frac{w\Delta E}{v^{\frac{2}{3}}} = w\left(\frac{\Delta E}{v}\right)v^{\frac{1}{3}} = w(CED)v^{\frac{1}{3}} \qquad (3\text{-}5)$$

where $\Delta E$ is the molar binding energy, $v$ is the molar volume, $w$ is a constant which incorporates the factor $m$ and other geometrical factors and $CED$ is the cohesive energy density, defined as the ratio of the binding energy to the volume, $\Delta E/v$. The values of surface tension for water and hexane demonstrate the effect of the $CED$. Water, with its hydrogen bonding, has much stronger molecular interactions than hexane, which has only weak Van der Waal's interactions, and has a value of surface tension that is 3.5 times larger than that of hexane.

### 3.1.2) ENTROPY OF SURFACE FORMATION

Entropy is quantitative measure of the number of possible states available to a system[41]. For the DICM model, each molecule is confined to a single cell. If the system is defined as a single cell, the number of states available to the molecule within the cell is directly proportional to the empty or free volume in the cell. The free volume, which is the volume due to thermal expansion, is defined as the volume occupied by a molecule less its Van der Waal's or hardcore volume. A molecule at the surface has a larger cell volume than in the bulk because of the density change from the liquid to the vapor state. Thus, surface molecules have a higher entropy than molecules in the bulk of the liquid, which leads to a positive entropy of surface formation. The entropy of surface formation, $\Delta s_s$, is modeled as the ratio of the surface and bulk free volumes, $v_{sf}$ and $v_{sb}$ respectively.

$$\Delta s_s = \ln\left(\frac{v_{sf}}{v_{bf}}\right) \qquad (3\text{-}6)$$

## 3.2) POLYMER LIQUIDS AND MELTS

Until now, the model for surface tension describes only simple liquids. The model is adapted to describe the surface tension of polymer liquids by joining each of the spheres in Fig. 3.1 to two of its nearest neighbours and the polymer molecules are represented by long chains of spheres. Each sphere represents a structural unit in the polymer chain. Equation (3-5) is expected to describe the enthalpy of surface formation of a polymer liquid where $V$ is now the molar volume per structural unit. However, the surface entropy of polymers is more complicated than that of simple liquids due to the large dimensions of the polymer chains. Silberberg[42] has shown that polymer molecules at the interface cannot retain a random coil configuration that is readily assumed in the bulk liquid phase. The restriction in the number of configurations of a polymer molecule at the surface reduces the surface entropy and the entropy of surface formation. The effect of entropic conformational restrictions on the surface tension of polymers has been estimated by several researchers[42-44] to be on the order of 10%, and Dee and Sauer[46] have found it to

be completely negligible. Therefore, the entropy of a polymer melt can be treated like that of a simple liquid, which is only a function of the average free volume per chain segment. Thus, equation (3-6) is also valid for polymer melts.

## 3.3) INTERFACIAL TENSION

The discrete interface cell model can be modified to describe the interfacial tension between immiscible polymer melts. The vapour phase is replaced by another set of cells that contain spherical molecules corresponding to the second immiscible polymer. For a polymer molecule at the interface, bonds or interactions with dissimilar polymer molecules on the other side of the interface replace a fraction of its bonds with similar polymer molecules. Stronger intermolecular interactions at the interface result in a lower enthalpy of surface formation. This reduces the value of interfacial tension, and it is usually much less than the values of surface tension for either liquid. Polymers with similar chemical compositions and densities, such as PE and PP, have strong intermolecular interactions, which reduces the enthalpy of surface formation and the interfacial tension significantly. Accordingly, the interfacial tension of PE/PP is approximately 1-2 dyne/cm, while the surface tension of either polymer melt is close to 30 dyne/cm.

It was established previously that the entropy of surface formation is a function of the ratio of the free volume at the surface to that in the bulk. The density difference across an interface separating two immiscible liquids is much smaller than the density difference across the interface of a liquid with a free surface. This reduces the free volume at the interface, which lowers the entropy of interfacial formation and further reduces the value of interfacial tension. The entropic contribution of the conformational restrictions of the polymer chains at the interface is no longer negligible, as is the case for a free surface, because of the lower values of interfacial tension.

## 3.4) VARIABLES AFFECTING SURFACE TENSION

### 3.4.1) CHEMICAL COMPOSITION

Sugden[47] has shown that the surface tension of a small molecule liquid is purely a function of chemical composition and density. For polymers, the chemical composition of the main chain structural unit is the most important factor to determine the interfacial tension. However, it is not the only factor. The cohesive energy density and the surface entropy are also affected by the arrangement of the structural units that form the polymer chains. Thus, the surface tension of polymers is also affected by variables such as the molecular weight and chain branching.

### 3.4.2) MOLECULAR WEIGHT

A linear macromolecule is composed of two types of units: main chain structural units, which account for most of the polymer mass, and the end groups. An end group has different properties than that of an internal unit because of structural differences. Any bulk polymer property, which is defined as a property that is strongly correlated with the bulk thermodynamic properties[87], is a function of the combined contributions of the main chain structural units and the end groups[45]. For polymer molecules with a degree of polymerization (*DP*) greater than 50, the concentration of end groups is small compared to the concentration of main-chain structural units. Thus, any bulk property is expected to be a linear function of the concentration of the end groups. An end group is connected to the polymer chain by only a single bond, which increases its external volume dependent degrees of freedom. Thus, the average free volume per structural unit of the polymer chain is directly proportional to the concentration of end groups and decreases as the chain length increases. It follows that bulk polymer properties are proportional to the free volume associated with the chain ends. The free volume contributed by the chain ends to the total free volume of the polymer chain is inversely proportional to the number average molecular weight of the polymer:

$$V_f = \frac{2N_o \rho \theta}{M_n} \qquad (3\text{-}7)$$

where $N_o$ is Avogadro's number, $\rho$ is the polymer density, $\theta$ is the free volume per end group and $M_n$ is the number average molecular weight. Equation (3-7) assumes a linear chain that has only two free ends. If the bulk polymer properties are linearly dependent on the free volume of the chain ends, then by equation (3-7), they are linearly dependent on the inverse of molecular weight, $M_n^{-1}$:

$$X = X_\infty - \frac{k}{M_n} \qquad (3\text{-}8)$$

where $X$ is a bulk polymer property at a given molecular weight, $X_\infty$ is the bulk polymer property at infinite molecular weight and $k$ is a constant for any homologous series. Patterson et al.[55] have shown that the surface tension of a liquid is strongly correlated with the bulk thermodynamic properties. Therefore, the surface tension can be expressed as a function of molecular weight[67], as in equation (3-8):

$$\gamma = \gamma_\infty - \frac{k}{M_n} \qquad (3\text{-}9)$$

where $\gamma$ is the surface tension at molecular weight, $M_n$ and $\gamma_\infty$ is the surface tension at infinite molecular weight. Jalbert et al.[48] developed a theoretical expression for $k$ using lattice theory:

$$k = (\gamma_\infty - \gamma_e)\left(\frac{2m_r v_e}{v_r}\right) \qquad (3\text{-}10)$$

where $\gamma_\infty$ is the surface tension at infinite molecular weight, $\gamma_e$ is the surface tension of the end group with molar volume $v_e$, and $m_r$ is the molecular weight of the repeat unit with volume $v_r$. Unfortunately $\gamma_e$ and $v_e$ are difficult to evaluate. Chee et al.[49] have developed a method to evaluate $k$ from P-V-T data using the principle of corresponding states.

The surface tension of polymer liquids increases with molecular weight because of two factors. The chain ends have a surface tension associated with them that is different

than that of a main-chain unit. A change in molecular weight also affects the density because of the additional free volume associated with the chain ends.

### 3.4.2.1) LOW MOLECULAR WEIGHT POLYMERS

Equation (3-9) describes the surface tension of macromolecules over a wide range of molecular weights, but deviations do occur for polymers of small molecular weight. As the molecular weight decreases, the concentration of the end groups increases and eventually reaches the same order of magnitude as the repeat units. The assumption in equation (3-9), which is the concentration of end groups is much less than the concentration of the repeat units, is no longer valid. This results in deviations from the dependence of bulk polymer properties on $M_n^{-1}$. For most properties, such as density, this occurs at very low molecular weights[42], $M_n < 50$. However, the surface tension of polymer liquids generally deviates from the $M_n^{-1}$ dependence at much larger molecular weights, $M_n <$ 1000-3000, depending on the type of polymer[46,50,51]. At the lower range of molecular weights, the surface tension of polymers depends on $M_n^{-\frac{2}{3}}$ rather than $Mn^{-1}$[46,50,51]. It is not known precisely why the surface tension depends on the molecular weight to the 2/3 power at the lower range of molecular weights or why deviations from $M_n^{-1}$ dependence occur at higher molecular weights for surface tension than for other bulk properties. However, it should be noted that several theoretical studies[52-55] have predicted the transition from the $M_n^{-1}$ to an approximate $M_n^{-\frac{2}{3}}$ dependence for surface tension at low molecular weights. Dee and Sauer[56] concluded that the power-law dependence of molecular weight varies from -1 to -2/3 because of a complicated interrelationship between density, compressibility and expansivity, which all vary with molecular weight.

### 3.4.3) TEMPERATURE

An increase in the temperature of a polymer liquid decreases its density, which reduces the value of surface tension. Surface and interfacial tension temperature

coefficients are constant for most liquids, including polymers, over large temperature ranges well below the critical temperature[10]. This is a reflection of the constant value of the thermal expansion coefficients over the same temperature ranges. The surface tension temperature coefficient, $d\gamma/dT$, of polymers (~0.5-0.8 dyne/cm/°C) is smaller compared to that of a small molecule liquid (~0.1 dyne/cm/°C) because polymers have smaller thermal expansion coefficients[12].

### 3.4.3.1) EFFECT OF MOLECULAR WEIGHT ON $D\gamma/DT$

The surface tension temperature coefficient, $d\gamma/dT$, decreases with increasing molecular weight because of a reduction in the macromolecules external, volume-dependent degrees of freedom which reduces the thermal expansion coefficient of the polymeric liquid[12,56] and $d\rho/dT$. Dee and Sauer have shown with polyethylene[40] and polytetrafluoroethylene[57] that the surface tension temperature coefficient decreases as the molecular weight increases with both experimental data and a discrete cell interface model. Demarquette and Kamal[58] measured the interfacial tension of PP/PS melts and showed that the interfacial tension temperature coefficient decreased with increasing molecular weight .

### 3.4.3.2) ENTROPY OF SURFACE FORMATION AND $D\gamma/DT$

It can be shown with thermodynamics[10], that the surface tension temperature coefficient, $d\gamma/dT$, is equal to the entropy of interfacial formation per unit area, $\Delta s_s$ (equation 3-2):

$$\frac{d\gamma}{dT} = -\Delta s_s \qquad (3\text{-}11)$$

Therefore, the entropy of surface formation is also related to the temperature dependence of the bulk density[40] and decreases with increasing molecular weight. The decrease in the entropy of surface formation with increasing molecular weight implies that the ratio of the free volume at the surface to the free volume in the bulk (equation 3-6) also decreases.

The physical manifestation of the relative decrease of the surface free volume is a decrease in the width of the interface.

It has been suggested[10] that the lower surface tension temperature coefficient, $d\gamma/dT$, of polymers is due to conformational restrictions of the polymer chains near the interface, which reduce the entropy of surface formation, $\Delta s_s$. However, the overall contribution of surface conformational effects to surface tension has been to be negligible[51], so its effect on the surface tension temperature coefficient is similarly limited[44].

#### 3.4.3.3) INTERFACIAL TENSION TEMPERATURE COEFFICIENT

The value of the interfacial tension temperature coefficient, $d\gamma_{12}/dT$, between two immiscible polymer melts, (.002-.03 dyne/cm/°C) is smaller than either value of the surface tension temperature coefficient, because the densities of both phases are affected by temperature changes. This reduces the effect of temperature on the strength of the molecular interactions across the interface and decreases the interfacial tension temperature coefficient.

### 3.4.4) POLYDISPERSITY

#### 3.4.4.1) INTERFACIAL TENSION

There are a number of studies[57-60] which have shown that the interfacial tension of a polydisperse polymer-polymer melt is lower than that of a monodisperse system of equal number average molecular weight. In order to affect the interfacial tension, a polydisperse system must change either the enthalpy or entropy of interfacial formation. It has been noted[58] that there is little effect of polydispersity on most bulk polymer properties, such as density and there is no change in the enthalpy of interfacial formation, as the intermolecular interactions per chain segment are the same for any size molecule.

Nam et al.[59] and Demarquette and Kamal[57] have measured a significant increase in the interfacial tension temperature coefficients of polydisperse systems, which implies

that the entropy of interfacial formation is also increasing (equation 3-11). Broseta et al.[58] concluded that the effect of polydispersity on the interfacial tension of a polymer-polymer system is purely entropic. They suggested that expelling the longer chains from the interface, which increases the interfacial concentration of the shorter chains, maximizes the interfacial entropy. The shorter chains have a higher entropy than longer chains, presumably due to the larger free volume of the smaller chains. The increase in the entropy of interfacial formation reduces the interfacial tension and broadens the interface.

### 3.4.4.2) SURFACE TENSION

Dee and Sauer[62] and Hariharan and Kumar[63] have studied the effects of polydispersity on the surface tension of polymer melts. Dee and Sauer[62] found through experiments and theory with bimodal blends of PDMS that the surface region had a much larger concentration of the shorter chain molecules, which reduced the surface tension, presumably through the free volume effect described previously. Hariharan and Kumar[63] theorized that conformational restrictions of the polymer chain at the surface would decrease the surface entropy. If the melt were polydisperse, the entropic loss suffered by longer chains would be greater than the loss incurred by a shorter chain. This would suggest that shorter chains would migrate to the surface to maximize the surface entropy and reduce the surface tension. However, the computer simulation found that surface enhancements due to configurational entropic effects are very small. This is in agreement with results obtained by Dee and Sauer[40], which indicate that the contribution of surface conformational entropic effects to the surface tension are negligible.

### 3.4.4.3) COMPARISON BETWEEN SURFACE AND INTERFACIAL TENSION

Polydispersity should have more of an effect on the value of interfacial tension because the conformational restrictions of polymers at the interface are more significant. This favors the migration of the shorter molecules to the interface, which should increase the effects of polydispersity. However, there are no known studies, which have compared the effects of polydispersity on the surface tension and interfacial tension of polymer melts.

### 3.4.5) CHAIN BRANCHING

#### 3.4.5.1) LITERATURE DATA

The effect of polymer chain branching on surface tension has not been extensively studied. Wu[8], Roe[12], Dettre and Johnson[63] and Allan and Neogi[64] are the only known researchers to have studied the surface tension of linear and branched polyethylene (B-PE). All the researchers found that branched polyethylene had a lower value of surface tension (~1-2 dyne/cm) compared to that of linear polyethylene at the same temperature. In fact Allan and Neogi[64] suggested that surface tension measurements could be used as a means of estimating the degree of branching in a polymer. Also, Wu[8] and Roe[12] found that B-PE had a larger surface tension temperature coefficient by approximately 0.01 dyne/cm/°C. Dettre and Johnson[63] studied the surface tension of several branched PE resins with different branching densities (Table 3.1).

| **Sample** | **Branching Density** (# methyl branches/100 C) | $M_n/M_w$ (g/mol) | **γ(160°C)** (dyne/cm) |
|---|---|---|---|
| $A^*$ | 6 | | 22.5 |
| $B^*$ | 5 | $M_n$=2000 | 25.4 |
| $C^*$ | 5.2 | $M_n$=7000 | 26.0 |
| $D^*$ | 3.5 | $M_w$=340000 | 26.6 |
| $E^*$ | 0.2 | $M_w$=67000 | 27.6 |

Table 3.1: Values of surface tension determined by Dettre and Johnson[63] for several PE resins with varying methyl branching density. The superscript * is used to differentiate Dettre and Johnson's samples from the LLDPE resins in this study.

Dettre and Johnson's[63] results suggest that an increase in branching density decreases the value of surface tension. However, the results also indicate that the molecular weight of the resins also plays a role in determining the value of surface tension (samples $B^*$ and $C^*$). An explanation for the effect of chain branching on the surface tension of branched PE was not given by any of the researchers. It was determined that the lower surface tension and higher surface tension temperature coefficient obtained by Roe[12] for the B-PE were not caused by a density difference. Wu[8] and Dettre and Johnson[63] did not publish the polymer densities.

Jasper et al.[65] studied the interfacial tension of hydrocarbons and water and determined that chain branching reduced the interfacial tension. The authors theorized that packing density differences caused by the chain branching in alkanes reduced the intermolecular forces. The decrease in cohesive energy density would then reduce the surface enthalpy and the surface tension. However, Owen[66] found that some of the experimental results were in error. The modified results indicated that while highly branched hydrocarbons do have lower surface tensions, there was no evidence that supported Jalbert et al.'s[65] claims that chain branching affected the cohesive energy density.

Carriere and Silvis[68] studied the effect of short chain branching and comonomer type on the interfacial tension of polypropylene-polyolefin elastomer blends. They determined that the interfacial tension of a blend with a branched polymer could be modeled with a modified form of equation (3-9):

$$\gamma = \gamma_{\infty} - \frac{k}{(M_n)_{eff}^{-z}} \qquad (3\text{-}12)$$

where the effective molecular weight is defined as the number average molecular weight between branch points and the exponent $z$ is an empirical constant which is commonly applied to equation (3-9) to model the interfacial tension between immiscible polymer melts. The effect of the comonomer type on the value of interfacial tension could not be determined conclusively.

## 3.5) THE PRINCIPLE OF CORRESPONDING STATES

The principle of corresponding states implies that any cell model which is based on simple spherical molecules that interact via an attractive potential that is characterized by a well depth, $\varepsilon$, and a hard core molecular radius, $r$, can be described by a partition function from which it is possible to deduce all thermodynamic properties of the system[69,70]. The partition function can be expressed in terms of the reduced temperature, $\tilde{T}$, and the

reduced volume, $\tilde{V}$. The energy and length scales, $\varepsilon$ and $r$, and the thermodynamic parameters $V$ and $T$ are used to form the reduction variables. The partition function is combined with an equation of state to relate the reduced pressure to the reduced temperature and volume:

$$\tilde{P}=f(\tilde{T},\tilde{V}) \qquad (3\text{-}13)$$

The nature of the function described in equation (3-13) depends only on the form of the potential function used to describe the molecular interactive potential, $\varepsilon(r)$. Equation (3-13) expresses the theorem of corresponding states, which implies that a single universal equation governs the $\tilde{P}$-$\tilde{V}$-$\tilde{T}$ behavior of all liquids.

Any physical property that is a function of the bulk thermodynamic parameters can be derived from the partition function. Therefore, a universal function also exists for such physical properties, which are solely a function of the thermodynamic reduced variables $\tilde{P}$, $\tilde{V}$ and $\tilde{T}$. This implies that such properties will also be described by a single universal function, regardless of molecular structure. For surface tension:

$$\tilde{\gamma} = \frac{\gamma}{\gamma^*(\tilde{P},\tilde{T})} = f(\tilde{V},\tilde{T}) \qquad (3\text{-}14)$$

where $\tilde{\gamma}$, is the reduced surface tension and $\gamma^*$ is the variable used to reduce the surface tension. As explained before, the form of the universal function describing each property depends on the function used to describe the interactive potential.

Without resorting to a specific model, the existence of such universal functions can be tested by scaling an observable property with the correct dimensional combination of thermodynamic properties of the bulk liquid. The reduced surface tension, $\tilde{\gamma}$, can be expressed as:

$$\tilde{\gamma}=\frac{\gamma}{\gamma^*}=\frac{\gamma}{\left(\frac{k}{\alpha}\right)^{\frac{1}{3}}\beta^{-\frac{2}{3}}} \qquad (3\text{-}15)$$

where $k$ is Boltzmann's constant.

To determine if a universal function exists, which governs the surface tension of all molecules, the reduced surface tension is plotted as a function of $\alpha T$ for a large number of molecules with varying chemical composition and molecular weight. Roe[71] and Patterson and Rastogi[72] were among the first to show that the principle of corresponding states does govern the surface tension of liquids. However, they found that two universal curves existed: one for simple molecules and another for polyatomic molecules, including polymers. More recently, Dee and Sauer[69] have confirmed the existence of the principle of corresponding states for the surface tension of macromolecules with new data and have showed that the surface tension of a polymer can be predicted to within ±6% from only bulk thermodynamic data. Figure 3.2 shows the data collected by Dee and Sauer[69] which demonstrates the existence of the corresponding states principle for surface tension.

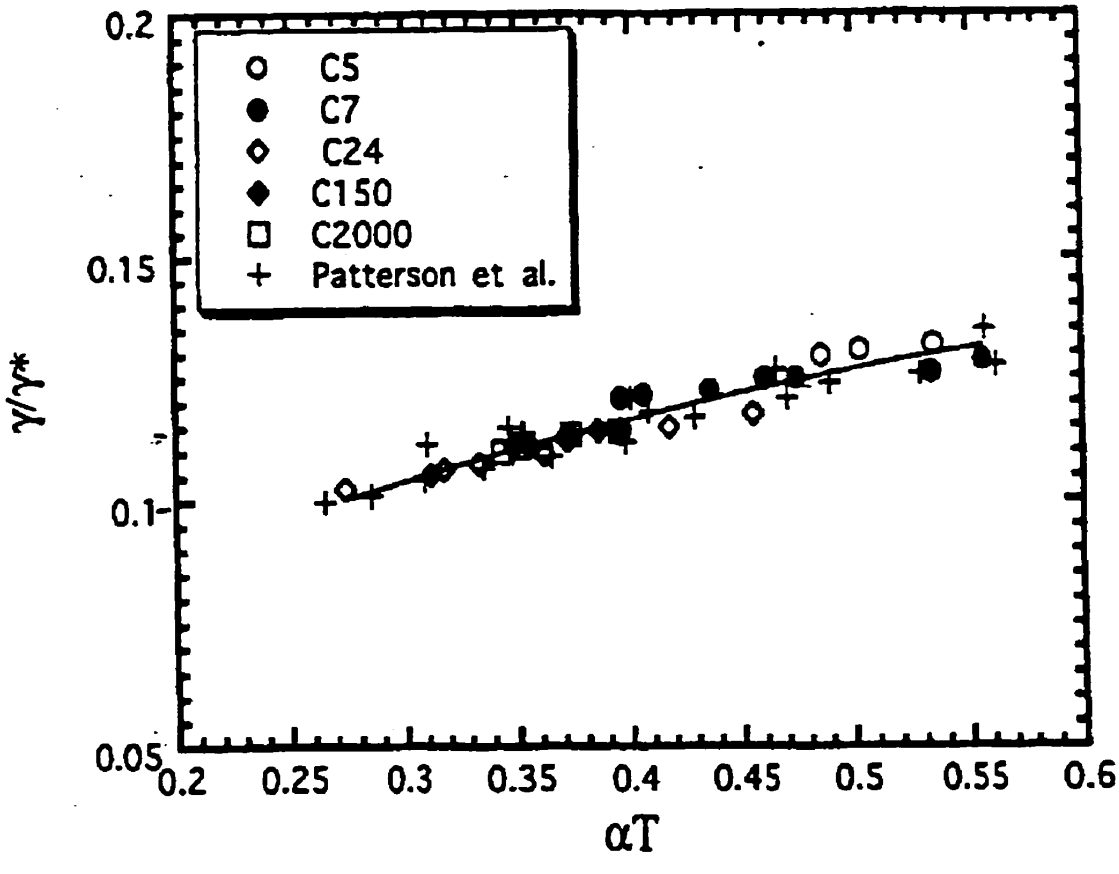


Fig. 3.2: Plot of reduced surface tension ($\gamma/\gamma^*$) as a function of αT for a series of alkanes. $\gamma^*=(k/\alpha)^{\frac{1}{3}}\beta^{\frac{2}{3}}$

# 4) RESULTS AND DISCUSSION: THE EFFECT OF STRUCTURAL AND MATERIAL PROPERTIES ON SURFACE TENSION OF LLDPE

A series of LLDPE α-olefin copolymers were characterized by Nova Chemicals and McGill University and exhibited differences in surface tension ($\gamma$), number average molecular weight ($M_n$), polydispersity ($PD$), branching density and pressure-volume-temperature relationships (Table 4.1-4.3). The objective of this section is to relate the differences in surface tension among the LLDPE copolymers to their material properties. To simplify matters, the analysis is initially restricted to the LLDPE 1-hexene copolymer.

## 4.1) DENSITY

Dee and Sauer[40] have shown that the surface tension of a linear polymer is affected by molecular weight because of changes in the density. The densities of the LLDPE copolymers were measured with the Gnomix® P-V-T apparatus to determine if the changes in surface tension could be attributed to differences in density (Fig. 4.1).

The difference in density between the LLDPE hexene resins, listed in Table 4.3, is very small. There is less than a 0.05% difference between three of the resins, *A*, *D* and *E* and resin *C* is only 0.2% larger than the others. In fact, the difference in the densities of the resins at 160 °C is so small, that it is less than or comparable to the experimental error of the P-V-T apparatus. Considering this, it is not surprising that the differences in surface tension (Fig. 4.1) do not appear to be related to the densities of the LLDPE resins. This indicates that the structural differences that exist between the LLDPE hexene copolymers probably had little effect on the cohesive energy density of the polymers. Thus, it is unlikely that the large differences in the surface tension of the LLDPE hexene copolymers were caused by a difference in density. Note that a significant density difference was not expected because the molecular weights of the LLDPE copolymers were all similar.

The limited data in the literature appears to support the fact that differences in surface tension between branched and linear polymers are not caused by differences in density. Roe[12], Wu[9] and Dettre and Johnson[63] all measured the surface tension of the exact same linear PE resin (DuPont Alathon® 7050) and the exact same branched PE resin (Union Carbide Bakelite® DYLT) and all the researchers found significant differences among the surface tension of branched and linear polymers. Roe[12] determined that the densities of both the linear and branched PE were equal. The data of the previous researchers supports the conclusion made from the experimental data with the LLDPE copolymers, that the differences in surface tension cannot be due to the effects of density alone.

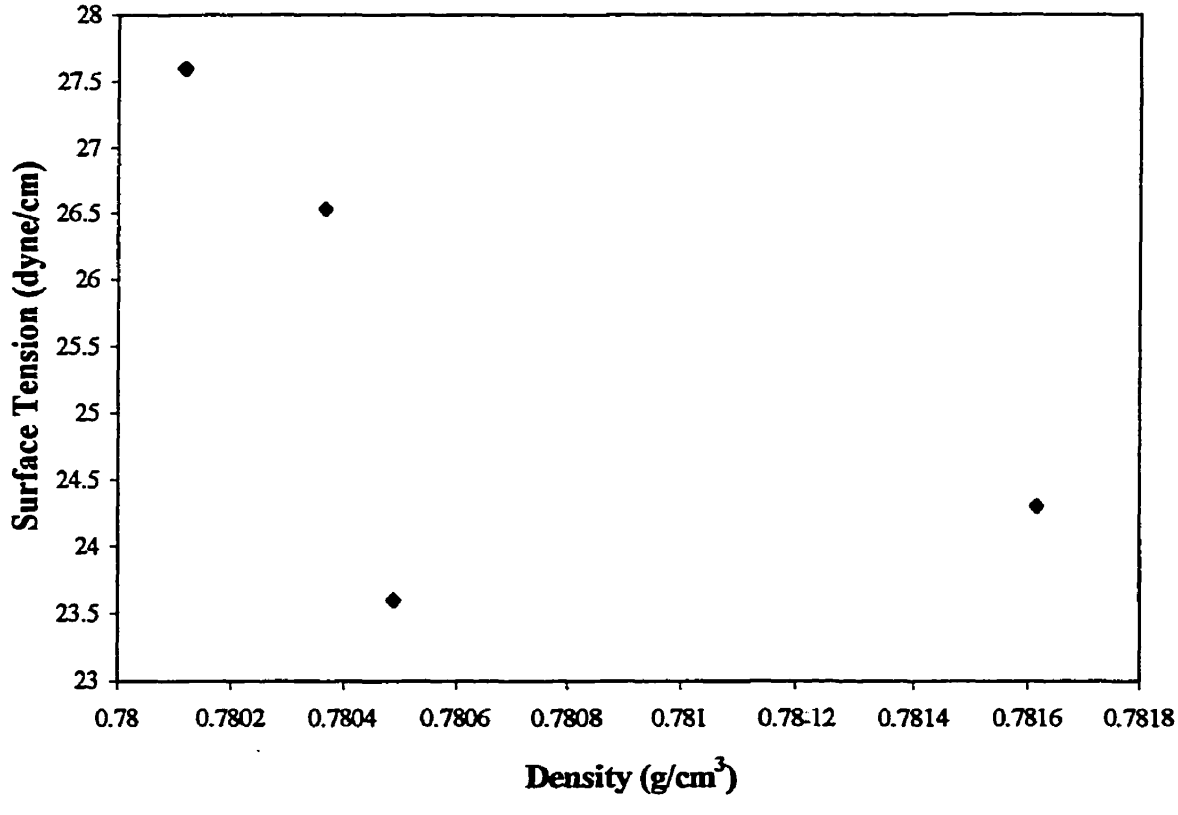


Fig 4.1 Surface Tension vs. density for LLDPE hexene copolymer series.

| Resin | Co-mer | Med / Cat | Surface Tension | % Co-mer | Branches per KC | $M_n*10^{-3}$ | $M_w*10^{-3}$ | PD $M_w/M_n$ | Term Unsat (MC) | Side Unsat (MC) | Internal Unsat (MC) | Total Unsat (MC) |
|---|---|---|---|---|---|---|---|---|---|---|---|---|
| B | But | Gas / ZN | 25.3 | 4.03 | 20.20 | 24.2 | 98.7 | 4.1 | 16.31 | 6.19 | 9.10 | 28.86 |
| H | But | Sol / ZN | 26.5 | 3.80 | 18.90 | 24.9 | 120.0 | 4.8 | 48.61 | 8.66 | 7.24 | 64.51 |
| | | | | | | | | | | | | |
| A | Hex | Gas / ZN | 23.6 | 3.94 | 19.72 | 30.0 | 111.0 | 3.7 | 18.90 | 12.48 | 6.55 | 37.92 |
| C | Hex | Sol / ZN | 24.3 | 3.77 | 18.87 | 36.0 | 111.3 | 3.1 | 18.21 | 16.17 | 4.59 | 38.96 |
| D | Hex | Gas / Met | 26.5 | 3.08 | 15.41 | 44.0 | 98.0 | 2.2 | 19.03 | 21.39 | 4.33 | 44.74 |
| E | Hex | Gas / Met | 27.6 | 2.56 | 12.80 | 43.0 | 94.0 | 2.2 | 12.31 | 12.03 | 8.11 | 32.45 |
| | | | | | | | | | | | | |
| G | Oct | Sol / ZN | 22.8 | 3.20 | 15.80 | 17.0 | 106.0 | 6.2 | 54.52 | 8.05 | 11.78 | 74.35 |
| I | Oct | Sol / Met | 26.0 | 5.00 | 24.80 | 22.0 | 53.0 | 2.4 | 39.45 | 10.16 | 27.64 | 77.25 |
| J | Oct | Sol / Met | 27.4 | 3.20 | 15.80 | 38.0 | 70.0 | 1.8 | 38.01 | 5.83 | 21.40 | 65.24 |

Table 4.1: Material properties of the LLDPE resins. Resin letter is sample designation. (Co-mer) indicates the α-olefin comonomer used in the LLDPE resin. But: 1-Butene, Hex: 1-Hexene, Oct: 1-Octene. Med/Cat: Polymerization medium (Gas & Solution) and catalyst (Metallocene & Ziegler-Natta) used respectively. Surface tension is in dyne/cm. % Co-mer indicates weight % of the α-olefin comonomer in LLDPE resin. Branches per KC is the number of branches per 1000 carbons and is a measure of the branching density. $M_n$ & $M_w$ are the number average molecular weight and the weight average molecular weight repectively. *PD* is the polydispersity represented by the ratio $M_w/M_n$. Unsat represents the number of unsaturated bonds per million carbons.

| Resin | Comonomer | Surface Tension 160 °C (dyne/cm) | $M_n$ (g/mol) | Branching Density (# branches/1000 C) | $(M_n)_{eff}$ (g/mol) | Polydispersity |
|---|---|---|---|---|---|---|
| B | But | 25.3 | 24200 | 20.20 | 680.5 | 4.1 |
| H | But | 26.5 | 24900 | 18.90 | 724.0 | 4.8 |
| | | | | | | |
| A | Hex | 23.6 | 30000 | 19.72 | 728.7 | 3.7 |
| C | Hex | 24.3 | 36000 | 18.87 | 764.0 | 3.1 |
| D | Hex | 26.5 | 44000 | 15.41 | 924.0 | 2.2 |
| E | Hex | 27.6 | 43000 | 12.80 | 1091.4 | 2.2 |
| | | | | | | |
| G | Oct | 23.5 | 17000 | 15.80 | 870.7 | 6.2 |
| I | Oct | 26.0 | 22000 | 24.80 | 612.4 | 2.4 |
| J | Oct | 27.4 | 38000 | 15.80 | 923.0 | 1.8 |

Table 4.2: Relevant LLDPE resin properties. $(M_n)_{eff}$ is the effective molecular weight which is equal to $M_n/(n+2)$, where $n$ is number of chain branches

| Resin | Comonomer | Surface Tension 160 °C (dyne/cm) | Density, ρ (g/cm3) | Thermal Exp Coefft, $\alpha \cdot 10^4$ ($K^{-1}$) | Volumetric Exp Coefft, $\beta \cdot 10^3$ ($MPa^{-1}$) |
|---|---|---|---|---|---|
| B | But | 25.3 | 0.7806 | 7.46 | 1.011 |
| H | But | 26.5 | 0.7787 | 7.39 | 0.996 |
| | | | | | |
| A | Hex | 23.6 | 0.7805 | 7.52 | 1.020 |
| C | Hex | 24.3 | 0.7816 | 7.54 | 1.013 |
| D | Hex | 26.5 | 0.7804 | 7.42 | 1.009 |
| E | Hex | 27.6 | 0.7801 | 7.44 | 1.011 |
| | | | | | |
| G | Oct | 23.5 | 0.7740 | 7.55 | 1.009 |
| I | Oct | 26.0 | 0.7756 | 7.26 | 1.009 |
| J | Oct | 27.4 | 0.7771 | 7.35 | 1.004 |

Table 4.3 PVT properties of LLDPE resins at 160 °C

## 4.2) MOLECULAR WEIGHT AND CHAIN BRANCHING

The data in Fig. 4.2 suggest that the surface tension of the LLDPE hexene copolymers is related to the number average molecular weight. However, there appears to be a discrepancy in the data, particularly for the two highest molecular weights. Resin *E* has a slightly lower molecular weight than *D*, but the surface tension of sample *E* is significantly larger. This appears to contradict published data and the theory that suggests surface tension increases with molecular weight.

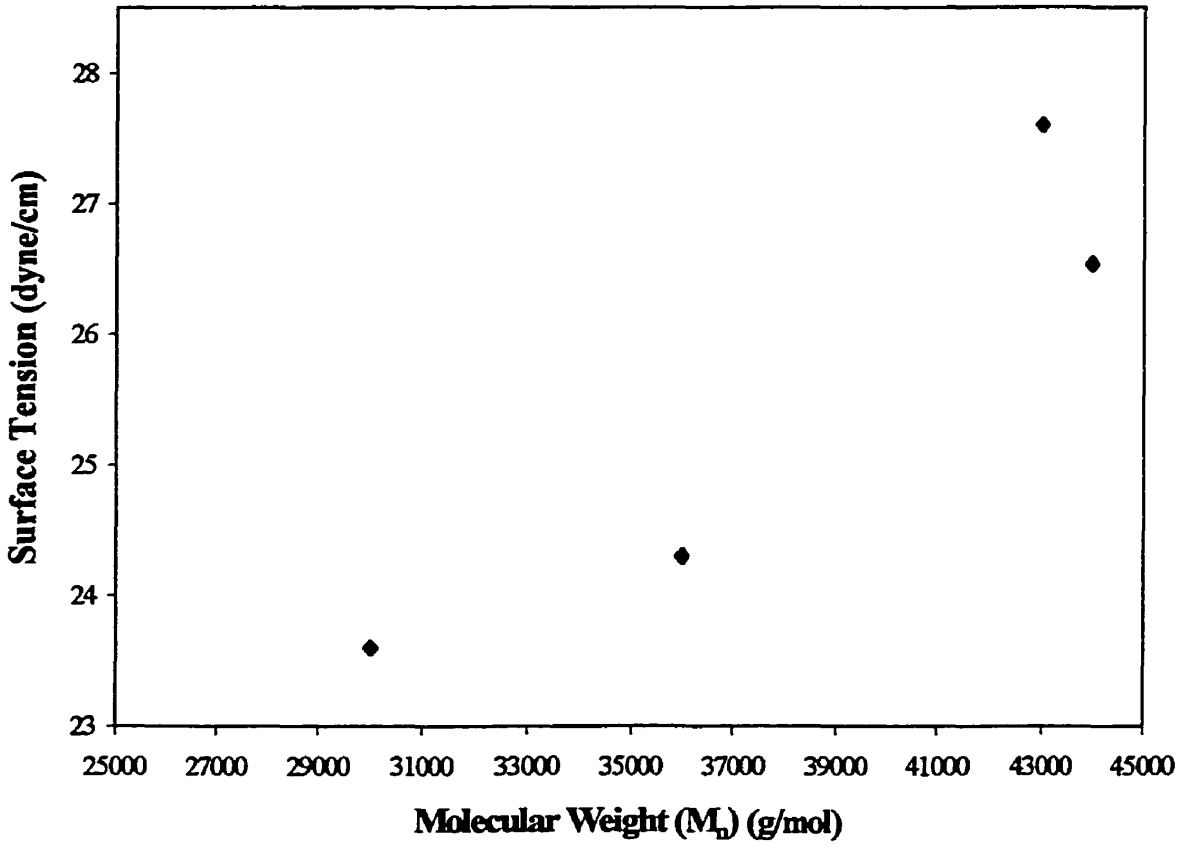


Fig. 4.2: Surface tension vs. number average molecular weight for LLDPE hexene copolymer series.

To explain the apparent contradiction, the effect of the short chain branches on the surface tension of the LLDPE copolymers must be examined in detail. For a branched molecule,

the free volume and properties of a branched end are comparable to those associated with a chain end because both terminal structures have additional volume dependent degrees of freedom. A bulk polymer property, such as surface tension, is now directly proportional to the total concentration of free ends, which includes branched and chain ends. The number of free ends can no longer be incorporated into the constant $k$, from equation (3-9). Therefore, the molecular weight term in equation (3-9) is modified:

$$\gamma = \gamma_\infty - \frac{k}{(M_n)_{eff}} \tag{4-1}$$

where $(M_n)_{eff}$ is the effective molecular weight and is equal to the number average molecular weight, $M_n$, divided by the total number of free ends, $(n+2)$:

$$(M_n)_{eff} = \frac{M_n}{(n+2)} \tag{4-2}$$

where $n$ corresponds to the number of chain branches. It is difficult to assign a physical meaning to the effective molecular weight that is universally applicable. For branched molecules with large molecular weights or high branching densities, the number of branched ends is much larger than the number of chain ends, $n>>2$. In this case, the effective molecular weight, $M_n/n$, is a measure of the branching density. At lower molecular weights or lower branching densities, the effect of the chain ends is not negligible and the effective molecular weight is affected by the number average molecular weight. Equation (4-1) is similar to that reported by Carriere and Silvis[68], except they defined the effective molecular weight as the number average molecular weight between branch points and did not account for the effect of the two main chain ends, which was negligible for the they polymers studied. Note that equation (4-1) reduces to equation (3-9) for the special case of a linear molecule with no chain branches, i.e. $n=0$. The surface tension of the LLDPE hexene copolymer resins are plotted as a function of $M_n^{-1}$ and $(M_n^{-1})_{eff}$ respectively to determine if the effective molecular weight is able to describe the surface tension of a branched polymer and compare it to the results obtained with the number average molecular weight.

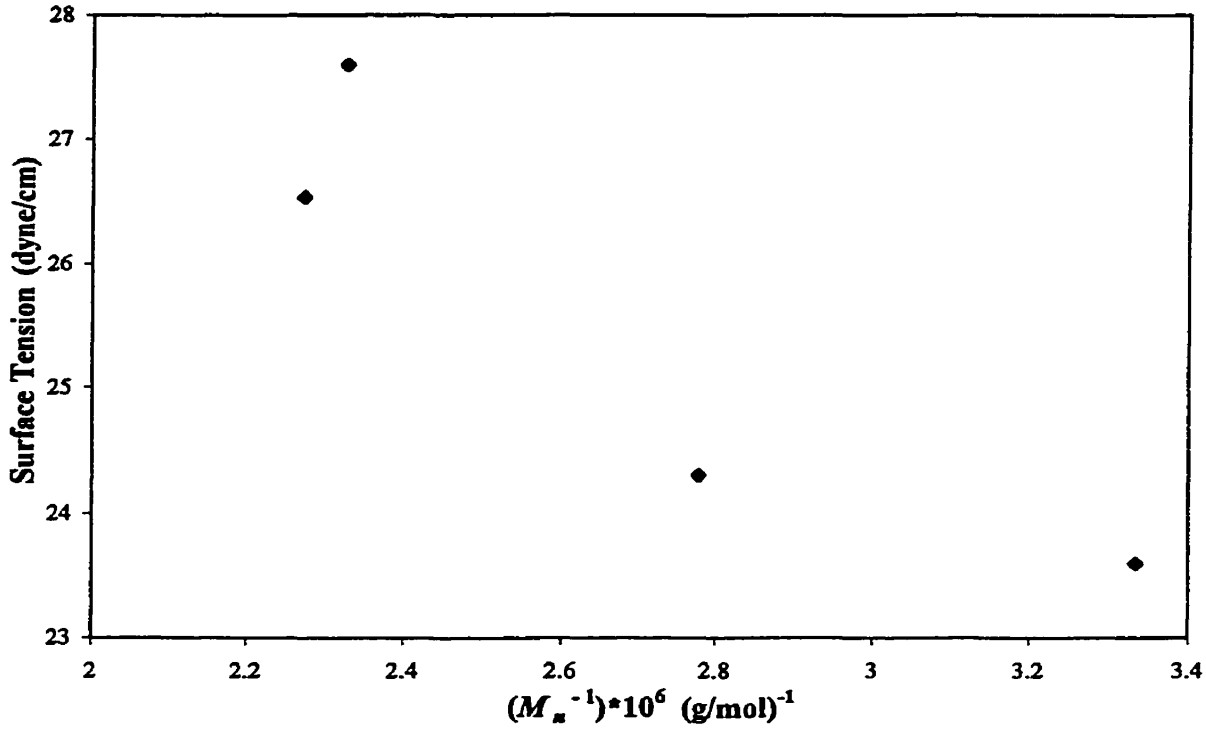


Fig. 4.3: Surface Tension as function of the inverse of number average molecular weight for LLDPE hexene copolymer series.

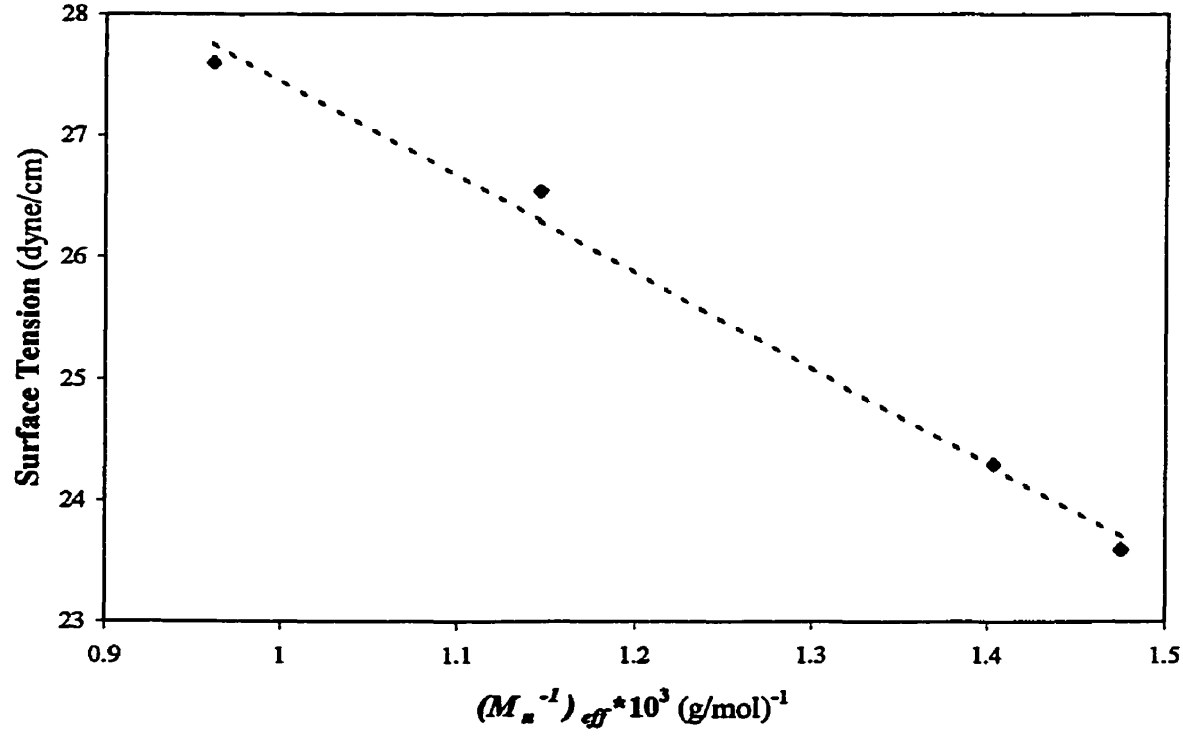


Fig. 4.4: Surface Tension as a function of the effective molecular weight for LLDPE hexene copolymer series. Dashed line represents the best fit of the data to equation (4-1).

The improved fit of the data in Fig. 4.4 indicates that the surface tension of the LLDPE 1-hexene copolymers depends on the inverse of the effective molecular weight, $(M_n^{-1})_{eff}$, rather than the inverse of the molecular weight itself. The standard form of equation (3-9) does not accurately describe the surface tension of a branched polymer because it does not account for the effect of the branched ends. It was impossible to accurately determine the exact dependence of surface tension on effective molecular weight, due to the small number of data points and the limited range of effective molecular weight spanned by the points. In fact, an adequate fit to the data is obtained with almost any power $z$, such that, $(Mn)_{eff}^{-z}$.

Clearly, the surface tension of the LLDPE copolymers is related to the effective molecular weight, although, the differences in surface tension cannot be attributed to changes in the density of the copolymers, as Dee and Sauer[40] have shown to be true for some linear polymers. It is not known exactly how the changes in effective molecular weight affect the surface tension. It is theorized that the surface tension of the free ends is smaller than the surface tension of the main-chain units. If this were true, the large number of free ends in an LLDPE copolymer molecule could cause large differences in the value of surface tension.

## 4.3) POLYDISPERSITY

Another factor which could influence the surface tension of the LLDPE hexene copolymer melts is the polydispersity index, *PD*. Table 4.2 shows the polydispersities of the LLDPE hexene copolymers and Fig. 4.5 shows the values of surface tension as a function of polydispersity.

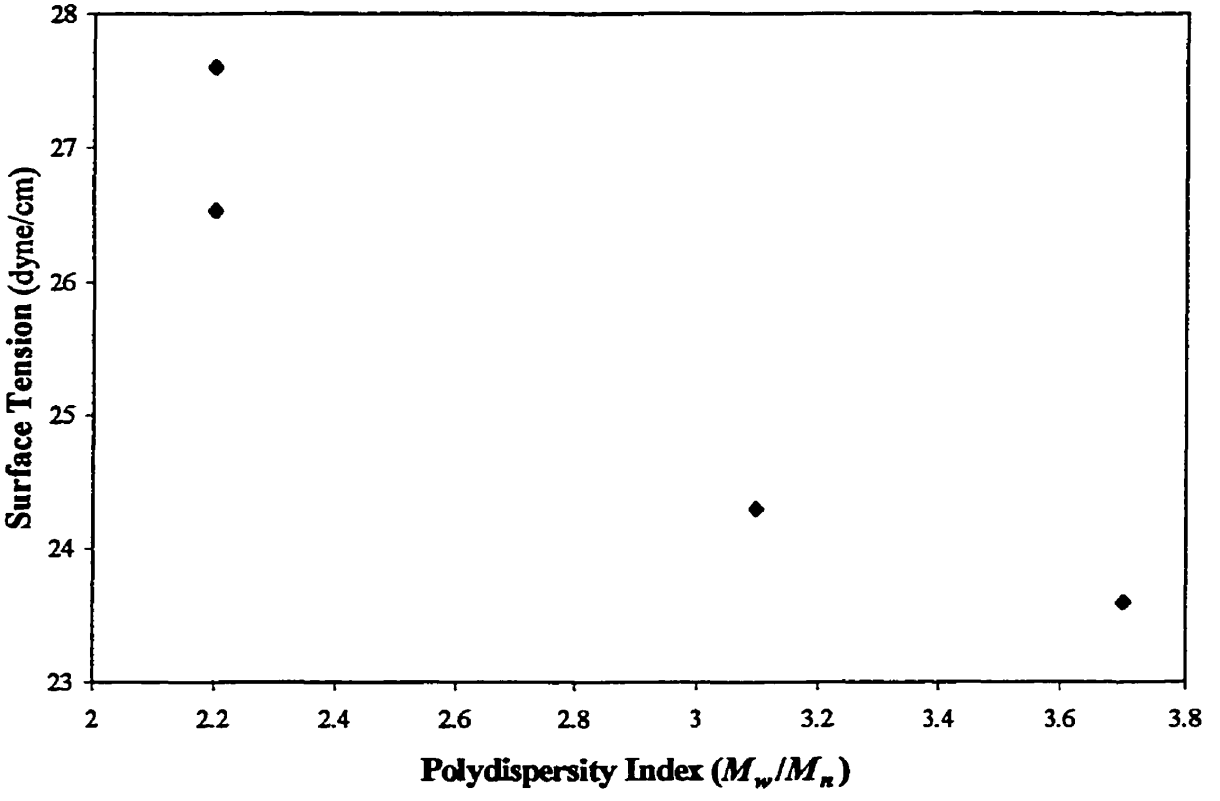


Fig. 4.5 Surface tension vs. polydispersity index of LLDPE hexene copolymer series.

Fig. 4.5 appears to imply that the surface tension decreases with an increase in polydispersity. However, a more plausible explanation is that the effect of polydispersity on surface tension is confounded with the effects of molecular weight. The effective molecular weight does not account for the polydispersity of the resin. If the effects of polydispersity were significant, the surface tension of the resins would be affected unequally, as there is a considerable difference in polydispersity between the hexene copolymers and equation (4-1) would be unable to accurately describe the surface tension of the resins. However, the effective molecular weight did account for the differences in surface tension of the LLDPE hexene resins, so it is assumed that the effects of polydispersity are negligible.

It is also important to consider how polydispersity affects the surface tension. The main factor in determining the free volume per chain segment of a large branched molecule is not its molecular weight, but rather its branching density. Metallocene catalysts produce polymer chains with low polydispersity indices and uniform chain branching, so the effects of polydispersity should be negligible. Ziegler-Natta catalysts, on the other hand, produce polymers with high polydispersity indices and non-uniform chain branching[76-77] which produces smaller chains with a much higher branching density than the larger chains[76]. This results in a large number of low effective molecular weight polymer chains. Thus, it is more likely that LLDPE copolymers produced with Z-N catalysts would exhibit a reduced surface tension due to the effect polydispersity. The only polymer produced with a Z-N catalyst from the hexene copolymer series is resin *A*. Two of the four LLDPE hexene copolymers are metallocene resins so their values of surface tension should not be affected by polydispersity. Although it cannot be determined with certainty what effect the polydispersity has on the surface tension of resin *A* and *C*, the hexene copolymers produced with a Z-N catalyst, the fact that they do not deviate from the $(M_n^{-1})_{eff}$ dependence followed by the other metallocene resins implies that the effect is minimal, if any.

## 4.4) SURFACE TENSION OF BUTENE AND OCTENE COPOLYMERS

Of the ten LLDPE copolymers studied, two samples contain the 1-butene comonomer and three samples contain the 1-octene comonomer (Table 4.2). For the LLDPE butene series, the surface tension increases with effective molecular weight and both resins have similar polydispersity indices. For the octene series, there is a large difference in surface tension between resins *G* and *J*. Both resins have similar effective molecular weights, due to identical branching densities, but resin *G* has a much lower surface tension. The difference in surface tension is thought to be due to the difference in polydispersity between the two resins. Resin *J* has the lowest polydispersity of all the samples and was produced with a metallocene catalyst. Resin *G* has the highest

polydispersity of all the samples, almost 3.5 times greater than sample *J*, and it was produced with a Ziegler-Natta catalyst.

A reasonable question would be: why did the polydispersity seem to have no effect on the surface tension of resin *A* and *C*, which were also produced with a Z-N catalyst, while significantly reducing the surface tension of resin *J*? First, sample *J* has a number average molecular weight that is roughly half of sample *A* and at 17000 g/mol, it is the lowest of all the samples. Sample *J* also has a higher polydispersity (almost double) that results in a broader molecular weight distribution. When all the factors are taken into consideration, sample *J* should have a much larger proportion of shorter chains with higher branching densities in comparison to the low effective molecular weight fraction of sample *A*. This could explain why a large decrease in surface tension was noted for sample *G* but not for sample *A* or *C*.

## 4.5) EFFECT OF α-OLEFIN LENGTH

The effect of the length of the α-olefin comonomer on the surface tension of the LLDPE copolymer is determined by observing differences in surface tension between the 1-butene, 1-hexene and 1-octene LLDPE copolymers. It is difficult to make any conclusions regarding the effect of the copolymer length due to the small amount of data available, but an attempt will be made to discuss certain aspects qualitatively. Fig. 4.6 and 4.7 show the surface tension of all the LLDPE copolymer resins as a function of the effective molecular weight and the inverse of the effective molecular weight respectively. Sample *G* will be omitted from the discussion, as the effects of polydispersity reduced its surface tension. The surface tension of each of the α-olefin LLDPE copolymer series, in relation to the inverse of effective molecular weight, lies along a separate curve. Accordingly, each series is characterized by a different set of constants, $k$ and $\gamma_\infty$, from equation (4-1) (Table 4.4). Within the range of effective molecular weight where data are available from all the α-olefin samples, 500-850 g/mol, the surface tension of both the butene and the octene copolymers is larger than the surface tension of the hexene copolymers. Both $k$ and $\gamma_\infty$ decrease significantly as the length of the α-olefin comonomer

is increased (Table 4.4), although the slopes of both the butene and octene series cannot be established with a large degree of confidence.

The differences in surface tension among the α-olefin series are probably due in part to differences in the polydispersity of the resins. The butene copolymers are of a relatively high polydispersity, ~4.5, and were produced with Z-N catalysts, so the values of surface tension may have been reduced. Therefore, it is difficult to make a distinction among the surface tension of the octene and butene series. However, it can be stated that the surface tension of the butene series is larger than that of the hexene series. The differences noted in the constants $k$ and $\gamma_\infty$ for the butene series could also have been influenced by the effects of polydispersity.

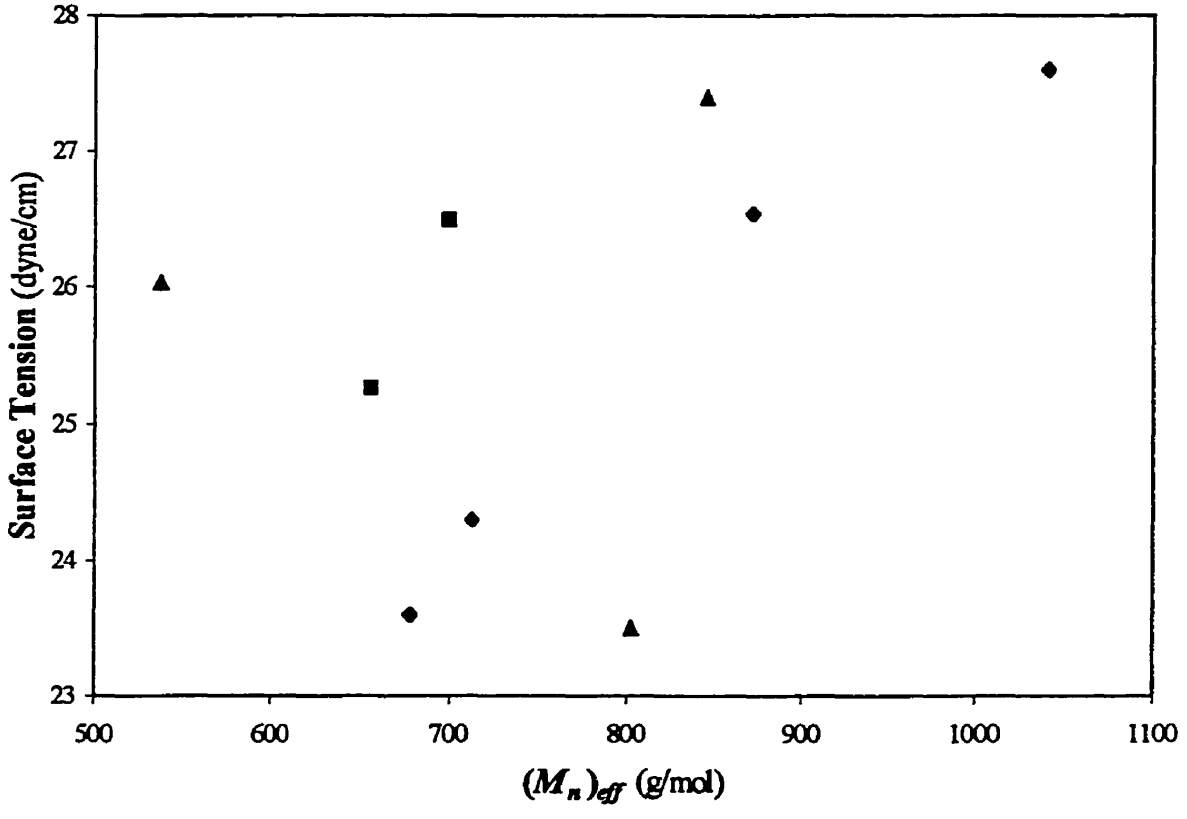


Fig. 4.6: Surface Tension vs. effective molecular weight for LLDPE α-olefin copolymer resins. α-olefin copolymer: ■: Butene, ◆: Hexene, ▲: Octene

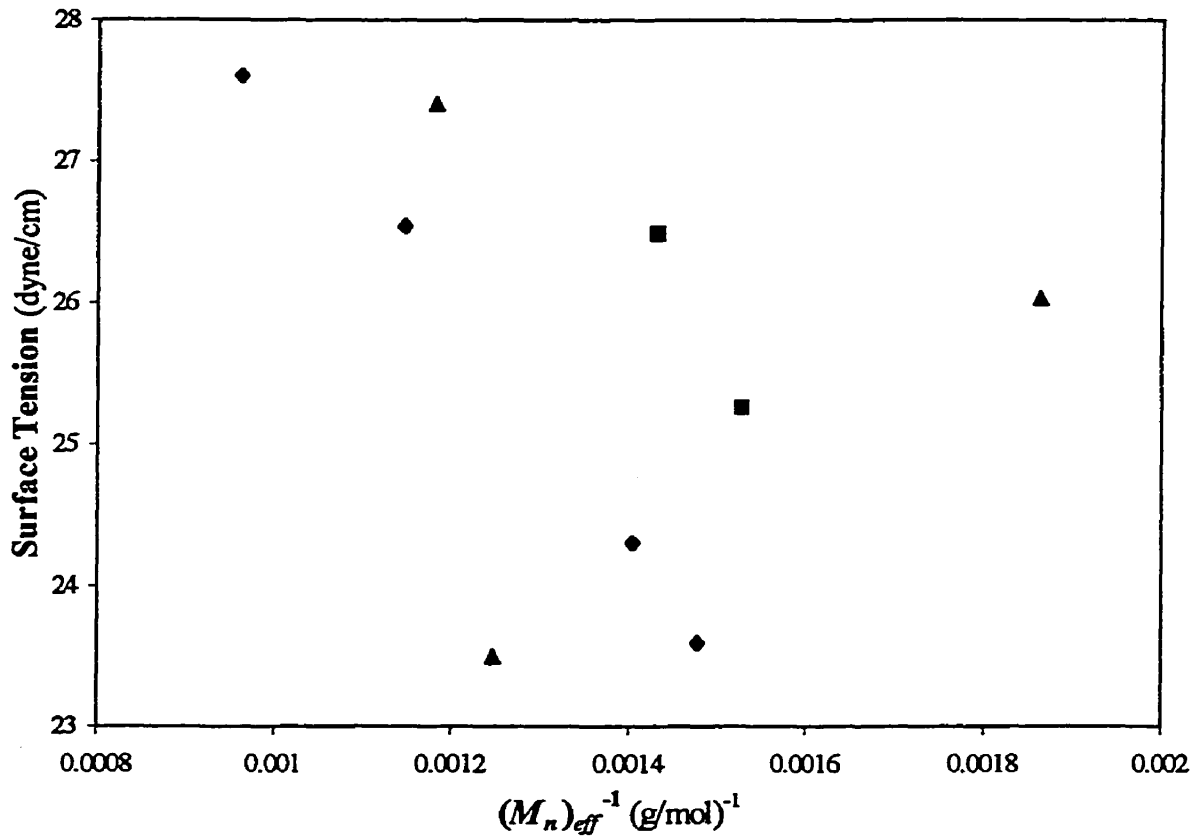


Fig. 4.7: Surface Tension vs. inverse of effective molecular weight for LLDPE α-olefin copolymer resins. α-olefin copolymer: ■: Butene, ◆: Hexene, ▲: Octene

It was theorized that the differences in surface tension among the LLDPE α-olefin copolymers could be partially due to differences in the density. However, the largest density difference between the resins is only about 1% (Table 2), which would not affect the value of surface tension significantly. If the effect of the α-olefin comonomer length on surface tension is not enthalpic, it may be an entropic effect that is related to the free ends of the short chain branches. It is possible that the properties of a branched end could vary significantly depending on the length of the branch, which would affect the value of surface tension. In theory, this would also change the value of the constant $k$ in equation (3-9), by changing the values of $v_e$ and $\gamma_e$. It should be stressed however, that this is only a theory and there is no direct experimental evidence that supports it.

| Resin | Comonomer | $M_n$ | $(M_n)_{eff}$ | $(M_n)_{eff}^{-1}$ | Surface Tension (dyne/cm) | Constants |
|---|---|---|---|---|---|---|
| B | But | 24200 | 656 | 0.00153 | 25.3 | $k$=-12906 |
| | But | 24900 | 699 | 0.00143 | 26.5 | $\gamma_\infty$=45.0 |
| | | | | | | |
| A | Hex | 30000 | 678 | 0.00148 | 23.6 | $k$=-7980 |
| C | Hex | 36000 | 713 | 0.00140 | 24.3 | $\gamma_\infty$=35.6 |
| D | Hex | 44000 | 872 | 0.00115 | 26.5 | |
| E | Hex | 43000 | 1041 | 0.00096 | 27.6 | |
| | | | | | | |
| G | Oct | 17000 | 802 | 0.00125 | 23.5 | $k$=-2010 |
| I | Oct | 22000 | 537 | 0.00186 | 26.0 | $\gamma_\infty$=29.8 |
| J | Oct | 38000 | 847 | 0.00118 | 27.4 | |
| | | | | | | |
| Literature | Prop | 7000 | 219 | 0.00457 | 25.4 | $k$=-1050 |
| Literature | Prop | 2000 | 250 | 0.00400 | 26.0 | $\gamma_\infty$=30.1 |

Table 4.4: Table of constants k and $\gamma_\infty$ used to fit the effective molecular weights and surface tensions to the relation $\gamma=\gamma_\infty-k/(M_n)_{eff}$. Literature values obtained from Dettre and Johnson[34] .

## 4.6) FREE VOLUME

The relation established between the surface tension and effective molecular weight for the LLDPE hexene copolymer series in Fig. 4.4 suggests that the surface tension depends on the number of branched ends. Free ends have a larger free volume than main-chain structural units due to their additional degrees of freedom. If the free volume of the LLDPE copolymers could be assessed independently of their surface tensions, the data could provide corroboration of the theorized relationship between surface tension and the concentration of branched ends.

Flory[73] proposed a model to determine the free volume of macromolecules which states that the free volume is a function of the thermal expansion coefficient of the liquid and the absolute temperature. The model accurately reflects the definition of free volume,

which is the expansion volume generated by thermal motion. Fig. 4.8 shows the relation between surface tension and the thermal expansion coefficients of the LLDPE copolymers.

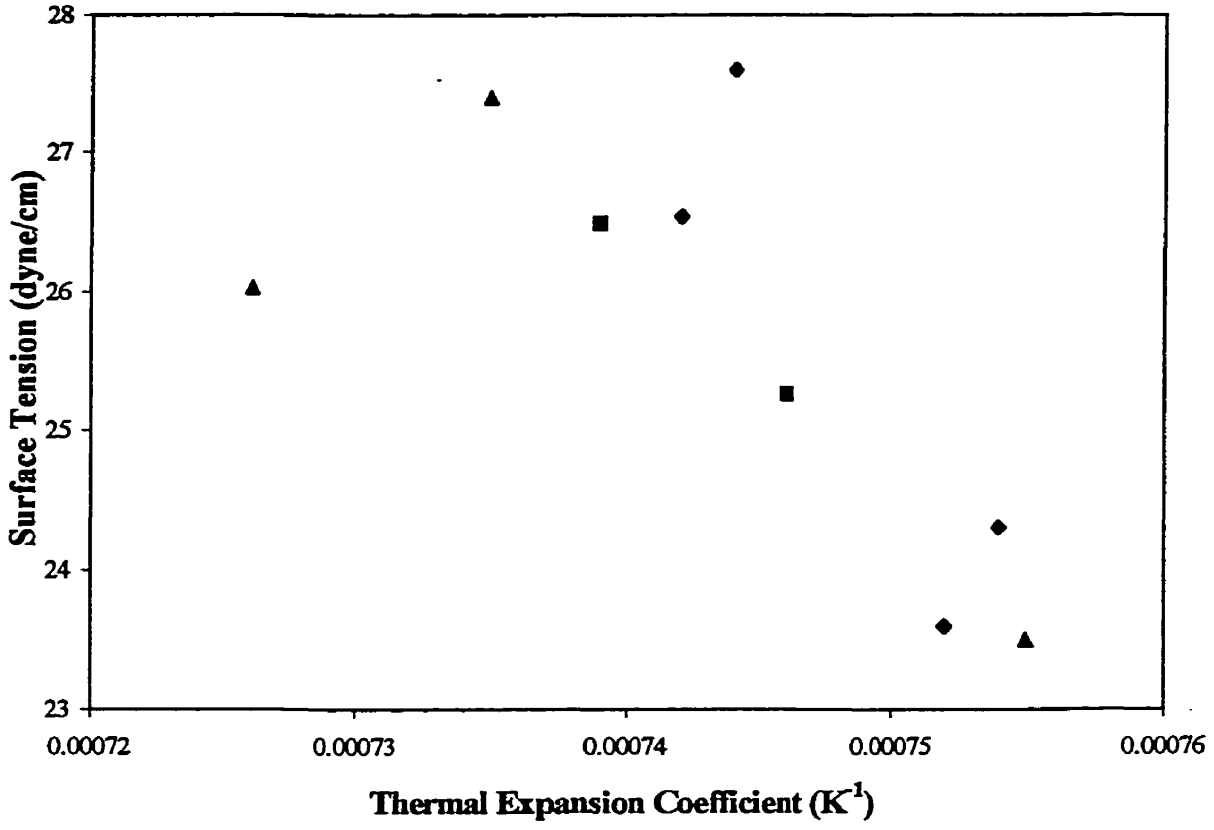


Fig. 4.8: Surface tension of LLDPE resins at 160 °C as function of thermal expansion coefficient

In Fig. 4.8, there appears to be a linearly decreasing relationship between the surface tension of the LLDPE resins and their thermal expansion coefficients, with the exception of two outlying points. It is not known what caused the deviation of the two points in Fig. 4.8, although it is interesting to point out that they represent the resins with the lowest and highest branching densities, resins *E* and *I* respectively. The rest of the data appear to support the theory that the differences in surface tension between the LLDPE copolymer resins are related to the concentration of the branched ends.

## 4.7) COMPARING VALUES OF SURFACE TENSION W/ LITERATURE

It has been shown that the effective molecular weight characterizes the surface tension of the LLDPE hexene copolymers (Fig. 4.4). The data of Dettre and Johnson[63] (Table 3.1) was reexamined to determine if the effective molecular weight could account for differences in the surface tension of the branched PE resins. Dettre and Johnson[63] only provided the number average molecular weight for two of the five branched PE resins studied so it could not be determined if the surface tension was a strict function of the effective molecular weight. However, the concept of effective molecular weight can be used to explain trends in the literature data. The surface tension decreases with increasing branching density for all of the samples except for $B^*$ and $C^*$. The surface tension of $B^*$ is lower than $C^*$ because the effect of the main chain ends is not negligible at the low number average molecular weights of the samples.

The range of values of surface tension for the LLDPE copolymers employed in this study (23.5-27.9) compares well with the range of literature values for methyl-branched PE (22.5-27.6) measured by Dettre and Johnson[63], at the same temperature. However, the samples used by Dettre and Johnson[63] had higher branching densities than the LLDPE copolymers, which resulted in lower effective molecular weights. It was noted previously that each of the LLDPE α-olefin series (butene, hexene and octene) had significantly different $\gamma$ vs. $(M_n)_{eff}$ relationships (Fig. 4.6, 4.7 and Table 4.4). Thus, it is not surprising that the branched PE resins tested by Dettre and Johnson[63], which all contain methyl branches, also have a different relationship with effective molecular weight.

The values of surface tension of LLDPE have been shown to be comparable to literature values of branched PE. However, they have not been compared to the values of surface tension of linear PE. To determine if the surface tension of a branched polymer is lower than that of a linear polymer, a comparison must be made between molecules of equal molecular weight. The question is: which molecular weight should be used as a basis for comparison, effective or number average molecular weight? To compare a branched and linear polymer, the comparison should be made on an effective molecular weight basis to account for the effect of the branched ends.

The effective molecular weight of the LLDPE resins ranges from 600~1100 g/mol. According to equation (4-2), the surface tension of the LLDPE copolymers should be compared to the surface tension of linear PE with a molecular weight ranging from 1200~2200 g/mol. Literature data for the surface tension of linear PE was taken from Dee and Sauer[40] and Wu[10]. The major difference between the two data sets is the value of surface tension at infinite molecular weight. At 150 °C, Wu[10] quotes a value of 29.4 dyne/cm while Dee and Sauer[40] have measured ~26.7 dyne/cm. Therefore, two separate data sets will be used to characterize the effect of molecular weight on the surface tension of linear PE. Both data sets use the data of Dee and Sauer[40] to determine the value of the constant $k$. The first data set will use $\gamma_\infty$, as determined by Dee and Sauer[40] and the second data set will use $\gamma_\infty$, as determined by Wu[10]. The surface tension of the LLDPE resins will be compared to the surface tension of linear PE determined from the two data sets described above, using both effective molecular weight and number average molecular weight, since there is no conclusive proof which is the correct basis for comparison.

The results of the comparison between the values of surface tension of the linear PE and the LLDPE copolymer are listed in Table 4.5. For the first data set, the values predicted with the absolute number average molecular weight appear to be closer to the values of surface tension of the LLDPE resins. For the second data set, the values of surface tension of the linear PE of equal effective molecular weight are comparable to the surface tension of the LLDPE resins, while the values of surface tension of the linear PE of equal molecular weight are clearly larger. The range of surface tension of the LLDPE copolymers is much larger than the corresponding range for linear PE, due to larger values of the constant $k$. From the data available, it cannot be stated conclusively that the surface tension of a branched polymer is smaller than the surface tension of a linear polymer of equal molecular weight. Also, it cannot be stated conclusively whether linear and branched polymers should be compared on a number average molecular weight or effective molecular weight basis due to inconsistencies in the literature data.

| Resin | Comonomer | $M_n$ | $(M_n)_{eff}$ | $\gamma_{exp}$ | $\gamma=f(M_n)$ (method 1) | $\gamma=f(M_n)_{eff}$ (method 1) | $\gamma=f(M_n)$ (method 2) | $\gamma=f(M_n)_{eff}$ (method 2) |
|---|---|---|---|---|---|---|---|---|
| **B** | But | 24200 | 656 | 25.3 | 26.1 | 24.4 | 28.1 | 26.4 |
| **H** | But | 24900 | 699 | 26.5 | 26.1 | 24.6 | 28.1 | 26.6 |
| | | | | | | | | |
| **A** | Hex | 30000 | 678 | 23.6 | 26.1 | 24.5 | 28.1 | 26.5 |
| **C** | Hex | 36000 | 713 | 24.3 | 26.1 | 24.6 | 28.1 | 26.6 |
| **D** | Hex | 44000 | 872 | 26.5 | 26.1 | 24.9 | 28.1 | 26.9 |
| **E** | Hex | 43000 | 1041 | 27.6 | 26.1 | 25.1 | 28.1 | 27.1 |
| | | | | | | | | |
| **G** | Oct | 17000 | 802 | 23.5 | 26.0 | 24.8 | 28.0 | 26.8 |
| **I** | Oct | 22000 | 537 | 26.0 | 26.1 | 24.1 | 28.1 | 26.1 |
| **J** | Oct | 38000 | 847 | 27.4 | 26.1 | 24.8 | 28.1 | 26.8 |
| | | | | | | | | |
| **Literature** | Prop | 7000 | 219 | 25.3 | 25.8 | 21.0 | 27.8 | 23.0 |
| **Literature** | Prop | 2000 | 250 | 25.9 | 25.0 | 21.7 | 27.0 | 23.7 |

Table 4.5: Comparison of experimental values of surface tension of LLDPE ($\gamma_{exp}$) to the surface tension of linear PE of equal number average molecular weight $M_n$ and equal effective molecular weight $(M_n)_{eff}$. The surface tension of the last four columns are calculated from the following equations $\gamma=f(M_n)$: $\gamma=\gamma_\infty - k/M_n$ $\gamma=f(M_n)_{eff}$: $\gamma=\gamma_\infty - k/(M_n)_{eff}$. Method 1: $k$=2249.5 $\gamma_\infty$=26.16 (data from Dee and Sauer). Method 2: $k$=2249.5 $\gamma_\infty$=28.16 (data from Wu). Calculations for 160 °C

## 4.8) SURFACE TENSION TEMPERATURE COEFFICIENTS

The surface tension temperature coefficients of the LLDPE resins *A*, *E*, *G*, *I* and *J*, listed in table 4.6, were determined for the temperature range 160-200 °C from a minimum of three points. It was theorized in section 4.3 that the smaller effective molecular weight fractions migrated to the surface and reduced the surface tension of sample *G* by increasing the ratio of the free volume at the surface to the free volume in the bulk. Theoretically, this should increase the entropy of surface formation and the surface tension temperature coefficient (Equation 3-6 and 3-11). Thus, if the effects of polydispersity reduced the surface tension of a polymer, it would be expected that the resin would have a higher surface tension temperature coefficient. However, the difference in the experimentally determined surface tension temperature coefficients was not statistically significant, so the free volume effect could not be confirmed.

## 4.9) COMPARING VALUES OF SURFACE TENSION TEMPERATURE COEFFICIENTS W/ LITERATURE

There is considerable variation among the reported values of surface tension temperature coefficients for branched PE. Wu[10], Roe[12] and Dettre and Johnson[63] all obtained different values of $-d\gamma/dT$, 0.067, 0.064 and 0.06 dyne/cm/°C for the exact same methyl-branched PE (DuPont Alathon 7050). In addition, Schonhorn and Sharpe[79] obtained a much higher value of $-d\gamma/dT$, 0.076 dyne/cm/°C, for a similar resin. The surface tension temperature coefficients of the LLDPE resins compare well with the literature values of branched PE. The LLDPE resins and the branched PE resins tested by other researchers have similar effective molecular weights. As a result, it was expected that they would have similar temperature coefficients. The polydispersities of the resins were not published, so it was not possible to determine if it affected the surface tension temperature coefficients.

Dee and Sauer[56,69] have shown that the surface tension temperature coefficient decreases as the molecular weight of a macromolecule increases. It has been noted that the temperature coefficients of branched PE are larger than those of linear PE, but these comparisons are often inaccurate as they are between samples of different molecular weight. Therefore, similar to the comparison made previously with the values surface tension, the surface tension temperature coefficients of the LLDPE copolymers will be compared to literature values of surface tension temperature coefficients for linear PE of equal molecular weight and equal effective molecular weight to determine if a difference exists.

The data of Dee and Sauer[40] and Wu[10] were used to determine the effect of molecular weight on the surface tension temperature coefficient of linear polyethylene. There is a disparity between the data point at infinite molecular weight quoted by Wu[10] (■) and the data points for the two largest molecular weights obtained by Dee and Sauer (◆) (Fig. 4.9). Therefore, it was decided to use two separate data series: Fit 1: data of Dee and Sauer[40] (◆), Fit 2: data point of Wu[10] (■) and the three lowest molecular weight data points of Dee and Sauer[40] (◆). The data sets were fit to the following equation that is valid for linear polymers:

$$\frac{d\gamma}{dT}=\left(\frac{d\gamma}{dT}\right)_{\infty}-\frac{k}{M_n} \qquad (4\text{-}3)$$

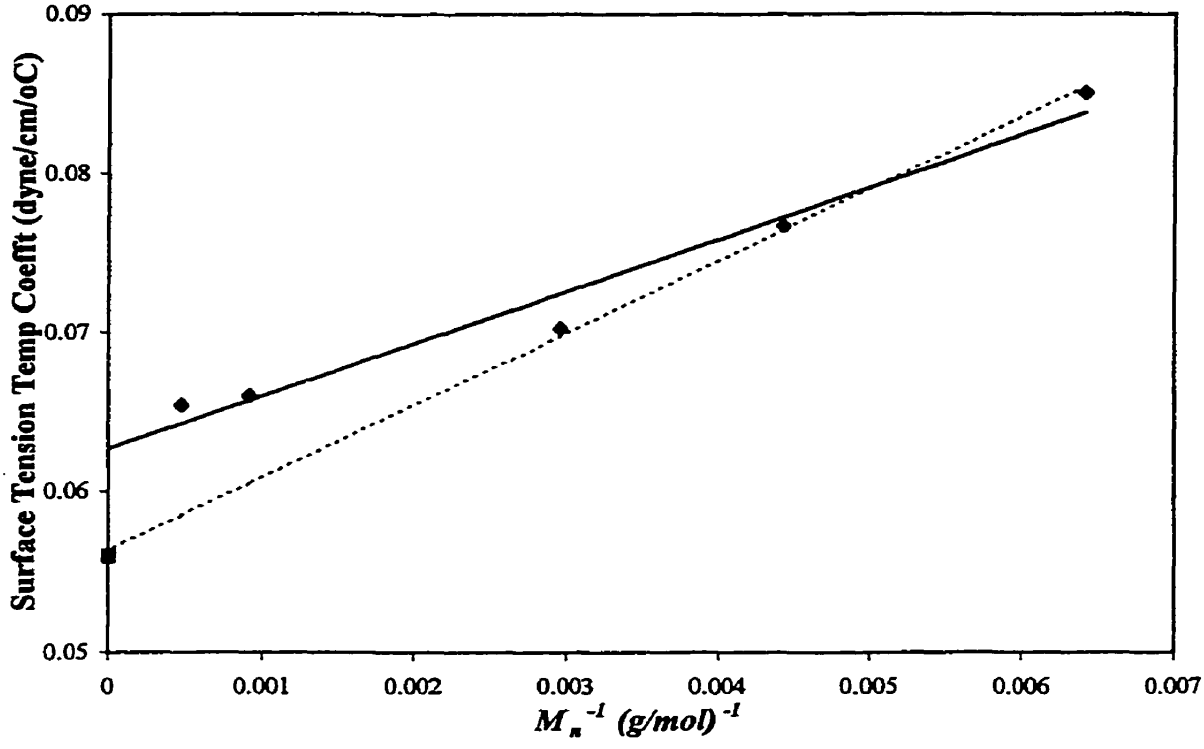


Fig. 4.9: Surface tension temperature coefficients ($-d\gamma/dT$) of linear PE as a function of the inverse of number average molecular weight. Data source: ■: Wu[10], ◆: Dee and Sauer[41]. Two lines represent two different fits to the combined data set. Dashed line: $k$=0.0564, $(-d\gamma/dT)_\infty$=4.55. Solid Line: $k$=0.0627, $(-d\gamma/dT)_\infty$=3.286

The values of $-d\gamma/dT$ predicted from the data of Dee and Sauer[40] (fit 1) appear to match the experimental surface tension temperature coefficients of the LLDPE copolymers more closely than the values of $-d\gamma/dT$ predicted from the combined data set of Dee and Sauer[40] and Wu[10] (fit 2). The surface tension temperature coefficients of the LLDPE resins compare reasonably well with the $-d\gamma/dT$ of the linear polymers calculated by fit 1 for both $M_n$ and $(M_n)_{eff}$. From the data available, it cannot be conclusively stated that the surface tension temperature coefficient of a branched polymer is any different than that of a linear polymer, when compared on either molecular weight basis.

| Resin | Comonomer | $M_n$ (g/mol) | $(M_n)_{eff}$ (g/mol) | $(-d\gamma/dT)_{exp}$ (dyne/cm/°C) | $-d\gamma/dT$ (fit 1, $(M_n)_{eff}$) | $-d\gamma/dT$ (fit 1, $M_n$) | $-d\gamma/dT$ (fit2, $(M_n)_{eff}$) | $-d\gamma/dT$ (fit 2, $M_n$) |
|---|---|---|---|---|---|---|---|---|
| **B** | But | 24200 | 656 | | 0.065 | 0.063 | 0.060 | 0.057 |
| **H** | But | 24900 | 699 | | 0.065 | 0.063 | 0.060 | 0.057 |
| | | | | | | | | |
| **A** | Hex | 30000 | 678 | 0.071 | 0.065 | 0.063 | 0.060 | 0.057 |
| **C** | Hex | 36000 | 713 | | 0.065 | 0.063 | 0.060 | 0.056 |
| **D** | Hex | 44000 | 872 | | 0.065 | 0.063 | 0.059 | 0.056 |
| **E** | Hex | 43000 | 1041 | 0.068 | 0.064 | 0.063 | 0.059 | 0.056 |
| | | | | | | | | |
| **G** | Oct | 17000 | 802 | 0.077 | 0.065 | 0.063 | 0.059 | 0.057 |
| **I** | Oct | 22000 | 537 | 0.07 | 0.066 | 0.063 | 0.061 | 0.057 |
| **J** | Oct | 38000 | 847 | 0.068 | 0.065 | 0.063 | 0.059 | 0.056 |
| | | | | | | | | |
| **Literature**[10] | Prop | 7000 | 219 | 0.067 | 0.070 | 0.063 | 0.067 | 0.057 |
| **Literature**[54] | Prop | 2000 | 250 | 0.06 | 0.069 | 0.064 | 0.065 | 0.059 |

Table 4.6: Comparison of experimental values of surface tension temperature coefficient of LLDPE $(-d\gamma/dT)_{exp}$ to the surface tension temperature coefficients of linear PE of equal number average molecular weight $M_n$ and equal effective molecular weight $(M_n)_{eff}$. The $(-d\gamma/dT)$ of the last four columns are calculated from the following equations $d\gamma/dT=f(M_n)$: $d\gamma/dT=(d\gamma/dT)_\infty - k/M_n$, $\gamma=f(M_n)_{eff}$: $d\gamma/dT=(d\gamma/dT)_\infty - k/(M_n)_{eff}$. Fit 1: $k$=0.0627, $(-d\gamma/dT)_\infty$=3.286, Fit 2: $k$=0.0564, $(-d\gamma/dT)_\infty$=4.55. Literature values from Wu[10] and Dettre and Johnson[54].

## 4.10) INTERFACIAL TENSION & INTERFACIAL TENSION TEMPERATURE COEFFICIENTS

The values of interfacial tension for the LLDPE *A*/PS, LLDPE *E*/PS and HDPE/PS were all similar and in general agreement with the literature (Table 4.7). Note that the interfacial tension of LLDPE *E*/PS is larger than the interfacial tension of LLDPE *A*/PS. This occurs because the interfacial tension of a polymer-polymer melt is a direct function of the surface tension of the individual components and the surface tension of LLDPE *E* is greater than that of LLDPE *A*.

The interfacial tension temperature coefficients of the LLDPE *A*/PS and LLDPE *E* /PS were both similar, however, their values were smaller than the corresponding literature values by a factor of 1.5-2. It is not known why the experimental interfacial tension temperature coefficients are lower than those determined by Wu[10]. It was confirmed that the densities of the polymers tested by Wu[10] were similar to the density of the LLDPE and PS resins used for this study. The number average molecular weights of the polymers used by Wu[10] are not known but the viscosity average molecular weights are quite high. This indicates that the molecular weights of the polymers are also relatively high. The molecular weight of the PS is not known but is assumed to be relatively large as the resin has a melt index of 4. Therefore, the molecular weights of the polymers used in this study are either comparable to or lower than those used by Wu. Then the experimental temperature coefficients should have been higher or equal to the literature values, which was not the case.

| Polymer Resins | $\gamma$ 200 °C | $\gamma$ 210 °C | $\gamma$ 220 °C | $-d\gamma/dT$ (dyne/cm/°C) |
|---|---|---|---|---|
| **LLDPE A / PS** | 4.57 | 4.39 | 4.28 | .014 |
| **LLDPE E / PS** | 4.78 | 4.70 | 4.57 | .010 |
| **HDPE / PS** | 4.71 | 4.62 | 4.51 | .012 |
| **LDPE / PS (lit)[10]** | 4.70 | 4.50 | 4.30 | .020 |

Table 4.7: Values of interfacial tension and interfacial tension temperature coefficients. Literature values from Wu[10].

# PART 2

# THE PENDANT DROP METHOD

# 5) BACKGROUND: PENDANT DROP METHOD

## 5.1) METHODS OF MEASURING INTERFACIAL TENSION

A number of different methods are available to measure the interfacial tension of low viscosity liquids. Unfortunately, the high viscosity of polymer melts makes most of these techniques irrelevant. The methods that can measure the interfacial tension of polymer melts can be separated into two categories: equilibrium and dynamic.

The equilibrium methods of determining the interfacial tension are the pendant drop and the spinning drop. Both techniques calculate the interfacial tension from the equilibrium shape of a drop profile.

The pendant drop method is the most widely used and accepted technique to measure the interfacial tension of most liquids, not just polymer melts. The Bashforth and Adams equation[2], derived in 1882, relates the equilibrium pendant drop profile to the interfacial tension. The pendant drop method has improved significantly since its inception, most recently with the use of computers, which simplifies the drop profile analysis and increases the accuracy of the results.

The spinning drop apparatus was developed more recently, by Vonnegut[16] in 1943. Although the spinning drop method has progressed significantly over the last thirty years, further research is needed before it is as widely regarded as the pendant drop method. One of the most troubling difficulties with the spinning drop method is a repeatable difference in the apparent equilibrium value of interfacial tension for some polymers, depending on whether the equilibrium state was approached from larger or smaller drop diameters[17].

The dynamic methods of measuring interfacial tension of polymer melts are based on the transient behaviour of selected phenomena, which varies depending on the method, rather than the observation of an equilibrium state. Two of the most popular dynamic methods are the breaking thread[18] and imbedded fiber retraction[19] techniques. Both relate the transient evolution of the shape of a fluid particle to the interfacial tension.

Another technique is based on inferring the interfacial tension from rheological measurements[20,21].

The dynamic methods of measuring interfacial tension are still in the early stages of development and experimental results are subject to large inaccuracies, often in excess of 10-20%. As such, dynamic methods are unable to reliably characterize the interfacial tension of polymer melts. In this work, the pendant drop apparatus was chosen over the spinning drop apparatus as the method of choice for determining the interfacial tension of polymer melts for two reasons. The pendant drop apparatus is considered to be the more reliable of the two and is generally the method of choice when determining the interfacial tension of polymer melts. In addition, the experimental procedure for the pendant drop apparatus is much simpler.

## 5.2) PENDANT DROP THEORY

The pendant drop method is based on the mechanical equilibrium of the surface and gravitational forces acting on a liquid drop suspended from a syringe in a second immiscible fluid. Tate's Law[21] characterized this relationship and noted that the maximum supported weight of a drop, $W_{max}$, is proportional to the interfacial tension, $\gamma$, and the syringe tip radius, $R$:

$$W_{Max} = 2\pi R\gamma \qquad (5\text{-}1)$$

The Laplace equation[21] relates the interfacial tension of a drop immersed in an immiscible fluid, to the pressure drop, $\Delta P$, across a curved interface.

$$\frac{1}{R_1}+\frac{1}{R_2}=\frac{\Delta P}{\gamma} \qquad (5\text{-}2)$$

The curvature of the pendant drop is specified by two mutually perpendicular radii of curvature $R_1(x,z)$ and $R_2(x,z)$ which vary with $x$ and $z$, the horizontal and vertical position coordinates, as shown in Fig. 5.1. $R_1$ swings in a plane parallel to the page along the drop profile, while $R_2$ swings in a plane perpendicular to the page around the drop profile:

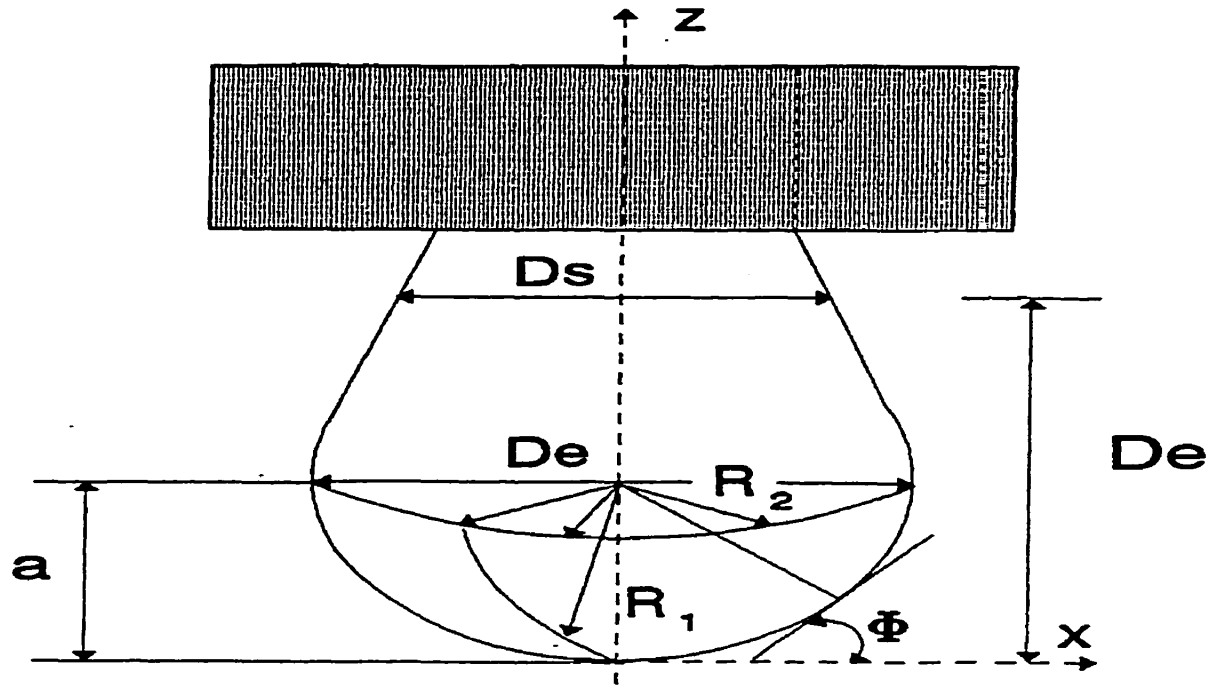


Fig. 5.1: Pendant Drop Geometry. $R_1$: radius of curvature swings in the plane of the page along drop profile. $R_2$: radius of curvature swings in a plane perpendicular to page around the drop profile. $\phi$ is the angle between the horizontal axis and a tangent to the drop profile at position $(x,z)$. $x$ and $z$ are the horizontal and vertical Cartesian coordinates respectively. Other quantities are not relevant.

If $\phi$ is the angle between the horizontal axis and a tangent to the drop profile at position $(x,z)$, then by geometry, the radius of curvature in the plane perpendicular to Fig. 5.1, $R_2$, is given by:

$$R_2 = \frac{x}{\sin\phi} \tag{5-3}$$

The pressure drop across the interface at any vertical position $z$, $\Delta P$, can be expressed as a function of the pressure drop across the interface at the bottom of the drop, $\Delta P_o$, the density difference between the two fluid phases, $\Delta\rho$, the gravity constant, $g$, and the vertical position coordinate, $z$.

$$\Delta P = \Delta P_o + \Delta\rho g z \tag{5-4}$$

At the bottom of the drop, a position also referred to as the drop apex, both radii of curvature are equal to a constant, $a$.

$$R_1 = R_2 = a \tag{5-5}$$

At the drop apex, $z$=0, so from equation (5-4), the pressure drop across the interface, $\Delta P$, is equal to $\Delta P_o$, the pressure drop across the interface at the bottom of the drop.

$$\Delta P = \Delta P_o \tag{5-6}$$

Substituting equations (5-5) and (5-6) into the Laplace equation (5-2) gives an expression for the pressure drop across the interface at the drop apex, $\Delta P_o$, in terms of the interfacial tension, $\gamma$, and the radius of curvature at the drop apex, $a$:

$$\Delta P_o = \frac{2\gamma}{a} \tag{5-7}$$

Equation (5-7) is used to eliminate $\Delta P_o$ from equation (5-4) which describes the pressure drop across the interface, $\Delta P$.

$$\Delta P = \frac{2\gamma}{a} + \Delta\rho g z \tag{5-8}$$

The new expression for $\Delta P$, equation (5-8), and the expression for $R_2$, equation (5-3), are substituted into the Laplace equation (5-2):

$$\frac{1}{R_1} + \frac{\sin\phi}{x} = \frac{2}{a} + \frac{\Delta\rho g z}{\gamma} \tag{5-9}$$

Equation (5-9) is rearranged by multiplying both sides of the equation by $a$, the radius of curvature at the drop apex. This leads to the Bashforth and Adams[2] equation:

$$\frac{1}{\frac{R_1}{a}} + \frac{\sin\phi}{\frac{x}{a}} = B\frac{z}{a} + 2 \tag{5-10}$$

The parameter $B$ is known as the dimensionless shape factor, where $a$ is the radius of curvature at the drop apex, $\Delta\rho$ is the density difference between the two fluid phases, $g$ is the gravitational constant and $\gamma$ is the interfacial tension:

$$B = \frac{a^2 g \Delta\rho}{\gamma} \tag{5-11}$$

The radius of curvature parallel to the page in Fig. 5.1, $R_1$, and the angle between the horizontal axis and a tangent to the drop profile at position $(x,z)$, $\phi$, can be expressed in a Cartesian coordinate system:

$$R_1 = \frac{\left[1+\left(\frac{dz}{dx}\right)^2\right]^{\frac{3}{2}}}{\left(\frac{d^2z}{dx^2}\right)} \tag{5-12}$$

$$\sin\phi = \frac{\frac{dz}{dx}}{\left(1+\left(\frac{dz}{dx}\right)^2\right)^{\frac{1}{2}}} \tag{5-13}$$

The Bashforth and Adams[2] equation is a nonlinear differential equation which relates the shape of the drop profile to the interfacial tension. Note that $R_1$, $x$ and $z$ all appear in the Bashforth and Adams[2] equation as ratios with respect to the radius of curvature at the drop apex, $a$. Thus, a given value for the constant $B$ gives the same drop shape regardless of drop size and changing $a$ influences only the drop size without changing its shape. When changing the size of a drop for a given liquid, both $B$ and $a$ should change to yield the same value of interfacial tension, $\gamma$ (Butler et al.[23]).

## 5.3) EVOLUTION OF THE PENDANT DROP METHOD

In 1882, Bashforth and Adams[2] derived the theoretical form of a sessile or pendant drop and calculated tables of drop contours. The interfacial tension of a pendant drop was determined by matching the experimentally measured drop profile to a theoretical drop contour. However, the visual comparison of drop profiles was time-

consuming, tedious and subjective. Consequently, interfacial tension measurements were subject to large experimental error.

Andreas et al.[28] proposed the following empirical relationship which simplified drop profile analysis:

$$\gamma = \frac{gD_e^2 \Delta\rho}{H(S)} \tag{5-14}$$

where $\Delta\rho$ is the density difference between the two phases, $g$ is the gravitational constant, $H$ is a correction factor related to the diameter ratio of the pendant drop, $S$, which is defined as the ratio of horizontal drop diameter $D_s$ located a distance $D_e$ from the drop vertex, as shown in Fig. 5.2:

$$S = \frac{D_s}{D_e} \tag{5-15}$$

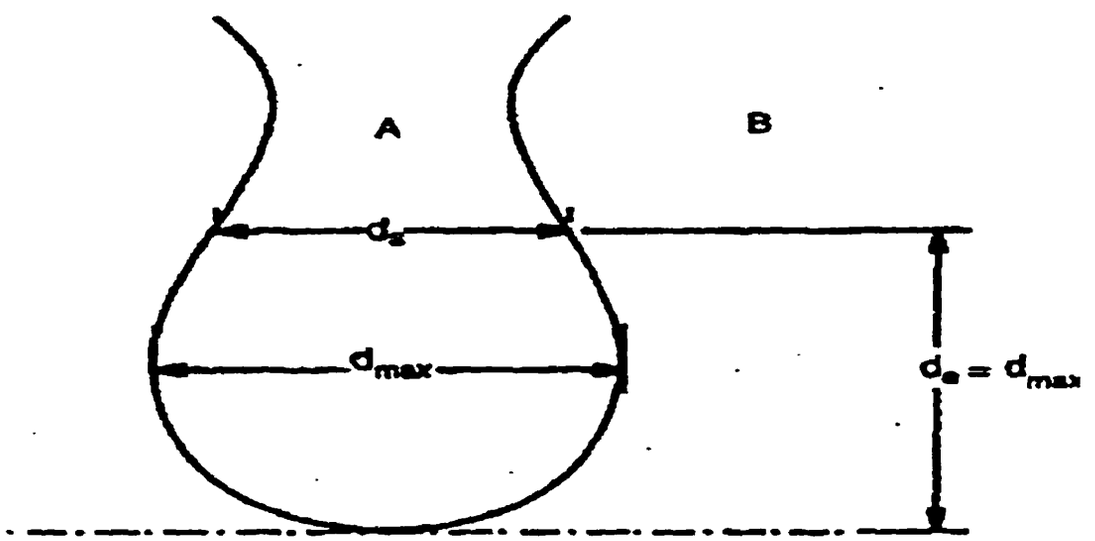


Fig. 5.2: Measurements defining the diameter ratio, $S=D_s/D_e$. $D_e$: Equatorial or maximum horizontal diameter. $D_s$: Horizontal drop diameter located a vertical distance $D_e$ from the drop apex.

Roe et al.[11] determined that interfacial tension measurements, calculated by the method proposed by Andreas et al.[28], were subject to large errors because the entire drop profile had been defined by a single diameter ratio, $S$. Roe et al.[11] improved the accuracy

of interfacial tension measurements by defining the drop profile with a series of diameter ratios, $S_n$:

$$S_n = \frac{D_n}{D_e} \tag{5-16}$$

Although the improved method of calculating the interfacial tension from drop profiles is more accurate, the calculations are still time-consuming, tedious and subject to human error.

Girault et al.[29,30] realized that computer systems, which had recently become affordable, were ideal for determining the interfacial tension from drop profiles. They used a digital camera to capture the image of a pendant drop, which was reduced to a profile by contrast analysis. A computer program was used to calculate the interfacial tension by optimizing the fit between the experimental profile and a numerically generated solution to the Bashforth & Adams[2] equation. Huh and Reed[31] developed an algorithm which independently optimized the fit of the dimensionless shape factor, $B$, and the radius of curvature at the drop apex, $a$. Rotenberg et al.[32] improved on Huh and Reed's[31] algorithm by optimizing five separate parameters, but the program suffered from long computational times and it did not always converge to reasonable solutions. Jennings and Pallas[4] made further improvements to the computer program by reducing the processing time required to calculate the interfacial tension and adding an error analysis routine. Anastasiadis[3] developed a program that used Siegel's[33,34] robust shape comparisons to optimize the fit between experimental and numerical drop profiles and a routine was added for rotationally resistant smoothing of the experimental drop profile. The shape comparison program used to determine the interfacial tension from pendant drop profiles for this study was a modified version of Anasatasiadis'[3] program developed by Demarquette and Kamal [5], who also studied the interfacial tension of polymer melts. Touhami et al.[35] reviewed the evolution of digital pendant drop profile analysis and should be referred to for more detail.

## 5.4) DYNAMIC ASPECTS OF PENDANT DROP EXPERIMENTS

### 5.4.1) EQUILIBRATION TIME

The Bashforth and Adams[2] equation, which characterizes the relationship between the interfacial tension and the drop profile, is only valid for a drop in its equilibrium state. Therefore, the equilibrium state of the drop must be verified to ensure accurate measurements of interfacial tension. Wu[9] states that a drop of a low-viscosity liquid, such as water, achieves equilibrium so quickly that it is assumed to occur instantaneously. However, the viscosity of polymer melts is several orders of magnitude larger than most low viscosity liquids. Accordingly, the shape of the drop profile may take anywhere from a few hours to several days to reach equilibrium, depending on the viscosities of the polymers involved.

The factors affecting the equilibration time, or the time required for the pendant drop to reach its equilibrium shape, has never been studied. However, Joseph et al.[83,86] studied interfacial tension equilibration times for polymer melts with the spinning drop apparatus. The pendant drop and spinning drop methods are similar as they both relate the equilibrium shape of a fluid drop to the interfacial tension. By analogy to the spinning drop method, the equilibration time for a pendant drop experiment should depend primarily on the viscosity of both polymer melts and to a lesser extent, the density difference between the two phases, the initial drop shape and dimensions and the equilibrium value of interfacial tension.

During the dynamic transition of the drop to equilibrium, the shape of the drop profile is a function of all the aforementioned variables. The Bashforth & Adams equation cannot determine the interfacial tension from an unstable drop as it does not account for the dynamic factors affecting drop shape. Once the pendant drop reaches equilibrium, its shape and magnitude are only a function of the interfacial tension and the density difference between the phases, and the Bashforth & Adams equation can be used to obtain accurate measurements of interfacial tension from the drop profile.

## 5.4.2) NECKING AND CAPILLARY EFFECTS

Tate's Law[2] states that the maximum supported weight, $W_{max}$, of a drop is proportional to the interfacial tension $\gamma$, and syringe tip radius, $R$:

$$W_{max}=2\pi R\gamma \qquad (5\text{-}17)$$

If the maximum drop weight is exceeded, surface forces are unable to support the drop mass and it necks, detaching from the syringe, as shown in Fig. 5.3. If the drop weight is less than that calculated by Tate's Law, surface forces exceed those exerted by the weight of the drop, retracting it into the syringe, as shown in Fig. 5.4. This is known as the capillary effect.

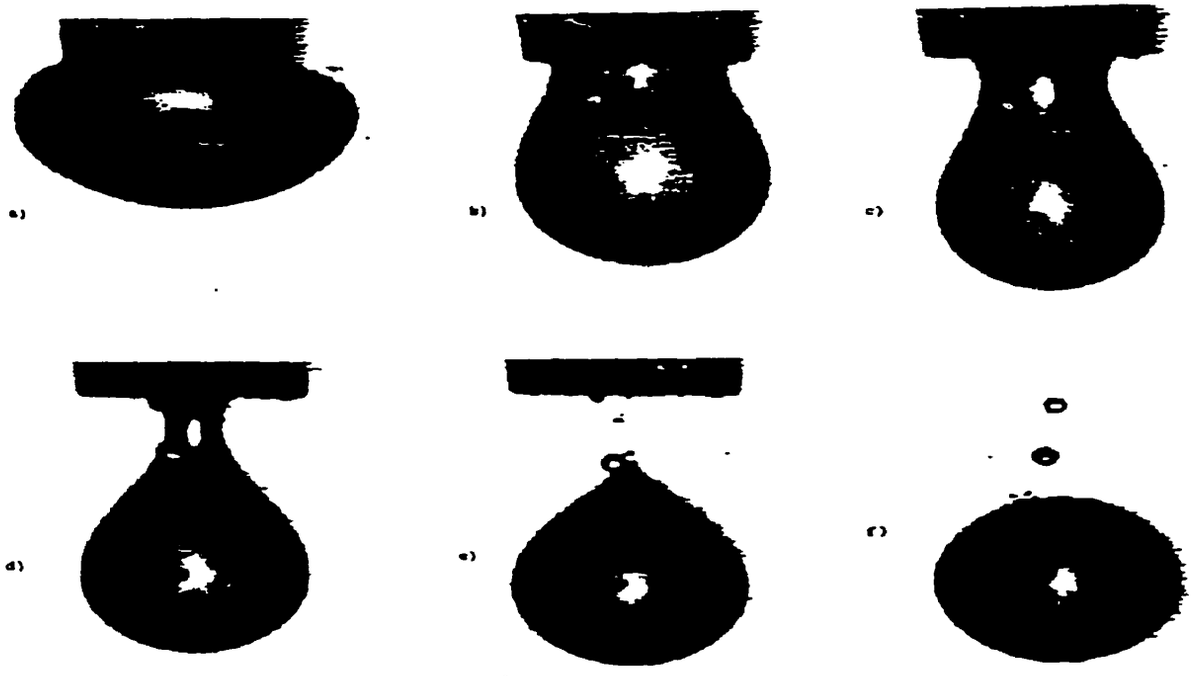

Fig. 5.3: Necking Pendant Drop

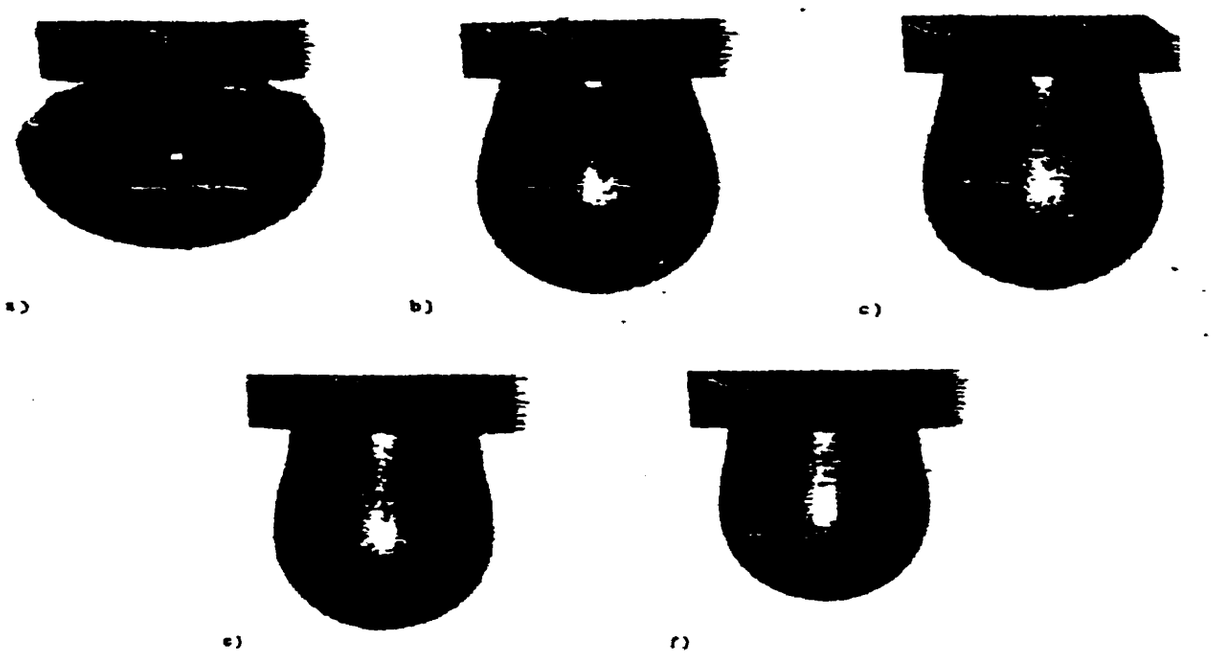


Fig. 5.4: Retracting Pendant Drop

Thus, a critical drop volume, $V_c$, exists which forms the largest, stable, pendant drop and is a function of the maximum, stable drop weight, $W_{max}$ and the density difference between the phases, $\Delta\rho$:

$$V_c = \frac{W_{max}}{\Delta\rho g} \qquad (5\text{-}18)$$

For low viscosity liquids, like water, a drop larger than the critical volume will neck and detach from the syringe in seconds. A polymer drop that exceeds the critical volume will also neck but the process may take days due to the high viscosity of polymer melts. The Bashforth & Adams[2] equation cannot accurately determine the interfacial tension from a drop which is necking or retracting because the drop is not in equilibrium.

In practice, $V_c$, cannot be accurately determined from Tate's Law because of significant deviations from ideal behavior. Using Tate's Law to determine the critical volume from the interfacial tension or vice versa is known as the drop weight method and the problems associated with it are discussed in Adamson's book[22]. An experimental

method of determining the critical drop volume is detailed in the materials and methods section (4.2.3.8).

Even when the critical volume is known, it is extremely difficult to obtain the exact volume needed experimentally due to the visco-elastic nature of polymer melts. The visco-elastic component of polymer melts causes the initially extruded drop volume to increase over time until a final drop volume is reached and it is difficult to establish a universal relationship between initial and final drop volumes. Thus, the majority of pendant drop experiments result in drop volumes which are not equal to $V_c$ and are unstable. Demarquette and Kamal[5] devised a mechanism to stabilize fluid polymer drops which facilitates pendant drop experiments. A Rulon ring was added to the syringe plunger, which expands when heated to form an impermeable seal between it and the syringe body. The seal prevents any drop smaller than the critical volume from retracting into the syringe. However, the Rulon ring does not prevent drops larger than the critical volume from necking. The device stabilizes any drop volume smaller than the critical drop volume, allowing the Bashforth and Adams[2] equation to accurately predict interfacial tension, once the drop reaches equilibrium.

## 5.5) EFFECT OF DROP VOLUME ON INTERFACIAL TENSION MEASUREMENTS

Niederhauser and Bartell[36] measured the surface tension of water for different drop sizes and concluded that drop volume had no effect on interfacial tension values. Efforts were made to obtain the report and inspect the experimental results which led to the conclusions, but the report proved unobtainable.

Stauffer[36] studied the effect of the diameter ratio, $S$, (equation 5-16) on the accuracy of surface tension measurements determined by the method developed by Andreas et al.[28]. The error of surface tension measurements was found to increase as the diameter ratio decreased, while the value of surface tension remained constant. Although the diameter ratio, $S$, does increase with drop volume, Stauffer's[36] results cannot be used

to draw any conclusions concerning the effect of drop volume on interfacial tension measurements. Surface tension was determined for only three drop volumes, each with a different syringe tip. In addition, only the diameter ratio, *S*, of the drops was specified. Neither the experimental drop volumes nor the three syringe diameters used to generate the drops were published. Therefore, while the conclusions regarding the effect of the diameter ratio, S, on the error of surface tension measurements may be correct, no conclusions could be made about the effect of the drop volume.

Roe et al.[11] improved the method developed by Andreas et al.[28] to analyze pendant drop profiles and studied the accuracy of surface tension measurements. Their conclusions were similar to those drawn by Stauffer[36], as the accuracy improved with an increasing diameter ratio, *S*, but the effect of drop volume on surface tension was not discussed.

Wu[6-10] and Roe[12-14] adapted the pendant drop method to determine the interfacial tension of polymer melts. However, their publications did not mention the effect of drop volume on interfacial tension measurements.

### 5.5.1) WORK OF JENNINGS AND PALLAS

Jennings and Pallas[4] examined the effect of drop volume on the accuracy of interfacial tension measurements. They studied drop profiles generated from numerical solutions of the Bashforth and Adams[2]equation. They assumed that the Bashforth and Adams[2] equation was valid for any drop volume. Jennings and Pallas[4] generated drop profiles numerically with the Bashforth and Adams[2] equation for a range of drop volumes. A component of random error was added to the individual coordinates defining the drop profile to simulate experimental measurement error which occurs when converting the image of an experimental drop profile to a series of discrete points which constitute the digital drop profile. Jennings and Pallas[4] determined that the error in calculated interfacial tension values, which is due to the digitization of the drop profile, decreases with increasing drop volume. The random error in the drop profile coordinates, which occurs when digitizing the drop profile is constant, so its effect on the overall shape

and magnitude of the drop profile decreases as the size or volume of the drop increases. Therefore, they concluded that the largest stable drop volume yields the most accurate determination of interfacial tension. To illustrate these effects, the largest stable drop volume would have an interfacial tension confidence interval of approximately 1%, while a drop 80% smaller than the maximum stable drop volume would have a confidence interval of 7%. The only significant error in the value of interfacial tension that is attributable to the shape comparison program of Jennings and Pallas[4] is caused by the digitization of the drop profile.

### 5.5.2) WORK OF LIN ET AL.

Lin et al.[38,39] studied the accuracy of surface tension measurements from experimental drop profiles. It was determined that the standard deviation of surface tension measurements decreases as drop volume increases, in accordance with the findings of Jennings and Pallas[4]. Surface tension measurements from the largest, stable drop yielded accurate results representative of literature values. However, for drop volumes smaller than the maximum stable drop volume, surface tension values decreased with decreasing drop volume, up to 15-30% lower than literature values. Fig. 5.5 illustrates the effect of drop volume on the measured surface tension of water. At the smallest drop volume, 1.5 $mm^3$, the measured value of surface tension is 62 dyne/cm, a full 10 dyne/cm lower than its true literature value of 72 dyne/cm. The surface tension measurements increase hyperbolically with increasing drop volume and level off at the literature value of the surface tension of water for drop volumes greater than 7 $mm^3$. The accuracy of the surface tension measurements improves as the drop volume is increased until a certain drop volume is reached, yielding the most accurate measurement of surface tension.

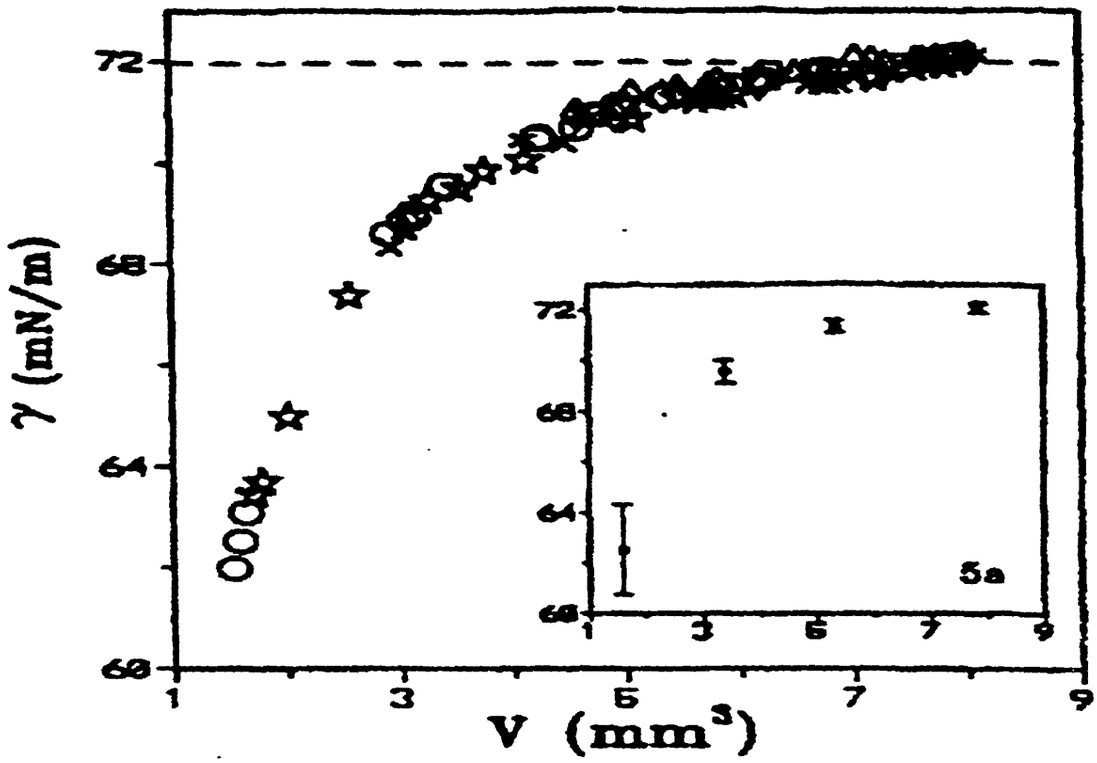


Fig. 5.5: Surface tension of water for different drop volumes. Each symbol represents a separate measurement. Dashed line indicates literature value for surface tension of water (72 dyne/cm). The inset plot (5a) indicates the decrease in the standard deviation of the measurements as the drop volume increases. Reprinted from Lin et al.[38].

The authors explained the effect of drop volume on surface tension by comparing the experimental drop profile, the best-fit profile and the theoretical profile for several drops. The computer program generates both the best fit and the theoretical drop profile. The best fit profile is the optimum fit of the experimental drop profile to the Bashforth and Adams[2] equation. The theoretical profile is derived from the Bashforth and Adams[2] equation with the literature value of the surface tension and a drop volume equal to the experimental drop volume.

For most drops, all three profiles seem to match perfectly except at a single point along the drop profile: the region of contact near the syringe, as shown in Fig. 5.6. The left and right sides within the dashed rectangular region in Fig. 5.6 have been expanded in Fig. 5.7.

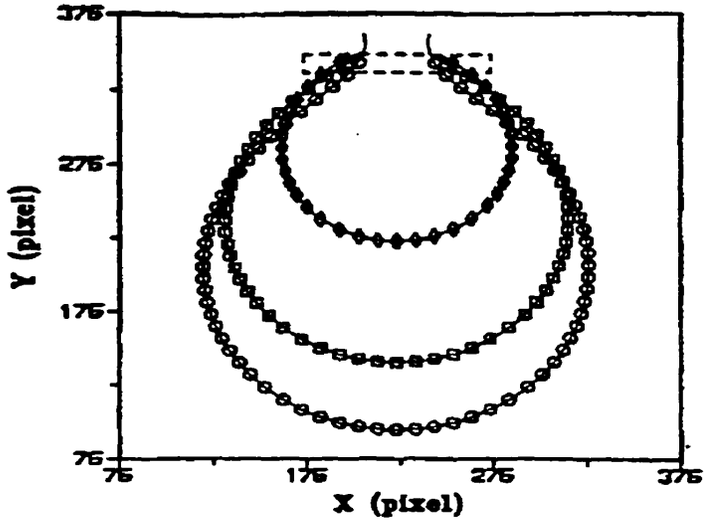


Fig. 5.6: Profiles of air drops in water with syringe diameter, d = 0.4 mm. Dashed rectangle indicates area where experimental, best fit and theoretical profiles do not match. Reprinted from Lin et al.[38].

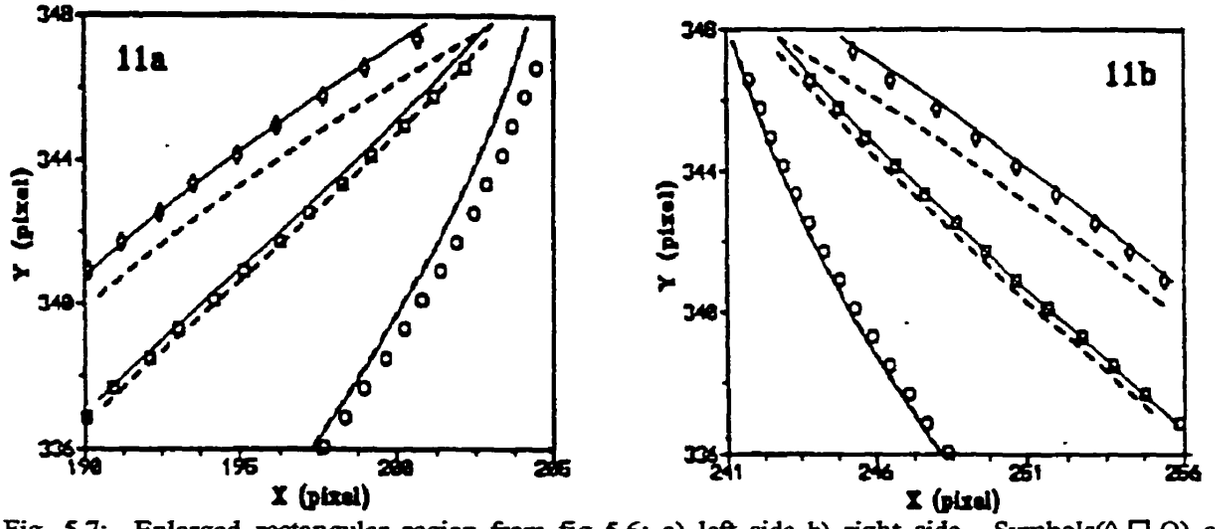


Fig. 5.7: Enlarged rectangular region from fig 5.6: a) left side b) right side. Symbols(◊,□,O) are experimental profiles in order of increasing drop volume. Solid line is best-fit curve to experimental drop profile. Dashed line is theoretical drop profile generated with Bashforth and Adams(2)equation and $\gamma$ literature value of water (72 dyne/cm). Reprinted from Lin et al.[38]

In Fig. 5.7, at the smallest drop volume(◊), the best fit curve matches the experimental profile well, but both are displaced from the theoretical curve by about a full pixel. The theoretical curve corresponds to the literature value of surface tension for water, 72 dyne/cm, while the best fit curve to the experimental profile(◊) yields a surface tension of 62.7 dyne/cm, over 10 dyne/cm lower than the literature value (Fig. 5.6). At the largest stable drop volume(O), using the same syringe, the best fit curve deviates from

the experimental profile at the contact point between the drop and the syringe, but the best fit curve matches the theoretical curve perfectly, yielding a measurement of 72 dyne/cm, the literature value of surface tension for water.

All the experimental profiles, (◊,□,O) deviate from the theoretical form of the Bashforth and Adams[2] equation, represented by the dashed line, at the syringe body, presumably due to the influence of the syringe itself. The deviation can be attributed to the boundary conditions used to derive the Bashforth and Adams[2] equation, which specifies that both radii of curvature, $R_1$ and $R_2$ are equal to a constant, $a$, at the drop apex. The boundary conditions do not account for the region of contact between the profile and the syringe tip, which explains the deviation between the experimental and theoretical drop profile. For smaller drop volumes(◊), the overall drop shape is affected by the syringe body. Thus, the best-fit curve to the experimental drop profile is significantly different from the theoretical profile, which yields the correct value of surface tension. For larger drop volumes, the syringe affects the experimental profile(O) close to the syringe body, but it has no effect on the overall drop shape as indicated by the perfect match between the best fit curve to the experimental drop profile and the theoretical profile. Thus, as the drop volume increases, the effect of the syringe on the overall drop shape decreases until it becomes negligible, at which point the drop profile yields the most accurate measurement of surface tension.

The above findings contradict the prevailing view that surface tension measurements are independent of drop size. To summarize, larger drops yield more accurate measurements of surface tension for two reasons. The effect of the syringe on the overall shape of the drop decreases as the drop volume increases, until it becomes negligible. Also, the relative error in determining the drop profile coordinates when digitizing the image of the pendant drop, decreases with increasing drop volume.

## 5.6) EFFECT OF SYRINGE DIAMETER ON INTERFACIAL TENSION MEASUREMENTS

### 5.6.1) WORK OF STAUFFER

Stauffer[36] used three different syringe diameters to generate pendant drops with significantly different diameter ratios to determine the effect of the diameter ratio, $S$, equation (5-16) on the accuracy of surface tension measurements. The syringe diameter had no noticeable effect on the mean value of surface tension, but Stauffer[36] did not vary the drop volume as he believed surface tension measurements were independent of drop size.

### 5.6.2) WORK OF JENNINGS AND PALLAS

Jennings and Pallas[4] analyzed numerically generated drop profiles corresponding to different syringe diameters and determined that the error for an interfacial tension measurement is minimized when the dimensionless syringe radius, $R_d$, is between 0.8 and 2.0. The dimensionless syringe radius, $R_d$, is a function of the actual syringe radius, $R$, the density difference between the two phases, $\Delta\rho$, and the surface tension, $\gamma$.

$$R_d = R\left(\frac{\Delta\rho g}{\gamma}\right)^{\frac{1}{2}} \qquad (5\text{-}19)$$

### 5.6.3) WORK OF LIN ET AL.

Lin et al.[39] studied the effect of syringe diameter on surface tension measurements with the pendant drop apparatus. They measured surface tension for a range of liquids, while varying the drop volume and the diameter of the syringe used to generate the drop. They determined that the dependence of surface tension measurements on drop volume is affected by the syringe diameter. To illustrate this effect, Fig. 5.8 shows the measured surface tension of water for a range of drop volumes and two syringe diameters: 16 gauge (1.2 mm i.d.) and 22 gauge (0.4 mm i.d.).

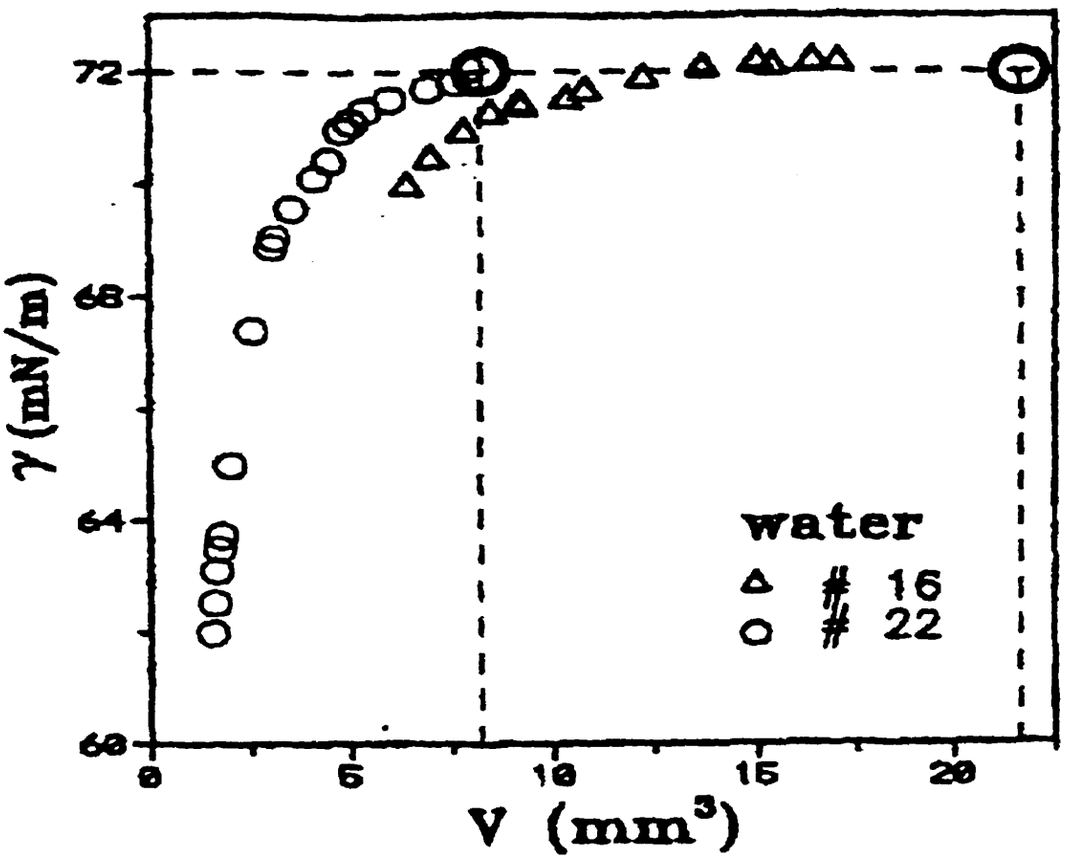


Fig. 5.8: Surface tension of water vs. drop volume for 2 syringe diameters. Symbols: Δ: 16 gauge (1.2 mm i.d.), O: 22 gauge (0.4 mm i.d.), **O**: Critical Drop Volume. Reprinted from Lin et al.[39]

The surface tension of water increases with increasing drop volume, eventually reaching its literature value of 72 dyne/cm for both syringes. For the larger syringe, surface tension measurements attained the true literature value, 72 ± 0.2 dyne/cm, for drop volumes greater than 11.5 $mm^3$. The maximum stable drop volume of water for the larger syringe, represented by the open circle in Fig. 5.5, is 21.6 $mm^3$. Therefore, a drop volume between 11.5 - 21.6 $mm^3$ is needed to obtain an accurate measurement of the surface tension of water with a 1.2 mm i.d. (inner diameter) syringe. For the smaller syringe diameter, a drop volume between 7.5 and 8.2 $mm^3$ is needed to obtain an accurate surface tension measurement. Therefore, the larger syringe diameter provides a larger range of drop volumes that yield accurate surface tension measurements of water, thus facilitating the experimental procedure.

The effect of syringe diameter on the dependence of surface tension on drop volume is explained by comparing the experimental profile, the best-fit profile and the theoretical profile for the two syringe diameters. The drop profiles for the smaller syringe are shown in Fig. 5.7 and the drop profiles for the larger syringe are shown in Fig. 5.9. For the drops generated by the larger syringe, Fig. 5.9b, all three profiles match almost perfectly, even at the smaller drop volumes, whereas in Fig. 5.7, the best-fit curve matches the theoretical profile for the largest drop only. Thus, it appears that the syringe has a diminished effect on drops produced from the larger syringe when compared to drops produced from the smaller syringe. Recall from section 5.5 that the effect of the smaller syringe on the drop profile decreases with increasing drop volume until the effect of the syringe becomes negligible. Drops produced from larger syringes are of a larger volume than drops from smaller syringes which explains the reduced the effect of the syringe on their drop profiles when compared to the effects on drops from smaller syringes.

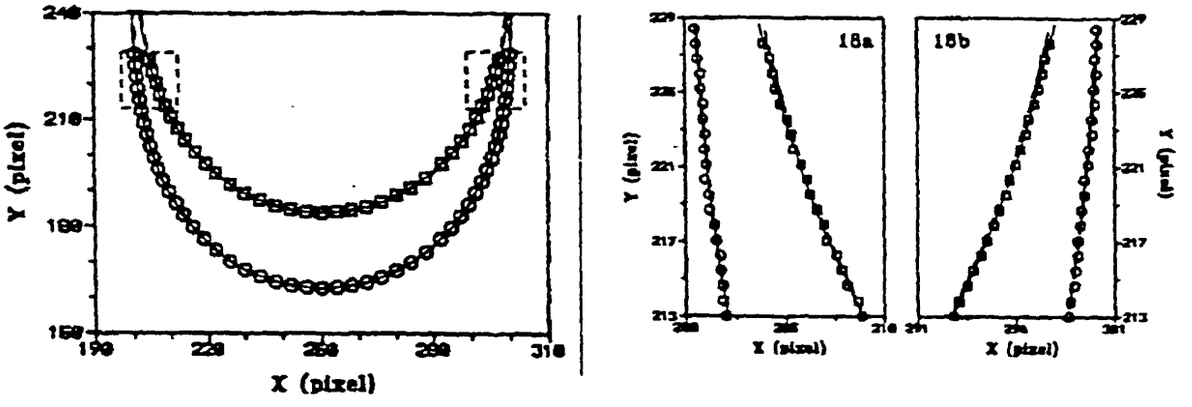


Fig. 5.9 (A): Drop profiles of air drop in water w/ syringe inner diameter = 1.2 mm. (B): Enlarged rectangular region from (A). Symbols (□,O): Experimental drop profiles. Solid Line: best-fit curve to experimental drop profile. Dashed line: theoretical drop profile generated with Bashforth and Adams(2)equation and γ literature value of water (72 dyne/cm)

# 6) MATERIALS & METHODS

## 6.1) PENDANT DROP APPARATUS

The pendant drop apparatus consists of several distinct components. The experimental cell is a heated sample holder that secures the syringe and pendant drop in an inert environment. A digital camera transfers the illuminated image of the pendant drop to a computer, where the drop profile is analyzed to determine the interfacial tension. The pendant drop apparatus and optical system are mounted on a vibration-proof table to avoid vibrations. Additional information on the pendant drop apparatus may be found in the thesis by Demarquette[74] or the paper by Demarquette and Kamal[5]. A general view of the apparatus is given in Fig. 6.1.

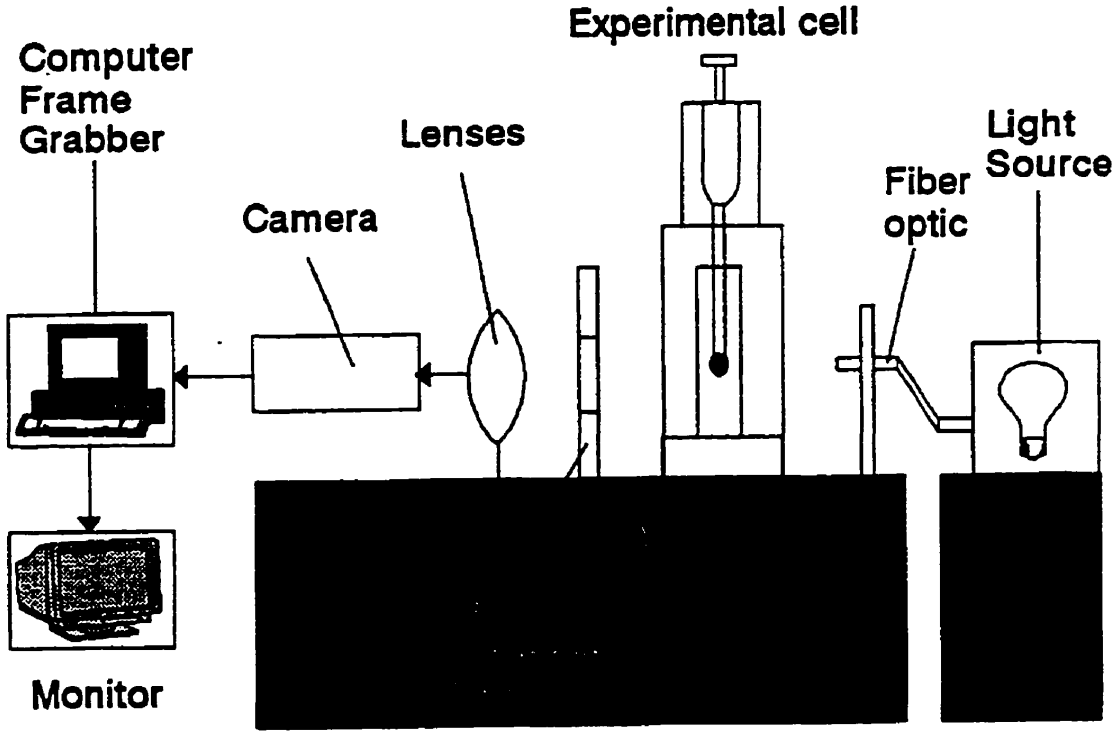


Fig 6.1: Pendant Drop Apparatus

### 6.1.1) OPTICAL SYSTEM

The pendant drop is illuminated by a fiber optic light source which allows the drop profile to be digitized. The wavelength of the light reaching the drop can be modified using colored filters, to detect small differences in the refractive index between the two phases. The digital camera and lens have a magnification factor of 960 pixels/cm which was verified by an optical calibration insert with a target of 100 +/- .01 mm. The intensity of the fiber optic light source is adjusted with a control dial.

### 6.1.2) EXPERIMENTAL CELL

The experimental cell of the pendant drop apparatus consists of an electrically heated, stainless steel chamber which has two quartz windows to permit illumination and viewing of the pendant drop (Fig. 6.2). The less dense fluid forms the matrix and is contained by a standard glass adsorption cell, held in place by a stainless steel insert. The insert is in firm contact with the experimental cell wall, improving heat conduction to the glass cell. A proportional temperature controller is capable of heating the cell to 300 +/- 0.5 °C.

Interfacial tension experiments with polymer melts involve exposure to high temperatures for long periods of time. A positive pressure of inert gas removes oxygen from the experimental cell, thus preventing oxidative degradation of the polymer melts. The experimental cell must be virtually airtight in order to maintain a stable positive pressure for long periods of time. All leaks are sealed with a high temperature silicone sealant. The area between the cell and the syringe holder is sealed by a standard silicone o-ring in the cell cover. During an experiment, the syringe holder should be in contact with the experimental cell cover to minimize the effects of a potential breach in the o-ring. Standard silicone degrades at about 200 °C, so the o-ring must be routinely replaced. The only detectable leak in the system should be from the area between the cover of the experimental cell and the experimental cell itself. When the cell is heated, the two metal surfaces expand, minimizing the leak. The leak from the cell cover is unavoidable but it is acceptably small and causes no problems.

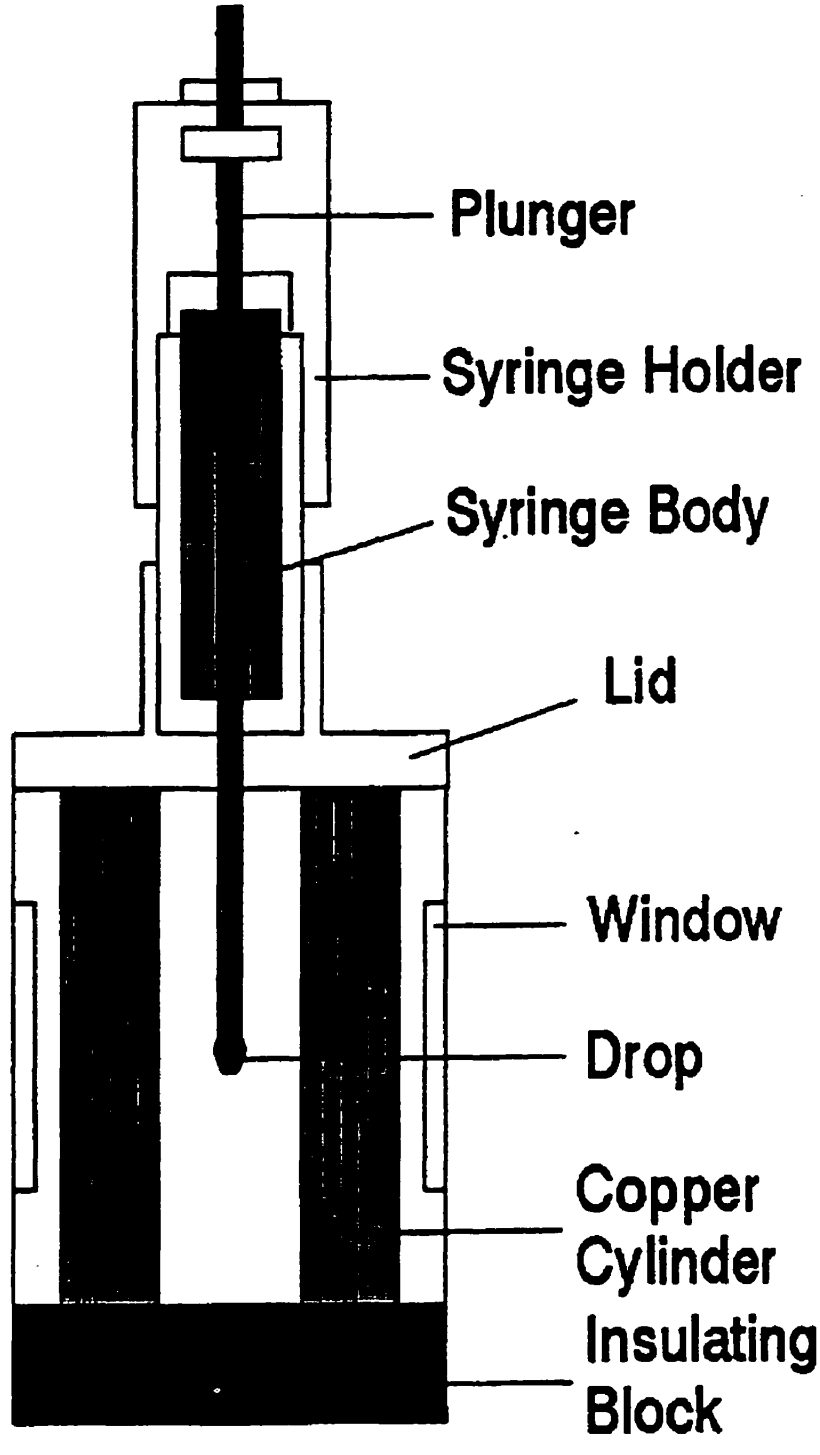


Fig. 6.2: Experimental Cell

### 6.1.3) DROP INSERTION DEVICE

The syringe, syringe holder and needle are collectively referred to as the drop insertion device, shown in Fig 6.3.

The syringe is a stainless steel tube of varying diameter encased in a copper body. The denser polymer, which forms the pendant drop, is inserted within the syringe tip. The syringe is secured in an electrically heated syringe holder which positions the syringe in the experimental cell.

The drop plunger or needle is attached to a micrometer and placed inside the syringe. This allows the drop to be slowly extruded or pushed out the syringe tip, forming a pendant drop. A Rulon ring, just above the tip of the drop plunger, expands when heated and forms a seal with the syringe body. This prevents drops smaller than the critical drop volume from retracting into the syringe. A plunger and Rulon ring should form a tight fit with the intended syringe to ensure an effective seal. Although the Rulon ring is capable of resisting temperatures up to 270 °C for prolonged periods of time, it does eventually lose its elasticity, at which point the entire plunger must be replaced. An ineffective seal, caused by either a degraded Rulon ring or a small plunger diameter, makes it difficult to obtain a stable pendant drop.

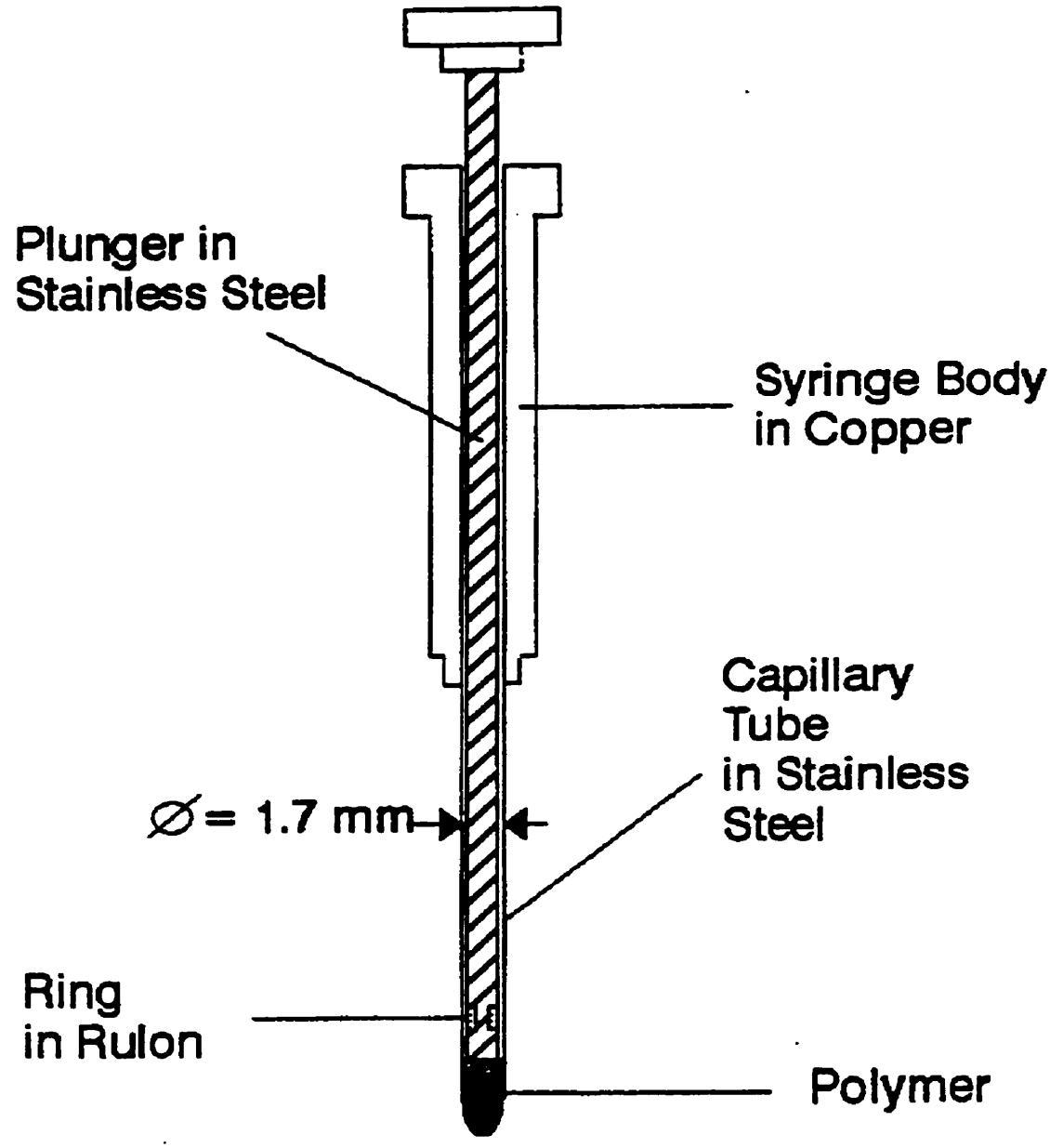


Fig. 6.3: Drop Plunger in Syringe

## 6.2) EXPERIMENTAL PROCEDURES

### 6.2.1) SELECTION OF SYRINGE DIAMETER

The selection of an appropriate syringe diameter for a pendant drop experiment is based on the findings of both Lin et al.[38-39] and Jennings and Pallas[4].

Lin et al.[38-39] determined that a larger syringe diameter affords a wider range of drop volumes which yield accurate interfacial tension measurements. However, they did not establish an ideal range of syringe diameters for interfacial tension measurements.

Jennings and Pallas[4] determined that the error for an interfacial tension measurement is minimized when the dimensionless syringe radius, $R_d$, is between 0.8 and 2.0. The dimensionless syringe radius, $R_d$, is a function of the actual syringe radius, $R$, the density difference between the two phases, $\Delta\rho$, and the surface tension, $\gamma$. Note that equation (5-19) is dimensionless because the product $\Delta\rho g/\gamma$ has units of length squared.

$$R_d = R\left(\frac{\Delta\rho g}{\gamma}\right)^{\frac{1}{2}} \qquad (5\text{-}19)$$

However, Jennings and Pallas[4] noted that their numerical analysis assumed ideal conditions and that it may be difficult to achieve the theoretical maximum drop volume for larger syringe diameters during an actual pendant drop experiment,.

From experience, it is recommended that a range of dimensionless tip radii, $R_d$, of 0.8 to 1.4, be used as a general guideline for establishing the syringe diameter for a pendant drop experiment. The reduced range of $R_d$ eliminated problems encountered with unstable drops that occurred at larger syringe diameters. A syringe diameter which satisfies a dimensionless tip radius of 0.8-1.4 is still relatively large and should ensure a wide range of drop volumes that yield accurate interfacial tension measurements, alleviating concerns raised by Lin et al.[38-39].

### 6.2.2) SAMPLE PREPARATION

#### 6.2.2.1) DENSER POLYMER WITH THE CAPILLARY RHEOMETER

The denser polymer, which constitutes the drop in an interfacial tension experiment, is prepared by extrusion with a capillary rheometer. The barrel of the capillary rheometer is packed with polymer pellets which form a continuous polymer melt under heat and pressure. A piston forces the polymer through a die to form long cylindrical samples. The diameter of the extruded polymer samples must match the syringe diameter as closely as possible. A tight fit between the sample and syringe is needed to form a stable pendant drop.

The parameters affecting the extruded polymer sample diameter can be categorized as either predetermined or adjustable parameters. Predetermined parameters are defined prior to the experiment and remain constant throughout its duration. They determine the approximate diameter of the extruded polymer sample. The predetermined variables include the die radius, the length to diameter ($L/D$) ratio of the die, and the barrel temperature. The adjustable parameters are varied during the experiment to improve the fit between the sample and syringe diameter. They include the piston speed and the drawdown length of the polymer sample.

When preparing samples for a pendant drop experiment, the processing temperature is usually set as low as possible to avoid polymer degradation. This is especially important for polymers lacking temperature stabilizers, which degrade rapidly at elevated temperatures. In addition, it is difficult to produce samples of a constant diameter at higher temperatures due to the low viscosity of the extruded polymer. However, temperatures close to the melting point of the polymer may induce melt fracture or an irregular surface structure in the samples. The onset of melt fracture can be shifted to higher shear rates by increasing the barrel temperature. A recommended processing temperature, $T$, for pendant drop sample preparation is $T_m < T < T_m+20°C$, where $T_m$ is the melting point of the polymer.

Both the diameter and the length to diameter ($L/D$) ratio must be considered when selecting a die. The effect of die diameter is obvious: the larger the die, the larger the

extruded sample diameter. The *L/D* ratio affects the die swell of the polymer sample. A longer *L/D* ratio increases the residence time of the polymer within the die constriction and aligns the long polymer chains in the axial direction, which reduces the expansion or swelling of the polymer sample when it exits the die. Therefore, a larger *L/D* ratio decreases the sample diameter. Dies with small diameters and long *L/D* ratios experience large pressure drops which can induce melt fracture. To summarize, the die diameter determines the approximate diameter of the extruded polymer sample which can be adjusted by varying the L/D ratio of the die.

The piston speed determines the shear rate which affects the die swell and in turn affects sample diameter. At lower shear rates, the polymer has a longer residence time in the die and the die swell decreases. At higher shear rates the opposite is true, but larger pressure drops are also experienced, which may lead to melt fracture.

The sample diameter may also be reduced by allowing the continuously extruded polymer to reach a distance below the die exit known as the drawdown length. The weight of the polymer exerts a tensile force which stretches the sample and reduces its diameter. Increasing the drawdown length at a given shear rate increases the tensile force which further reduces the sample diameter. The tensile effect is controlled by cutting small samples at the bottom of the polymer strand, which maintains a constant drawdown length.

Low shear rates and long drawdown lengths are recommended to produce polymer samples of a consistent diameter, as the conditions ensure a slow, stable extrusion process. The exact values of the parameters needed to match the diameter of the extruded polymer sample to the syringe diameter can only be determined by trial and error, using the general guidelines established. Fig. 6.4 is an iterative action plan which should help users adjust the capillary rheometer parameters to match syringe and sample diameters.

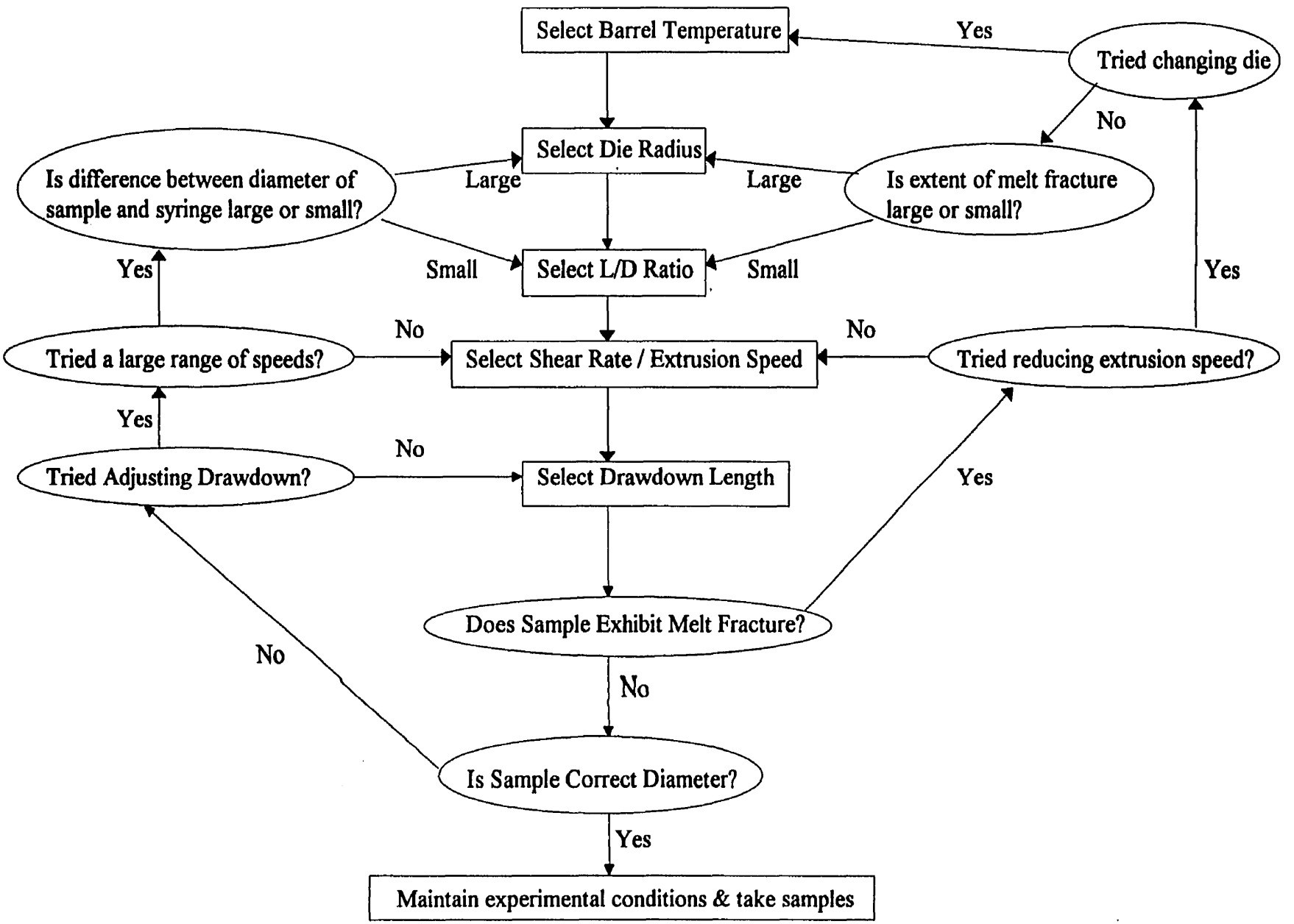


Fig. 6.4: Iterative action plan to manipulate diameter of filaments of denser polymer phase using capillary rheometer

#### 6.2.2.2) LESS DENSE POLYMER WITH COMPRESSION MOLD

The less dense polymer is prepared by compression molding of the polymer pellets. The mold is placed between by thin metal sheets covered with a polyester film, which assures a clean mold surface that does not adhere to the metal. The thin steel sheets are flexible under pressure and ensure proper contact and heat transfer between the compression molding heating plates and the mold itself. The mold should be filled with an excess of polymer pellets to ensure that molten polymer completely fills the mold. High molding pressures are used to eliminate voids or air pockets in the mold.

The mold assembly is placed between the heated compression molding plates, which causes the polymer pellets to melt gradually over 5-10 minutes. The hydraulic pump is used to maintain contact between the mold assembly and the hot plates during this period to improve heat transfer to the mold. Pressure should not be applied to the mold before the polymer pellets are completely melted to prevent air from being trapped within the mold interior. Once the polymer has melted, the mold is pressurized to 10000 psig for 4 minutes, 20000 psig for 3 minutes and finally 30000 psig for 2 more minutes. The heaters are turned off and the mold is cooled to room temperature prior to releasing the pressure and removing the mold.

Processing temperatures for compression molding are generally 20-30 °C above the melting point of the polymer. If polymer degradation is a concern, the temperature and/or the molding time may be reduced.

### 6.2.3) PENDANT DROP EXPERIMENTS

#### 6.2.3.1) PENDANT DROP APPARATUS ALIGNMENT

The experimental system must be properly aligned to avoid non-symmetrical drops. Drop asymmetry may be corrected but it is not a trivial task[28]. The experimental cell must be secured on a level vibration-proof table. Then, the digital camera is aligned with the optical calibration insert. Finally, the alignment of the syringe in the syringe holder is verified with the digital camera.

### 6.2.3.2) SAMPLE PREPARATION

The surface of the polymer samples should be cleaned with an appropriate solvent, such as acetone. The samples are then dried under vacuum to eliminate surface moisture and any residual traces of solvent. Polystyrene is moderately polar, as its repeat unit contains a phenyl group. It is dried under vacuum at 70 °C for about three hours. Polymers with a higher degree of polarity, such as polyamide, should be dried at about 90 °C for the same amount of time. While not essential, the vacuum accelerates the drying process and retards degradation of the polymer by reducing available oxygen.

The denser polymer sample, prepared by extrusion in a capillary rheometer, should measure approximately 1.7 cm in length. The sample is inspected for dirt or contamination and quickly cleaned with compressed air prior to insertion in the syringe. In surface tension experiments, the polymer insert tended to slide out of the syringe before it was fully melted. This problem was minimized by pushing a tightly fit sample 1 cm inwards from the base of the syringe tip. In interfacial tension experiments, this was not a problem, and the sample was set flush with the syringe tip.

The compression-molded polymer sample is cut into rectangular sections: the length of the sample is ¾ of the height of the glass cell. The cross-sectional area should match the dimensions of the glass cell as closely as possible. Firm contact between the solid polymer and the opaque walls of the glass cell improves heat conduction to the sample, causing it to melt quickly. In addition, a sample matching the dimensions of the glass cell has less chance of trapping air in the polymer melt.

### 6.2.3.3) ESTABLISHING AN INERT ATMOSPHERE

A 2-stage regulator, with a needle valve, controls the gas pressure and the flowrate to the experimental cell. The gas cylinder is fully opened with both regulator valves fully closed. Then, the flow valve (smaller valve) is fully opened before slowly opening the pressure valve while monitoring the pressure in the experimental cell, which should not exceed a few psig. The system should be routinely checked for leaks, specifically, the

regulator valve and its seal with the gas cylinder, the line from the cylinder to the experimental cell and the cell itself.

### 6.2.3.4) INTERFACIAL TENSION EXPERIMENT

The glass cell containing the less dense polymer is placed in the experimental cell. The cover is firmly secured over the experimental cell with the two screws provided. The temperature of the cell is raised to melt the polymer matrix. To prevent polymer degradation, the cell is maintained under a positive pressure of inert gas. Once the polymer is completely melted, which may be verified with the digital camera, the syringe containing the denser polymer is secured in the syringe holder. The needle is placed in the syringe, fully raised, so it does not prematurely force the denser polymer out of the syringe. A compressed gas canister is used to clean the syringe tip from any dirt it may have picked up from the syringe holder. The syringe assembly is lowered into the polymer melt and locked into position. Only then are the syringe heaters raised to the appropriate temperature. When the unheated syringe contacts the polymer melt, the still solid polymer insert (denser polymer) will emerge a small distance out of the syringe into the melt. The insert will begin to melt and then should retract within the syringe. Once the polymer drop has completely retracted into the syringe, it is allowed an additional 5-10 minutes, depending on the temperature of the cell, to fully melt. Protracted melting periods in the syringe can lead to misshapen pendant drop profiles, the reason for which is unknown. The polymer drop is extruded from the syringe into the surrounding melt by lowering the plunger with the micrometer. See section 6.2.3.8 to determine the critical volume which yields the most accurate determination of interfacial tension. Do **not** disturb the drop once a significant amount of time has elapsed after it was extruded, as this may result in an abnormal drop shape.

### 6.2.3.5) OPTICAL CORRECTION FACTOR

For an interfacial tension experiment involving two liquid phases, the matrix magnifies the image of the drop. The real drop dimensions are related to the apparent image dimensions by an optical correction factor, $n$, which is determined by inserting a rod of known diameter into the polymer melt and observing its apparent dimensions, as a function of temperature. The thermal expansion of the rod at the temperatures involved is negligible.

$$n(T) = \frac{d_{app}(T)}{d_{real}} \qquad (6\text{-}1)$$

### 6.2.3.6) SURFACE TENSION EXPERIMENT

Surface tension experiments are simpler than interfacial tension experiments as the second phase is air or an inert gas. The differences between a surface tension and interfacial tension experiment will be outlined. The syringe is placed in the unheated experimental cell and both heaters are raised to the desired set point. Once the polymer insert in the syringe has fully melted, which requires approximately 20-30 minutes depending on the temperature, the polymer is extruded to the desired volume or length. See section 6.2.3.8 to determine the critical volume which yields the most accurate determination of surface tension. With surface tension experiments, a positive pressure cannot be established until the drop melts in the syringe and seals the cell. To prevent degradation, the polymer was melted and extruded at lower temperatures, at which point an inert environment was established and then the temperature was raised to the desired set point.

### 6.2.3.7) RECORDING PENDANT DROP IMAGES

The design of the pendant drop system allows for on-line monitoring of the apparent interfacial tension, $\gamma_{app}$, defined as the interfacial tension from a drop in a dynamic state. In principle, an experiment is monitored and once conditions for

equilibrium are satisfied, the equilibrium value of interfacial tension is recorded and the experiment is terminated. The procedure works well for surface tension experiments with polymer melts of medium to low viscosity, as they reach equilibrium relatively quickly (less than 2-3 hours). However, interfacial tension experiments require much longer to reach equilibrium, often 10-24 hours, for polymers of comparable viscosity. Also, the apparent interfacial tension approaches its equilibrium value very slowly, especially as the experiment nears completion. If the experiment is monitored on-line, fatigue may influence the researcher to terminate the experiment prematurely which could lead to inaccurate estimations of the interfacial tension.

To solve this problem, a program was developed which automatically records images of the pendant drop for a period of time that is much longer than the estimated equilibration time of the experiment. The images are analyzed collectively at a later time and equilibrium can be determined with a greater degree of confidence.

#### 6.2.3.8) CRITICAL DROP VOLUME

As outlined in the background and confirmed by experiments conducted for this study, interfacial tension results depend on drop size. The maximum stable drop volume or critical drop volume, $V_c$, yields the most accurate measurement of interfacial tension for a given set of conditions. Theoretically, the critical volume depends on the syringe diameter, the interfacial tension and the density difference between the phases, the last two of which are functions of temperature.

The critical drop volume must be determined from experiments because of deviations from Tate's Law. First, estimate the critical drop volume using Tate's Law (equation 2-24) with the radius of the syringe and an estimate of the interfacial tension. Assume the shape of the drop is approximately cylindrical, with the same radius as the syringe, and calculate the length of the cylinder with the estimated critical drop volume. For the first pendant drop experiment, extrude the drop to the length estimated from Tate's Law. The drop length is monitored, as it can be determined instantly on-screen, as opposed to the drop volume, which must be determined by numerically integrating the

drop profile with a spreadsheet program. Once the drop is extruded, its dimensions are monitored to determine equilibrium, as described in section 6.3.1. If the drop reaches equilibrium, its drop volume is calculated (section 6.3.3) and it is assumed to be less than the true critical drop volume, $V_c$. Further experiments are conducted, gradually increasing the initial drop length, which increases the equilibrium drop volume. Once the critical drop volume is surpassed, the drop will be unstable and its length will increase until the drop necks and detaches from the syringe. The largest stable drop, prior to that point, can be considered equal to the critical or maximum stable drop volume, $V_c$.

#### 6.2.3.9) TERMINATING PENDANT DROP EXPERIMENT

At the end of a pendant drop experiment, the syringe needle is removed from the heated cell and syringe holder and placed aside. A small piece of kimwipe tissue is placed within the needle and pushed with a steel rod until it contacts the polymer located in the syringe tip. This can be confirmed by observing an increase in drop volume on the monitor. The syringe assembly is then raised, which lifts the glass cell filled with the less dense polymer out of the experimental apparatus. The glass cell is removed and the excess polymer on the syringe exterior is wiped away with a tissue before it can harden. The glass cell is quickly placed in a preheated oven at a temperature of 400 °C. The cell is positioned upside down at an angle to the oven wall which allows the polymer to melt and flow out of the cell onto the oven floor where it burns away. This minimizes the residue buildup on the glass cell wall, which is difficult to clean. The tissue is pushed out of the syringe, removing most of the polymer from the syringe interior. If it has solidified, lower the syringe assembly back into the heated experimental cell, where it should quickly soften. The syringe is then placed in the oven along the floor, to avoid bending the syringe capillary tube, and the remaining polymer is burned away.

The syringe should remain in the oven for a minimum of one hour, after which time it may be removed and allowed to cool. The syringe is cleaned with medium steel wool followed by kimwipe tissue paper. The cleaning material is carefully packed in the syringe

interior and pushed back and forth with a steel rod . Care must be taken not to jam the steel wool in the syringe. If it becomes stuck, it is difficult to remove.

The glass cells should be left in the heated oven for a few days to burn away as much of the polymer residue as possible. The oven is then turned off and the glass cells within are gradually cooled, keeping the oven doors closed. Rapid cooling can cause the glass cells to crack. With repeated use, a polymer residue builds up on the surface of the glass cells which prevents the digital camera from obtaining a clear image of the pendant drop. The residue is removed by placing the glass cells in a solution of aqua regia (2/3 nitric acid, 1/3 sulfuric acid) overnight. The cells are rinsed with water and allowed to dry. Finally, they are gently cleaned with a kimwipe tissue to remove any remaining residue. The acid solution is dangerous and should be handled under a fume hood with a lab coat, rubber gloves and eye protection.

## 6.3) ANALYZING PENDANT DROP PROFILES

### 6.3.1) PENDANT DROP EQUILIBRIUM

The lengthy transition of the pendant drop to equilibrium for viscous polymer melts makes the determination of the equilibrium time difficult. The first criterion for equilibrium is a static pendant drop profile for a predetermined amount of time (20–40% of the equilibration time itself). Drop profile dimensions, specifically the maximum drop length and radius, are quickly inspected with the TCPro imaging software. When equilibrium is reached, drop dimensions should remain constant. If drop dimensions are not carefully monitored, equilibrium can be declared prematurely or unstable drops may be misidentified as the drop profile changes in shape very slowly due to the high viscosity of the polymers involved. An unstable drop greater than the critical volume will neck and slowly increase in length until it detaches from the syringe. A drop smaller than the critical volume which is not sealed in place by a Rulon ring will shrink and eventually completely retract into the syringe.

### 6.3.2) EQUILIBRIUM VALUE OF INTERFACIAL TENSION

The interfacial tension is monitored after the maximum drop dimensions appear stable, because further small changes occur in the shape of the drop profile and are reflected in the value of the apparent interfacial tension. The dynamic transition of interfacial tension is characterized by an exponential decay function, approaching equilibrium very slowly in the later stages. When equilibrium is finally attained, the data will indicate a random error with no observable trend. The equilibrium state is determined with the correlation coefficient, $r^2$, which measures the strength of association between interfacial tension and time. Prior to equilibrium, the apparent interfacial tension decreases with time and is characterized by a large correlation coefficient. At equilibrium, the interfacial tension no longer varies with time and so the correlation coefficient should be negligible. The exact criteria used to assess equilibrium for an interfacial tension measurement in this study were: (1) a correlation coefficient between interfacial tension and time of less than 0.1 and (2) the standard deviation of the measurements at equilibrium should not exceed 2%. Both criteria must be applied to a period of time equal to 20-40% of the equilibration time itself.

### 6.3.3) DROP VOLUME

The drop volume is calculated by numerically integrating the drop profile with a spreadsheet program:

$$V_d = \iiint dV \qquad (6\text{-}2)$$

$$V_d = \iiint r(drdzd\theta) \qquad (6\text{-}3)$$

$$V_d = \pi \int_{z=0}^{z=h} r^2 dz \qquad (6\text{-}4)$$

where $h$ is the drop height and $r$ is the drop radius which varies as a function of $z$.

### 6.3.4) INTERFACIAL TENSION

The interfacial tension is calculated with the dimensionless shape parameter, $B$, the radius of curvature at the drop apex, $a$, the magnification factor $M$, the optical correction factor, $n$, and the density difference, $\Delta\rho$, between the two polymer phases which is obtained experimentally or by equations of state. The dimensionless shape parameter, $B$, is calculated from the shape comparison routine developed by Anastasiadis and modified by Kamal et al.(5), and the radius of curvature at the drop apex, $a$, is calculated from the drop profile with Sigmaplot. See sections (6.4.2) and (6.4.3) for more details on the calculation of $B$ and $a$.

$$\gamma = \frac{\Delta\rho g a^2}{\left(\sqrt{B}\right)^2 n^2 M^2} \qquad (6\text{-}5)$$

### 6.3.5) ERROR ANALYSIS

The possible sources of error in an interfacial tension measurement are from the estimation of the dimensionless shape parameter, $B$, the radius of curvature at the drop apex, $a$, the magnification factor $M$, the optical correction factor, $n$, and the density difference between the phases, $\Delta\rho$. Additional error is incurred if drops smaller than the critical volume or unstable drops are used to determine the interfacial tension.

#### 6.3.5.1) ERROR IN $B$ AND $a$

The error in estimating the dimensionless shape parameter, $B$, and the radius of curvature at the drop apex, $a$, occurs during the analysis of the drop profile. Note that if the program is properly coded, the contribution to the total error from the estimation of $a$ and $B$ would be negligible. See section 6.4.2.3 for more details on the errors in the shape comparison program.

The error in estimating the dimensionless shape parameter, $B$, depends on the portion of the experimental drop profile omitted when fitting the Bashforth and Adams equation. The fraction of the profile excluded from the curve-fitting procedure usually decreases with increasing drop volume. Therefore, drops from the smaller syringe have a

larger % error than drops from larger syringes. From experience, values of $B$ from drops with the 1.8 mm syringe have an error of approximately 1.5%, and drops from the 4 mm syringe have an error of approximately 0.7%.

The error in estimating the radius of curvature at the drop apex, $a$, was determined to be approximately 1% of the radius of the fitted circle itself.

#### 6.3.5.2) ERROR IN $\Delta\rho$

The error in the difference in densities depends on the method used to characterize the individual polymer melt densities. If characterization equipment is not available, equations of state can be used, but are subject to relatively large errors, ranging from 2-4%. For an interfacial tension experiment, where there are two polymer phases, the additive errors can be substantial. In this study, the Gnomix P-V-T apparatus was used to estimate the polymer densities and it is considered very accurate with an error of less than 0.5%.

#### 6.3.5.3) ERROR IN $M$

The lens on the digital camera has a magnification factor which is precisely determined with an optical insert consisting of a circular target with a radius specified to three decimal places. The error of the magnification factor is relatively small at approximately 1%.

#### 6.3.5.4) ERROR IN $n$

The optical correction factor, $n$, is related to the refractive index of the matrix liquid, which magnifies the drop in an interfacial tension experiment. Note that this error does not apply to surface tension experiments as the refractive index of air is negligible. The optical correction factor is determined by observing the change in the dimensions of a rod inserted within the polymer melt. The error is relatively high at approximately 3%, because the refractive index itself is a relatively small quantity.

### 6.3.5.5) PROCEDURAL ERRORS

If the experimental procedure is not carefully followed, interfacial tension measurements can be subject to large additional errors. Procedural errors are related to interfacial tension measurements from either reduced drop volumes or unstable drops.

This study has determined, in accordance with the findings of Lin et al.[38,39], that interfacial tension results depend on drop size. Therefore, the interfacial tension should be measured from the largest stable or critical drop volume. Smaller drop volumes can reduce the measured value of interfacial tension and should be avoided. See section (6.2.3.8) for more details on determining the critical drop volume.

The Bashforth and Adams[2] equation used to determine the interfacial tension from the drop profile is only valid under equilibrium conditions. If the interfacial tension is measured from an unstable drop, the errors can be substantial, reaching values up to 100%. The further the drop is from its equilibrium state, the larger will be the resulting error in the interfacial tension measurement. These errors can be completely eliminated by confirming that the drop has reached equilibrium before determining the interfacial tension.

### 6.3.5.6) TOTAL ERROR IN DETERMINING INTERFACIAL TENSION

If an independent variable, $R$, is a function of $m$ independent variables $x_i$ with individual errors, $e_{xi}$, then the error in $R$ is defined by Holman[75] as:

$$e_R = \left[ \sum_{i=1}^{i=m} \left( \frac{\partial R}{\partial x_i} e_{x_i} \right)^2 \right]^{\frac{1}{2}} \qquad (6\text{-}6)$$

If the interfacial tension is calculated by equation (6-7):

$$\gamma = \frac{\Delta \rho g a^2}{B n^2 M^2} \qquad (6\text{-}7)$$

where $B$ is the dimensionless shape parameter, $a$ is the radius of curvature at the drop apex, $M$ is the magnification factor, $n$ is the optical correction factor and $\Delta\rho$ is the density

difference between the phases. Then, the total error in the value of the measured interfacial tension is defined as:

$$e_\gamma = \left[\left(\frac{\partial\gamma}{\partial\Delta\rho}e_{\Delta\rho}\right)^2 + \left(\frac{\partial\gamma}{\partial a}e_a\right)^2 + \left(\frac{\partial\gamma}{\partial B}e_B\right)^2 + \left(\frac{\partial\gamma}{\partial M}e_M\right)^2 + \left(\frac{\partial\gamma}{\partial n}e_n\right)^2\right]^{\frac{1}{2}} \qquad (6\text{-}8)$$

After calculating the derivatives and substituting terms from equation (6-7) into (6-8), equation (6-9) becomes:

$$e_\gamma = \left[\left(\frac{\gamma}{\Delta\rho}e_{\Delta\rho}\right)^2 + \left(\frac{2\gamma}{a}e_a\right)^2 + \left(\frac{\gamma}{B}e_B\right)^2 + \left(\frac{2\gamma}{M}e_M\right)^2 + \left(\frac{2\gamma}{n}e_n\right)^2\right]^{\frac{1}{2}} \qquad (6\text{-}9)$$

Then the percent error in the interfacial tension is obtained by dividing both sides of the equation by $\gamma$ and multiplying by 100:

$$\frac{e_\gamma}{\gamma} = \left[\left(\frac{1}{\Delta\rho}e_{\Delta\rho}\right)^2 + \left(\frac{2}{a}e_a\right)^2 + \left(\frac{1}{B}e_B\right)^2 + \left(\frac{2}{M}e_M\right)^2 + \left(\frac{2}{n}e_n\right)^2\right]^{\frac{1}{2}} * 100 \qquad (6\text{-}10)$$

Table 6.1 lists a typical set of percent errors for a surface tension experiment with a 4.0 mm diameter syringe which lead to a final percent error of approximately 4.5%.

| Variable | % Error |
|---|---|
| $B$ | 0.7 |
| $a$ (pixels) | 2.0 |
| $\Delta\rho$ (g/cm$^3$) | 0.5 |
| $M$ (pixels/cm) | 1.0 |
| $n$ | 0 |

Table 6.1: Percent errors for surface tension experiment with 4.0 mm diameter syringe. $B$ is the dimensionless shape parameter, $a$ is the radius of curvature at the drop apex, $M$ is the magnification factor, $n$ is the optical correction factor and $\Delta\rho$ is the density difference between the phases.

Table 6.2 lists a typical set of percent errors for an interfacial tension experiment with a 1.8 mm diameter syringe which lead to a final percent error of approximately 8%. The larger percent error is due mainly to the error in the refractive index, $n$.

| Variable | % Error |
|---|---|
| $B$ | 1.5 |
| $a$ (pixels) | 2.0 |
| $\Delta\rho$ (g/cm$^3$) | 1.0 |
| $M$ (pixels/cm) | 1.0 |
| $n$ | 3.0 |

Table 6.2: Percent errors for interfacial tension experiments with 1.8 mm diameter syringe. $B$ is the dimensionless shape parameter, $a$ is the radius of curvature at the drop apex, $M$ is the magnification factor, $n$ is the optical correction factor and $\Delta\rho$ is the density difference between the phases.

## 6.4) COMPUTER PROGRAMS

The code for Sigmaplot which determines the radius of curvature at the drop apex and the Winbatch program used to automate the measurements are reprinted in the appendix.

### 6.4.1) AUTOMATED RECORDING OF DROP IMAGES

After extruding the pendant drop, the user initiates the program which independently records images of the pendant drop profile at specified time intervals. Once the pendant drop experiment is finished, the images are analyzed to determine the equilibrium value of interfacial tension. The program works by automating keystrokes within the imaging software, TCPro. It was written using the WinBatch language developed by Wilson WindowWare.

### 6.4.2) DROP PROFILE ANALYSIS PROGRAM

The drop profile analysis program has three main components. The code for the pendant drop profile analysis program can be found in Demarquette's thesis[74].

#### 6.4.2.1) EDGE DETECTION

An edge detection program is used to obtain the drop contour from a digitized drop image. The program scans the image and detects the contours of objects by differences in gray levels. Once a pixel reaches a gray level higher than a threshold value it is defined to be part of the object. Girault[29] proved that the value of interfacial tension is affected by less than 1%, depending on whether the threshold value or the previous pixel is taken as the drop contour. The outermost points form the contour of the object.

#### 6.4.2.2) PROFILE SMOOTHING

The smoothing program fits a continuous polynomial curve to the drop contour points. It eliminates small irregularities in the drop profile. The smoothing is done piecewise (point by point replacement) along the whole profile of the drop. Due to an error in the smoothing routine, the program is unable to analyze certain images of drop profiles. The effects of the error can be minimized by changing the vertical position of the pendant drop on the recorded image and by recording a large number of images.

#### 6.4.2.3) SHAPE COMPARISON

A robust shape comparison between the experimental and theoretical profiles is performed by optimizing five separate parameters: three parameters for aligning the experimental drop profile to the coordinate system of the theoretical drop profile ($x$ and $z$ translation plus a rotation, $\theta$), one parameter for the dimensionless shape factor, $B$, which describes the shape of the drop, and one parameter for the scale factor of the drop, $c$, which adjusts the absolute size of the drop. The theoretical profile is obtained from

numerical solutions of the Bashforth and Adams[2] equation. The interfacial tension is then calculated from the scale factor, $c$, corresponding to the set of five parameters which minimizes the overall error and provides the optimal fit to the experimental profile, where $c$ is defined as:

$$c = \sqrt{\frac{\Delta\rho g}{\gamma}} \tag{6-11}$$

and $\Delta\rho$ is the density difference between the two fluid phases, $g$ is the gravity constant and $\gamma$ is the interfacial tension.

The modified version of Anastasiadis'[3] drop analysis program used in this study has two flaws, both of which occur during the shape comparison of the experimental drop profile to solutions of the Bashforth & Adams[2] equation.

The program can only generate a theoretical profile which matches the experimental drop profile if a portion of the experimental drop profile closest to the syringe is eliminated. This reduces the accuracy of the dimensionless shape factor, $B$, because it is not derived from the entire experimental drop profile. For large drop volumes, the fraction of the drop profile eliminated is relatively small (less than 10%) and it only marginally increases the total error. However, the relative fraction increases as the drop volume is decreased, further increasing the error for smaller drops. As a general rule, if the fraction of the drop profile omitted from the curve-fitting procedure exceeds 25%, the results should be discarded, as they are not necessarily representative of the entire drop profile.

In addition, the shape comparison program used for this study provided only the value of the dimensionless shape factor, $B$. The program does not give the value of the scale factor, c, which is used to calculate the interfacial tension. Therefore, a fix was implemented which calculates the radius of curvature at the drop apex, $a$, by fitting the equation of a circle to the drop profile. The interfacial tension can then be calculated with both $B$ and $a$ as in equation (6-7). Although the method works, it introduces additional error into the calculation of interfacial tension because of the uncertainty in estimating a

differential quantity at a single point from a series of discrete points that comprise the drop profile.

It is important to note that the reduction in accuracy caused by the problems with the shape comparison program does not invalidate interfacial tension results. In fact, the overall errors for the measurements are still relatively low and the accuracy and repeatability of the apparatus has been proven with several fluids. See section (6.3.5) for details on the error analysis and section (6.2) for details on the accuracy and standard deviation of surface tension measurements.

### 6.4.3 RADIUS OF CURVATURE

The radius of curvature at the drop apex, $a$, is calculated as the radius of the largest possible circle fitted to the drop profile whose average residual error does not exceed 1% of the radius of the fitted circle itself. SigmaPlot is used to fit the equation of a circle to the drop profile and a WinBatch program is used to automate the keystrokes to reduce analysis time.

## 6.5 MATERIALS

The high-density polyethylene is HDPE 04452N and the polystyrene (PS) is Styron 685D, both from Dow Chemicals. The linear low-density polyethylene (LLDPE) copolymers are experimental resins from Nova Chemicals. The densities of the linear low-density polyethylenes resins are found in Table 4.3. The Gnomix P-V-T apparatus was used to determine equations of state for the polymer resins in the melt state. Densities are in g/cm$^3$ and temperatures are in °C.

$$\rho_{HDPE} = 0.868 - 5.66 \cdot 10^{-4} T \qquad (6\text{-}12)$$

$$\rho_{PS} = 1.10 - 6.80 \cdot 10^{-4} T \qquad (6\text{-}13)$$

# 7) RESULTS AND DISCUSSION: EVALUATION OF THE PENDANT DROP METHOD

## 7.1) DETERMINATION OF EQUILIBRIUM STATE

Two criteria were established to determine the equilibrium state of a pendant drop: (i) the shape of the drop profile must remain constant for a predetermined period of time; (ii) the interfacial tension, which depends on the shape of the pendant drop, must also remain constant for a predetermined period of time. At first, it may appear that only one of the above criteria would be sufficient, as they both reflect the shape of the drop over time. However, the results presented will demonstrate the need for the two separate criteria.

The period of time required to establish equilibrium for either of the criteria is usually 20-40% of the equilibrium time itself. An interfacial tension experiment with polymer melts at relatively low temperatures, may take 24 hours to reach equilibrium. To properly determine equilibrium in this case, the two criteria would have to be satisfied for a period of time of approximately 4.8 hours or 20% of the equilibrium time itself. On the other hand, a surface tension experiment may take only 2-3 hours to reach equilibrium, in which case the time required to establish equilibrium would be approximately 40% of the equilibrium time itself or 60 minutes.

### 7.1.1) DROP DIMENSIONS

The first criterion to determine equilibrium requires a static or unchanging drop profile for a predetermined amount of time. The maximum length and diameter of the pendant drop are easily measured and characterize the shape of the drop profile. The drop dimensions are monitored over time with the TCPro imaging software. The pendant drop is assumed to have reached equilibrium once the maximum drop length and diameter reach a constant value.

During experiments to measure the interfacial tension between LLDPE *A* and PS, the dimensions of a pendant drop were monitored and the initial extruded drop volume was varied. The maximum length (Fig. 7.1) and diameter (Fig. 7.2) of the largest drop (1) did not stabilize. Drops 2 and 3 reached a stable drop length and diameter between 5 and 6.5 hours. Therefore, drops 2 and 3 were assumed to have reached equilibrium and had a drop volume less than the critical volume while the first drop did not reach equilibrium and its volume was assumed to be larger than the critical volume.

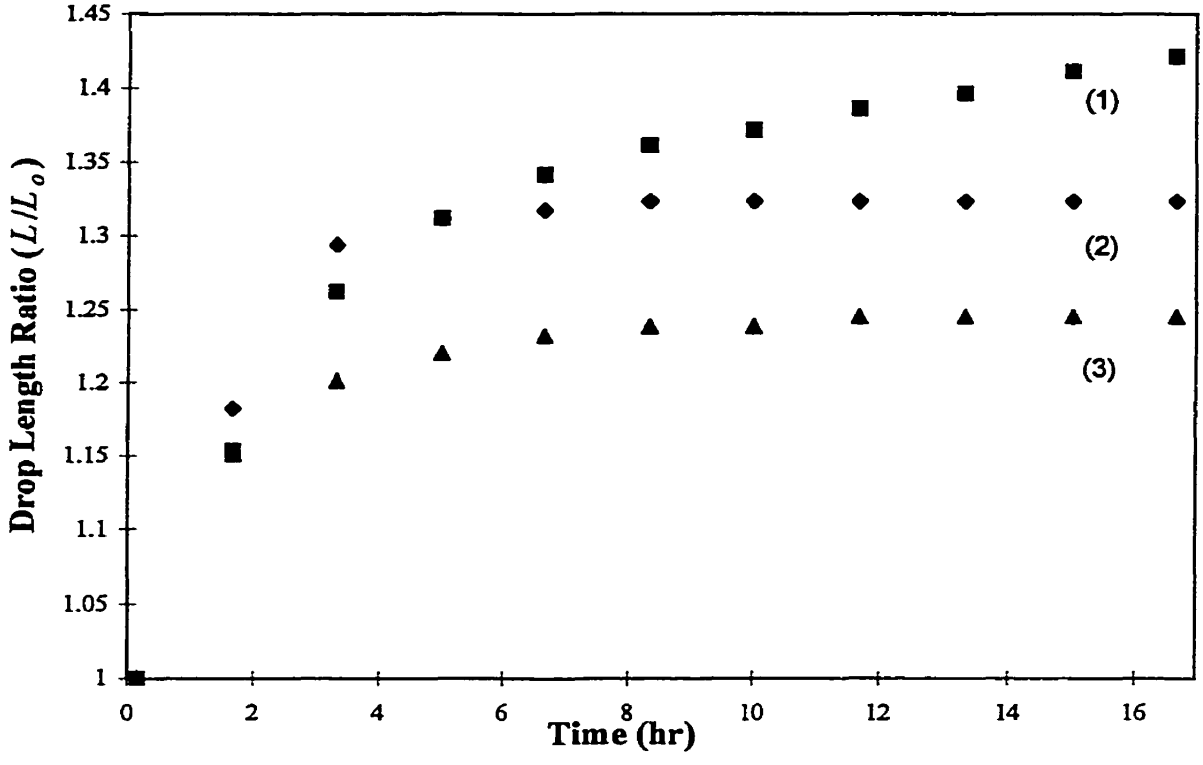


Fig. 7.1: Drop Length Ratio ($L/L_o$) as a function of time for LLDPE A/PS at 200 °C, where $L$ is drop length at time $t$ and $L_o$ is initial drop length. Symbols: 1(■): $L_o$=0.21cm, 2(◆): $L_o$=0.18cm, 3(▲)$L_o$=0.16 cm

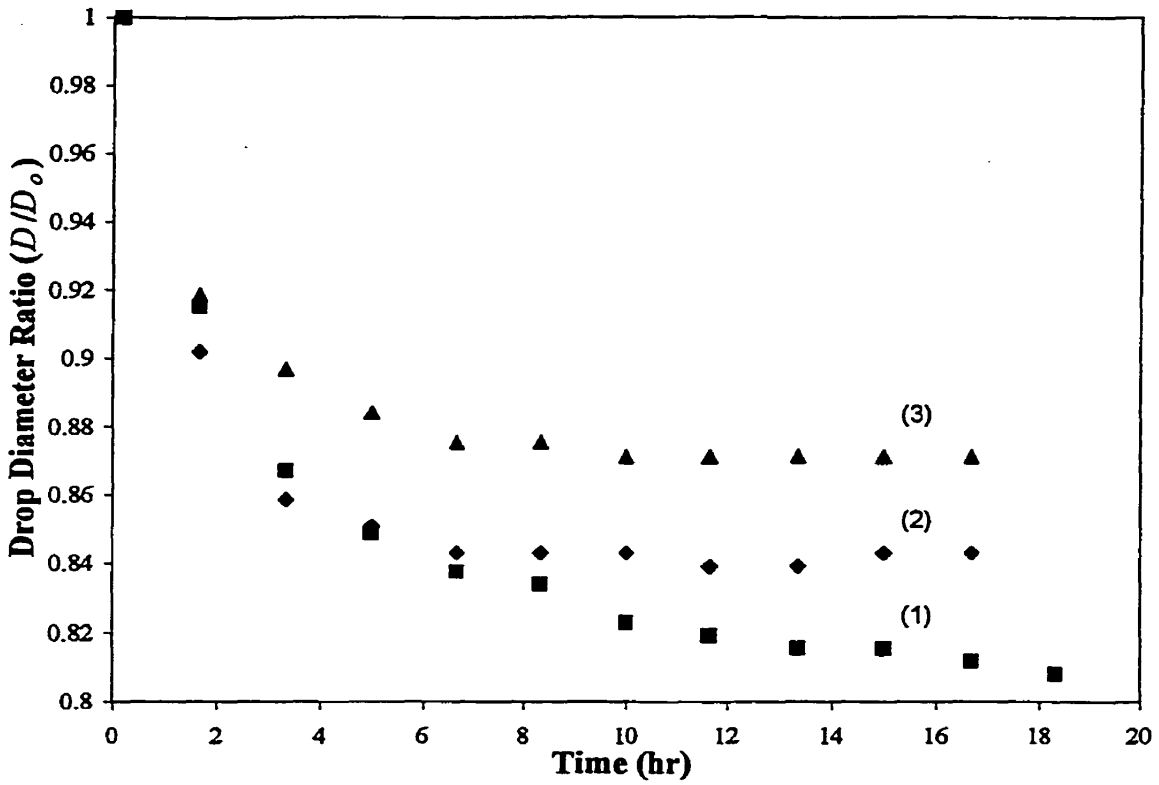


Fig. 7.2: Drop Diameter Ratio ($D/D_o$) as a function of time for LLDPE A/PS at 200 °C, where $D$ is drop diameter at time t and $D_o$ is initial drop diameter. Symbols: 1(■):$D_o$=0.13cm, 2(◆):$D_o$=0.11cm, 3(▲): $D_o$=0.08 cm

In the later stages of the pendant drop experiment, the drop length ratio (Fig 7.1), for curve (1) is increasing by approximately 0.007 $hr^{-1}$ and the drop diameter ratio (Fig 7.2) is decreasing by approximately 0.003 $hr^{-1}$. The drop length ratio, $L/L_o$, is defined as the ratio of the drop length at time $t$, $L$, to the initial drop length, $L_o$, and the drop diameter ratio, $D/D_o$, is defined as the ratio of the drop diameter at time $t$, $D$, to the initial drop diameter, $D_o$. Although the change in the drop dimensions is very slow, due to the high viscosity of both polymer melts, it clearly indicates that the first drop is not in equilibrium. If the drop dimensions are not carefully monitored over time, an unstable drop can be mistaken for a drop that has reached equilibrium, and this would increase the error in an interfacial tension measurement.

To summarize, the inspection of drop dimensions accomplishes two goals: (i) it can quickly assess equilibrium without the need to calculate the interfacial tension from the

drop profiles, which is a time-consuming process; (ii) it identifies unstable drops which reduce the accuracy of interfacial tension measurements.

### 7.1.2) INTERFACIAL TENSION

Once a stable drop is obtained, as indicated by the length and diameter measurements, the drop profiles are analyzed to determine the equilibrium value of interfacial tension.

The interfacial tension for the stable drop, (curve (2), Fig. 7.3), reaches equilibrium within 7-8 hours. Recall, that the equilibrium time, first determined by monitoring the maximum drop length and diameter (Fig. 7.1 and 7.2), occurs between 5 and 6.5 hours. The equilibrium time determined by monitoring drop dimensions is only an approximation to the true equilibrium time, which must be determined by the interfacial tension. The drop profile only reaches equilibrium when the entire drop shape is constant. By monitoring only the maximum drop length and diameter, further small changes in the drop shape are ignored, but are detected by the profile analysis program, as it determines the interfacial tension from the entire drop profile. Therefore, the true equilibrium time, determined by the interfacial tension, usually occurs some time after the maximum drop dimensions appear to reach a constant value.

The most common criterion for equilibrium requires a minimum variation in several measurements of interfacial tension over a predetermined period of time. An example is the criterion employed by DeMarquette et al.[5]: equilibrium was assessed when the variation of interfacial tension was less than 2% from measurements taken every 10 minutes over a period of two hours. Curve (1) in Fig. 7.3 shows the apparent interfacial tension as a function of time for the unstable drop, which was confirmed by measuring the drop dimensions over time (Fig. 7.1 & 7.2). Applying the criterion for equilibrium established by DeMarquette et al.[5] to the apparent interfacial tension data in curve (1), the drop would qualify for equilibrium, as the standard deviation in the data during the period of time, 11.5-14.5 hours, is only 0.025 dyne/cm or 0.5%, even though the drop is

unstable. In fact, the standard deviation in the apparent interfacial tension for the unstable drop from 8-16 hours is only 2.2%. This example demonstrates that the standard criterion to determine equilibrium may be inadequate for interfacial tension experiments with long equilibration times. An incorrect determination of equilibrium will increase the error in the reported value of interfacial tension. If equilibrium were determined for the unstable drop (curve (1) in Fig. 7.3) according to the criterion established earlier, it would result in a value of interfacial tension of 4.85 dyne/cm. This is almost a full 0.3 dyne/cm greater than the true value of interfacial tension, 4.57 dyne/cm, obtained from curve (2) in Fig. 7.3, which was based on the largest stable drop, as confirmed by monitoring drop dimensions. Generally, the increased drop volume associated with a necking drop is accompanied by an increase in the apparent value of interfacial tension. On the other hand, drop retraction decreases the drop volume and usually causes a reduction in the apparent value of interfacial tension.

The criterion presently used by most researchers to determine equilibrium is inadequate as it only accounts for the variation of the interfacial tension over a short period of time, which can lead to an incorrect assessment of equilibrium. A more precise method to determine equilibrium uses the correlation coefficient to measure the strength of association between the value of interfacial tension and time. The data from curve (2) in Fig. 7.3 after 7.7 hours has a correlation coefficient of 0.096 indicating that the interfacial tension is not changing with time and has reached equilibrium. The standard deviation in the data is 0.03 dyne/cm or 0.65% and is due to random experimental error. On the other hand, the data from curve (1) in Fig. 7.3 has a correlation coefficient that is higher than 0.96 for any period of time after 4 hours and this indicates that the first drop is unstable.

The recommended criteria for establishing the equilibrium state are: (i) a correlation coefficient of less than 0.1 and (ii) a percent standard deviation of less than 2%. Both criteria should be based upon a period of time approximately 20-40% of the equilibrium time itself. The limit for the correlation coefficient can be increased to compensate for the potential effects of thermal degradation, which can slowly reduce the measured value of interfacial tension over time.

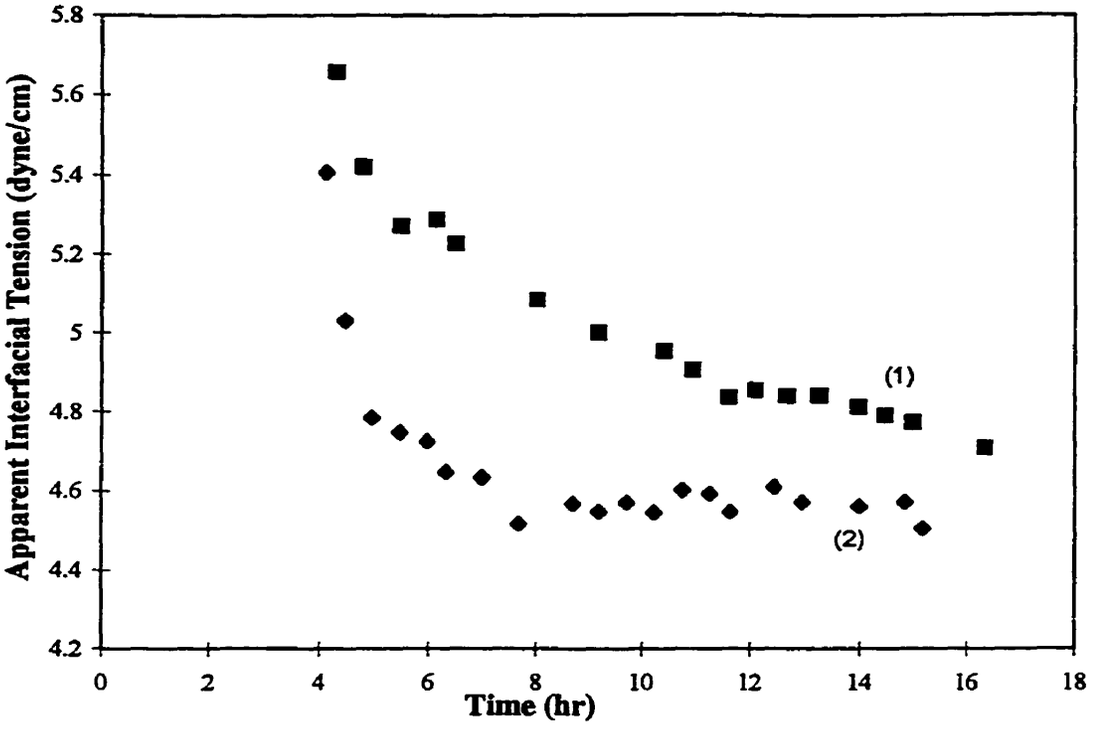


Fig. 7.3: Apparent interfacial tension as a function of time for LLDPE A/PS at 200 °C. Symbols: 1(■): $L_o$=0.21 cm, 2(◆): $L_o$=0.18 cm

## 7.2) ACCURACY AND STANDARD DEVIATION OF SURFACE TENSION MEASUREMENTS

### 7.2.1) ACCURACY

The accuracy of the pendant drop apparatus was confirmed with the 1.8 and 4.0 mm diameter syringes with ethylene glycol and water (Table 7.1), two liquids whose surface tensions are well defined in the literature. It is difficult to assess the accuracy of pendant drop apparatus with polymer melts because their surface and interfacial tensions depend on composition. The values of surface tension were determined from drops close to the critical drop volume, as it has been proven by Lin et al.[38,39] that the largest, stable drop yields the most accurate determination of drop volume.

| Liquid | Syringe diameter (mm) | $\gamma_{Exp}$ (dyne/cm) | $\gamma_{Lit}^{(22)}$ (dyne/cm) | % Error |
|---|---|---|---|---|
| **Water** | 1.8 | 68.7 | 72.0 | 4.6 |
| **Ethylene Glycol** | 4.0 | 43.1 | 47.3 | 8.9 |

Table 7.1: Experimentally determined values of surface tension, $\gamma_{Exp}$, for water and ethylene glycol compared to literature values, $\gamma_{Lit}$. Values for 25 °C.

The experimental error for the values of surface tension are significant, particularly for the 4 mm diameter syringe, and is uncharacteristic of measurements with the pendant drop apparatus. The pendant drop apparatus at McGill University was designed to measure the surface and interfacial tensions of viscous polymer melts, not low viscosity liquids, such as water and ethylene glycol. It was not possible to produce stable pendant drops with the liquids without making major modifications to the pendant drop apparatus. Therefore, all the surface tension measurements with low viscosity liquids were from unstable pendant drops, which introduces additional experimental error. Unstable drops of low viscosity liquids can still yield reasonably accurate measurements of interfacial tension because the drop profile is assumed to reach equilibrium almost instantaneously (Wu[8]). Drops from the 1.8 mm diameter syringe either necked or retracted slowly and their profiles were used as reasonable approximations to equilibrium profiles of the same drop volume. However, drops formed with 4 mm diameter syringe fluctuated rapidly in size and shape for an unknown reason and increased the experimental error of the measurements. This behavior was not observed with drops from the smaller syringe.

### 7.2.2) STANDARD DEVIATION

The standard deviation of surface tension measurements with the pendant drop apparatus was assessed from blind tests with several LLDPE resins. The surface tensions were calculated from the largest stable drop volume.

| Resin | Surface Tension (dyne/cm) | Standard Deviation |
|---|---|---|
| A | 23.3<br>23.6<br>23.9<br>23.4<br>23.7<br>23.4 | 0.22 |
| C | 24.0<br>24.4<br>24.5 | 0.30 |
| D | 26.5<br>26.4 | 0.11 |
| E | 27.9<br>27.9 | 0.01 |

Table 7.2: Standard deviation of surface tension measurements from several LLDPE resins with the 1.8 mm diameter syringe. Values for 160 °C.

## 7.3) EFFECT OF DROP VOLUME ON SURFACE TENSION MEASUREMENTS

### 7.3.1) SURFACE TENSION OF HEPTANE

The surface tension of heptane was determined experimentally from a range of drop volumes, with two different syringe diameters, 1.8 and 4 mm to verify the dependence of surface tension on drop volume, as experimental results of Lin et al.[38,39] have not been independently reproduced or confirmed in the literature. A simple liquid was chosen, because its surface tension is well defined in the literature.

#### 7.3.1.1) SURFACE TENSION OF HEPTANE W/ 1.8 mm DIAMETER SYRINGE

The surface tension of heptane is clearly a function of drop volume for the smaller syringe diameter (Fig. 7.4). The surface tension increases linearly with drop volume between 5.5 and 11.5 $mm^3$, before reaching a constant value of 19.7 dyne/cm between 11.4-13.3 $mm^3$, which is within 2.2% of the literature value of heptane (20.14 dyne/cm).

The drop profile analysis program could not fit the Bashforth and Adams[2] equation to drop volumes smaller than 5.5 $mm^3$.

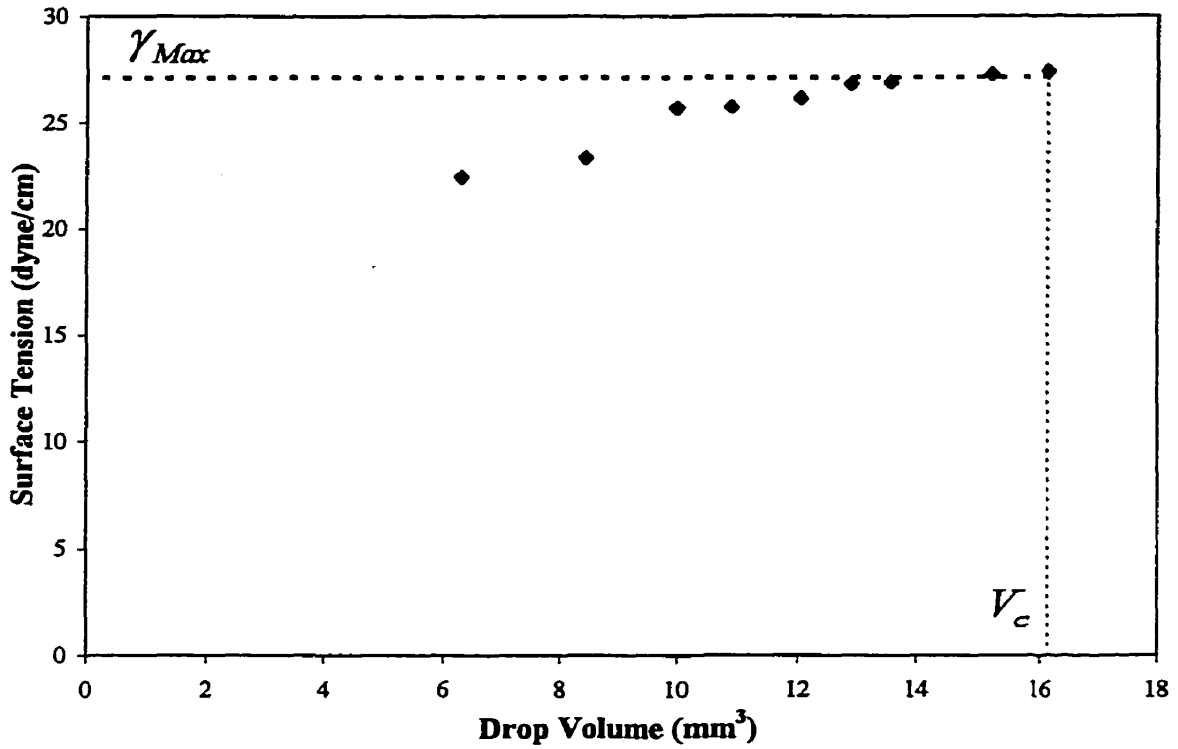


Fig. 7.4: Surface Tension as function of drop volume for heptane at 23 °C with inner syringe diameter, $d$=1.8 mm. $\gamma_{Lit}$: Literature surface tension value of heptane, 20.14 dyne/cm. $V_c$: Critical Drop Volume

### 7.3.1.2) SURFACE TENSION OF HEPTANE W/ 4 mm DIAMETER SYRINGE

For the larger syringe, it was difficult to assess the effect of drop volume on the surface tension of heptane due to the degree of scatter in the data (Fig. 7.5). The scatter in the surface tension measurements of heptane with the large syringe diameter is related to problems with drop stability and is explained in section (7.2.1). A correlation coefficient ($r$) of 0.7 was calculated with the data that indicates that the surface tension of heptane is increasing with drop volume. In addition, it appears that the surface tension data can be divided into two groups: drop volumes less than 19 $mm^3$ and those greater than 19 $mm^3$. It was confirmed with statistical analysis (t-test) that the means of the two

groups were different: for drop volumes less than 19 $mm^3$, the surface tension has a mean of 19.0 ± 0.4 dyne/cm, while for drop volumes greater than 19 $mm^3$, the surface tension has a mean of 20.9 ± 0.4 dyne/cm. It is not known why an abrupt change in the surface tension occurs at 19 $mm^3$, but it is possible that the scatter in the surface tension measurements masks a smooth linear increase of surface tension with drop volume, like that found previously with the smaller syringe (Fig. 7.3). Note that the average surface tension of all the measurements is 19.9 dyne/cm, which is very close to the literature value of the surface tension of heptane, listed at 20.14 dyne/cm.

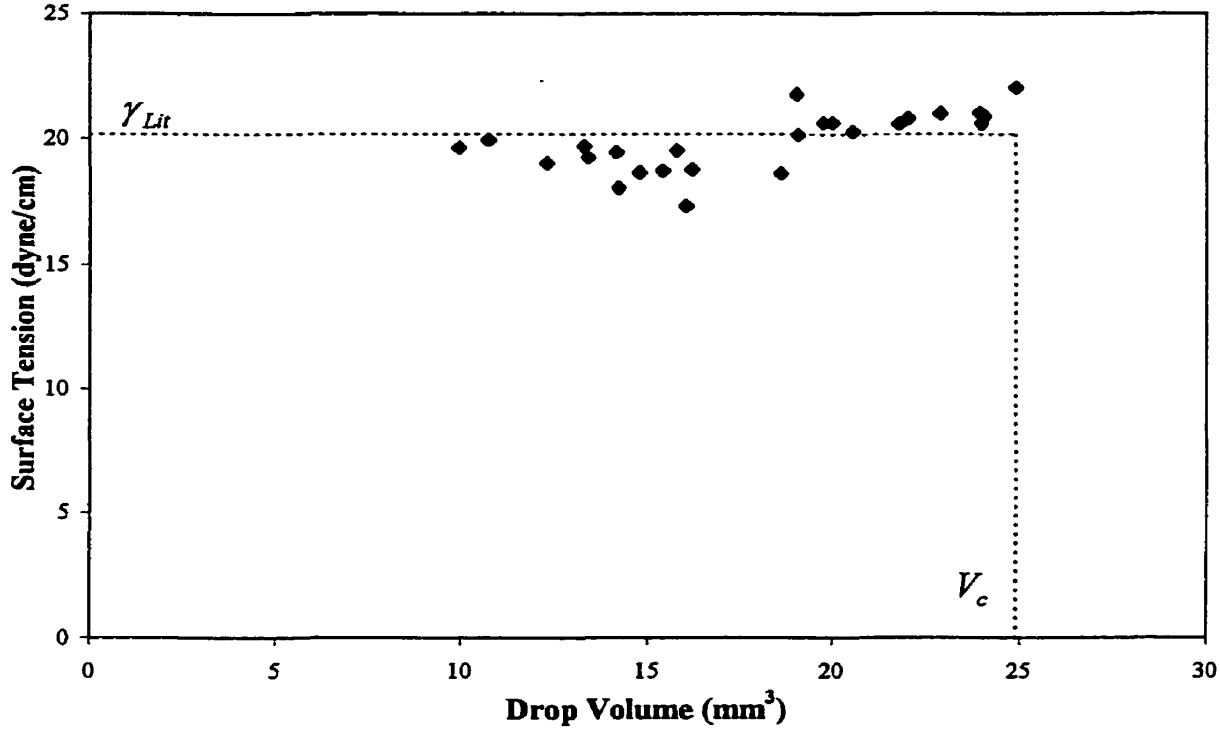


Fig. 7.5: Surface Tension as function of drop volume for heptane at 23 °C with inner syringe diameter $d$=4 mm. $\gamma_{Lit}$: Literature surface tension value of heptane, 20.14 dyne/cm, $V_c$: Critical Drop Volume

## 7.3.2) SURFACE TENSION OF LLDPE E

To evaluate the effect of drop volume, for polymer melts, the surface tension of LLDPE E was measured with both the 1.8 mm and 4 mm diameter syringe. It is suggested that the maximum experimental value of surface tension is the most accurate

surface tension measurement, which is justified by the results obtained with heptane and the results published by Lin et al.[38-39].

### 7.3.2.1) SURFACE TENSION OF LLDPE E W/ 1.8 mm DIAMETER SYRINGE

The surface tension of LLDPE E was determined experimentally from a range of drop volumes, 6-16 $mm^3$, with the 1.8 mm diameter syringe. The data in Fig. 7.6 indicate that the surface tension of LLDPE E is a function of drop volume for the 1.8 mm diameter syringe. The surface tension increases asymptotically with drop volume and reaches a maximum value of 27.1 dyne/cm for drop volumes greater than 12.9 $mm^3$. Note that the value of surface tension increases slightly for drop volumes greater than 12.9 $mm^3$, but the difference (2.2%) is not significant as it less than the experimental error of the measurements.

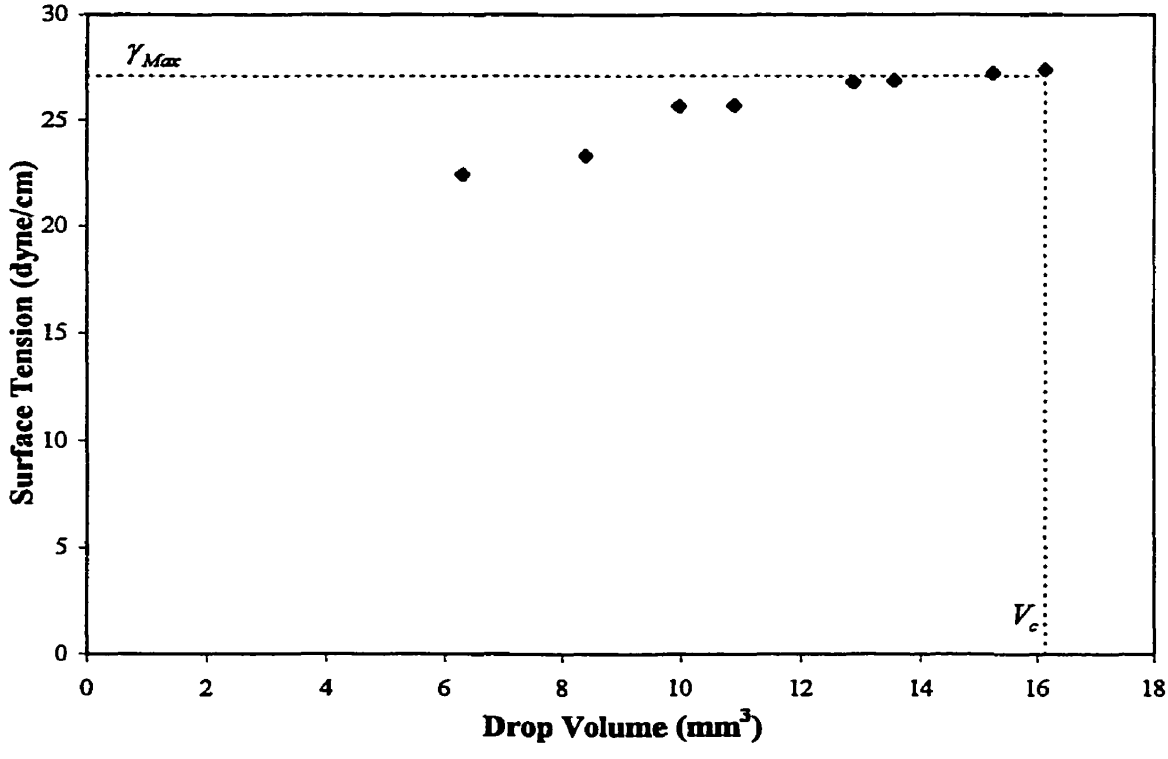


Fig. 7.6: Surface Tension of LLDPE E as a function of drop volume at 160 °C with syringe diameter $d$ = 1.8 mm. $\gamma_{Max}$: Maximum surface tension $V_c$: Critical Drop Volume

### 7.3.2.2) SURFACE TENSION OF LLDPE E W/ 4 mm DIAMETER SYRINGE

The surface tension of LLDPE E was determined with the 4 mm diameter syringe from a range of drop volumes, 12.3-30.8 $mm^3$. The data, displayed in Fig. 7.7, suggest that the experimentally determined surface tension of LLDPE E is also a function of drop volume. The surface tension of LLDPE E increases asymptotically from its lowest value, 22.3 dyne/cm at 12.3 $mm^3$, to its maximum value of 28.7 dyne/cm 22.5 $mm^3$. The values of surface tension do increase slightly from 22.5 $mm^3$ to the critical drop volume (30.8 $mm^3$) but the difference is not significant.

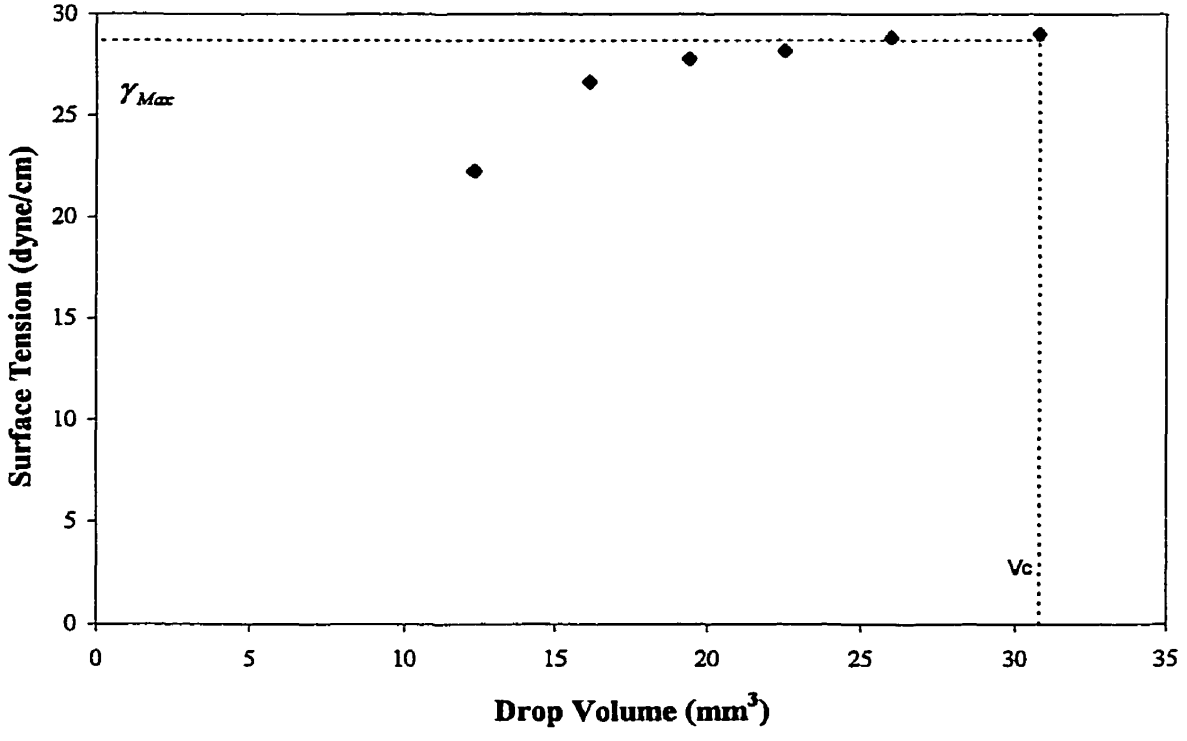


Fig. 7.7: Surface Tension of LLDPE E as a function of drop volume at 160 °C with syringe diameter $d$ = 4 mm. $\gamma_{Max}$: Maximum surface tension $V_c$: Critical Drop Volume

## 7.4) EFFECT OF SYRINGE DIAMETER

The effect of the syringe diameter on surface tension measurements is determined by comparing the data obtained from pendant drop experiments with the 1.8 and 4.0 mm syringe diameter for the two fluids: heptane and LLDPE E. The results which will be compared for the two syringe diameters are; (i): the maximum value of surface tension, (ii): The minimum drop weight to surface force ratio, $\xi_{Min}$, which represents the ratio of the smallest drop volume that yields the literature value of surface tension, (iii): the range of drop volumes that yield the maximum value of surface tension and (iv): the dependence of surface tension on drop volume, $d\gamma/dV$.

$$\xi_{Min} = \frac{\Delta\rho V_\gamma g}{2\pi R\gamma} = \frac{GravitationalForce}{SurfaceForce} \qquad (7\text{-}1)$$

Table 7.3 lists the results obtained with heptane and LLDPE E for the two syringe diameters.

| Fluid | Syringe Diameter (mm) | (i) $\gamma_{Max}$ (dyne/cm) | (ii) $\xi_{Min}$ | (iii) Volume Range ($mm^3$) | (iv) $d\gamma/dV$ (dyne/cm/$mm^3$) |
|---|---|---|---|---|---|
| **Heptane** | 1.8 | 19.7 | .68 | 1.9 (11.4-13.3) | 0.72 |
| **Heptane** | 4.0 | 20.9 | .48 | 5.9 (19.0-24.9) | 0.17 |
| **LLDPE E** | 1.8 | 27.1 | .64 | 3.2 (12.9-16.1) | 0.65 |
| **LLDPE E** | 4.0 | 28.7 | .48 | 8.3 (22.5-30.8) | 0.24 |

Table 7.3: Comparing results for heptane and LLDPE for two syringe diameters: 1.8 and 4.0 mm. (i) $\gamma_{Max}$: Maximum value of surface tension. (ii) $\xi$: Drop weight to surface force ratio where the drop volume is the smallest drop to yield the maximum value of surface tension. (iii) Volume range: Range of drop volumes which yield the maximum value of surface tension. Bracketed term shows the absolute values of the range. (iv) $d\gamma/dV$: The dependence of surface tension on drop volume for volumes less than in (iii).

The maximum value of surface tension for both syringe diameters compared reasonably well, but the larger syringe yielded a 6% higher value of surface tension with both fluids. The minimum drop weight to surface force ratio, $\xi_{Min}$, is decreasing for both fluids as the syringe diameter is increased. The range of drop volumes that yield a constant, maximum value of surface tension increases as the syringe diameter is increased for both fluids. The

dependence of surface tension on drop volume, $dy/dV$, was calculated from the linear region in the data before the surface tension reached a constant, maximum value. For both fluids, the slope, $dy/dV$, decreased as the syringe diameter was increased. The decrease in $\xi_{Min}$ implies that a smaller drop volume, relative to the syringe diameter, is needed to obtain the maximum value of surface tension for the syringe with the larger diameter syringe. The range of drop volumes that provide the maximum constant value of surface tension is also larger for the 4.0 mm diameter syringe. It can be concluded from the previous results that it is easier to obtain an accurate measurement of surface tension with a larger syringe diameter.

Next, the data will be compared to results obtained by Lin et al.[38,39]. Comparing the values for $\xi_{Min}$, (Table 7.3 and Fig. 7.8), the results for the 1.8 and 4 mm diameter syringes are similar to those obtained by Lin et al. with 0.4 and 1.2 mm diameter syringes, respectively. The range of drop volumes which provide the maximum value of surface tension and the effect of drop volume on surface tension also compare well (see section 5.6.3 for results of Lin et al.[38,39]). Therefore, the trends observed with increasing syringe diameter are in agreement with results obtained by Lin et al., but we are observing similar effects at larger syringe diameters. It is theorized that the effects of drop volume on surface tension are due to the influence of the syringe body on the shape of the drop profile as explained in sections (5.5.2) and (5.6.3). Both studies used a typical grade stainless steel for the syringe body, so the increased effect is probably not caused by a difference in materials. It is not known precisely what caused the increased effect of drop volume on the value of interfacial tension compared to the results obtained by Lin et al.[38,39].

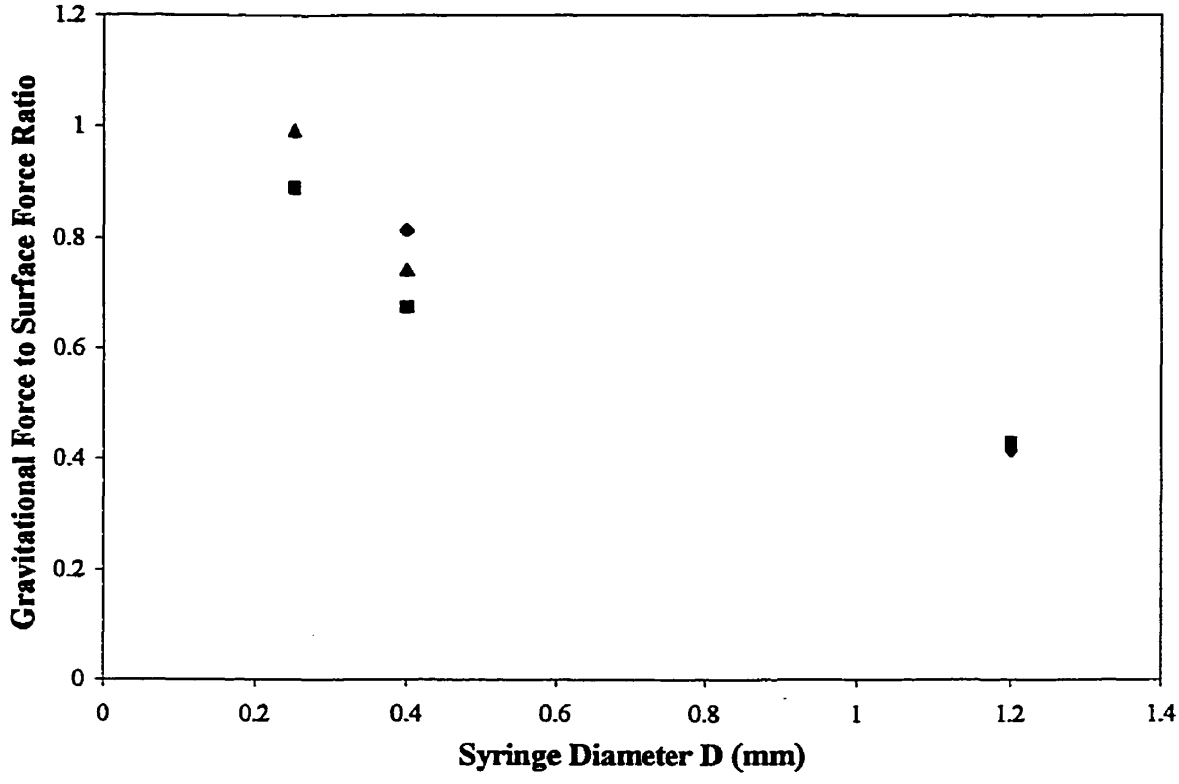


Fig. 7.8: Gravitational to surface force ratio, $\xi=\Delta\rho V_\gamma g/2\pi R\gamma$ for 3 syringe diameters (0.2, 0.4 and 1.2 mm) and 3 fluids (◆: water, ■: glycerol, ▲: ethylene glycol), where $\Delta\rho$ is the density difference between the phases, $V_\gamma$ is the smallest drop volume which yields the literature value of surface tension, $\gamma$, $g$ is the gravitational constant, and $R$ is the syringe radius. Data from Lin et al.[38].

# 8. CONCLUSION

## PART 1: SURFACE TENSION OF LLDPE

### 8.1) DENSITY

The structural differences between the resins had no significant effect on their melt densities. The largest density difference between the resins was less than 1% and is of the same order of magnitude of the measurement error of the P-V-T apparatus. This implies that the cohesive energy densities of the resins are similar and are not responsible for the apparent differences in surface tension.

### 8.2) EFFECTIVE MOLECULAR WEIGHT

For a linear polymer, the number average molecular weight represents the molecular weight between chain ends and can be used to characterize bulk polymer properties because it accurately reflects the concentration of free ends compared to the number of main chain units. For a branched polymer, it was theorized that the number average molecular weight does not characterize bulk polymer properties because it does not account for the branched ends, which are similar to main chain ends. The effective molecular weight considers the concentration of all the free ends. The effective molecular weight accounts for the surface tension differences among the LLDPE hexene copolymer series. The relationship could not be confirmed for the other α-olefin copolymers due to lack of data.

### 8.3) POLYDISPERSITY

It was theorized that the effects of polydispersity on the value of surface tension were minimal for LLDPE copolymers produced with Metallocene catalysts and were significant for those produced with Ziegler-Natta catalysts. The difference in the effect of polydispersity among catalyst type is due to structural differences that exist among the resins. The effects of polydispersity are believed to be responsible for a large surface tension reduction noted in sample G.

### 8.4) EFFECT OF α-OLEFIN COPOLYMER

It was difficult to assess the effect of the α-olefin copolymer (length of the alkyl branches) on the surface tension of the LLDPE resins due to the limited data available. However, from the experimental results, it is clear that differences between the α-olefin series exist, although no clear trends are apparent.

## 8.5) FREE VOLUME

Branched ends have a larger free volume than a repeat unit and the thermal expansion coefficient is a partial measure of free volume. As the thermal expansion coefficient of the LLDPE copolymer resins increased, the surface tension decreased linearly, which appears to support the relationship between the surface tension and the concentration of the branched ends.

## 8.6) COMPARISONS OF LLDPE SURFACE TENSION WITH LITERATURE

The values of surface tension of the LLDPE resins compared well with the surface tension of several branched PE resins measured by Dettre and Johnson[63]. Also, the concept of effective molecular weight appeared to explain observed trends in the literature data.

The surface tension of the LLDPE resins was compared to literature values of surface tension of linear PE, in order to determine if there was a difference in surface tension between a linear and branched polymer of equal molecular weight. From the data available, there is no conclusive proof that branched polymers have lower values of surface tension than linear polymers of the same molecular weight. It was also unclear from the data whether the polymers should be compared on a number average molecular weight basis or effective molecular weight basis due to inconsistencies in the literature data.

## 8.7) SURFACE TENSION TEMPERATURE COEFFICIENTS

The surface tension temperature coefficients ($d\gamma/dT$) of the LLDPE resins compared reasonably well with literature values of branched PE. The surface tension temperature coefficients of the LLDPE resins compared well with values of linear PE calculated on an equal molecular weight and equal effective molecular weight basis. From the data available, it cannot be concluded that branched polymers have significantly different values of surface tension temperature coefficients than linear polymers of the same molecular weight.

## 8.8) COMMENTARY

The most important finding of this study is the concept of effective molecular weight and its effect on the surface tension of the LLDPE copolymers. If the effective molecular weight governs the surface tension of branched polymers, it should also apply to any other bulk polymer property. Future work should consist of the following: It should be verified independently that bulk polymer properties of branched polymers are governed by effective molecular weight. These tests should not be limited to the surface tension of polymers. Examples of other properties that could be tested are the glass transition temperature, density, thermal expansion coefficient etc.. Preferably the property tested should have well established values for linear polymers in the literature and the property should experience large changes with molecular weight. This would facilitate the comparison between linear and branched polymer properties and it could be determined whether the correct basis for comparison is effective or number average molecular weight. Once the effect of chain branching on polymer properties is verified, future work could study the effect of the α-olefin copolymer length on the bulk properties of polymers. The concept of predicting properties of branched polymers from linear polymers of equal effective molecular weight could prove useful as large amounts of data have been collected for linear polymers but data for branched polymers is limited.

# PART 2: PENDANT DROP METHOD

A detailed experimental procedure was proposed to measure the interfacial tension of polymer melts with the pendant drop apparatus. The procedure improves confidence in experimental results by establishing strict criteria to determine the equilibrium state of a pendant drop. This ensures that the interfacial tension measurements are not affected by dynamic factors of unstable drops. Measurements of interfacial tension were found to be dependent on drop volume and the maximum stable drop volume was shown to yield accurate interfacial tension measurements representative of literature values.

Drop volumes smaller than the maximum stable drop volume yielded reduced values of interfacial tension. At smaller drop volumes, it is believed that contact between the drop and the syringe body, which is unaccounted for in the Bashforth and Adams equation, alters the shape of the drop profile and reduces the measured value of interfacial tension. This explains the effect of syringe diameter on interfacial tension measurements. Larger syringes produce larger drops and their profiles are less

susceptible to the effects of the syringe due to their larger drop volumes. Thus, as syringe diameter increases, the effect of drop volume on the measured value of interfacial tension decreases.

The detailed experimental procedure was used to determine values of interfacial and surface tension with various polyethylene and polystyrene resins over a range of temperatures. The excellent agreement of the experimental results with the corresponding literature data validates the effectiveness of the experimental method.

## 9. References


1. A. Luciani, M. F. Champagne and Utracki L. A., *Polym. Networks Blends*, **6**, 51 (1996)
2. S. Bashforth, J. C. Addams, *An attempt to test the theory of capillary action*, Cambridge University Press, London (1882)
3. S. H. Anastasiadis, J. K.Chen, J. T. Koberstein, J. E. Sohn, J. A.Emerson, *Polym. Eng. Sci.*, **26**, 1410 (1986)
4. J. W. Jennings, N. R. Pallas, *Langmuir*, **4**, 959 (1988)
5. N. R. Demarquette, M. R. Kamal, *Polym. Eng. Sci.*, **34**, 1823 (1994)
6. S. Wu, *J. Colloid Interface Sci.*, **31**, 153 (1969)
7. S. Wu, *J. Phys. Chem.*, **74**, 632 (1970)
8. S. Wu, *J. Polym. Sci., Part C*, **34**, 19 (1971)
9. S. Wu, *J. Macromol. Sci. - Revs. Macromol. Chem.*, **c10**, 1 (1974)
10. S. Wu, *Polymer Interface and Adhesion*, Marcel Dekker Inc., New York (1982)
11. R. J. Roe, V. L. Bachetta, P. M. G. Wong, *J. Phys. Chem.*, **71**, 4190 (1967)
12. R. J. Roe, *J. Colloid Interface Sci.*, **31**, 228 (1969)
13. R. J. Roe, *J. Phys. Chem.*, **72**, 2013 (1971)
14. R. J. Roe, *J. Colloid Interface Sci.*, **31**, 228 (1971)
15. R. J. Roe, *J. Phys. Chem.*, **62**, 490 (1975)
16. B. Vonnegut, *Rev. Sci. Instrum.*, **13**, 6 (1942)
17. D. D. Joseph, M. Arney, G. Ma, *J. Colloid Interface Sci.*, **148**, 291 (1992)
18. S. Tomotika, *Proc. R. Soc.*, **150**, 322 (1935)
19. C. J. Carriere, A. Cohen, *J. of Rheol.*, **33**, 681 (1991)
20. D. Graebling, R. Muller, *Colloids and Surfaces*, **55**, 89 (1991)
21. H. Grassmespacher, J. Meissner, *J. Rheol.*, **36**, 1127 (1992)
22. A. W. Adamson, *Physical Chemistry of Surfaces*, Wiley, New York (1967)
23. J. N.Butler, B. H. Bloom, *Surface Science*, **4**, 1 (1966)
24. E. Helfand, Y. Tagami, *J. Phys. Chem.*, **56**, 3592 (1972)
25. J. W. Cahn, J. E. Hilliard, *J. Phys. Chem.*, **28**, 258 (1958)
26. S. H. Anastasiadis, I. Gancarz, J. T. Koberstein, *Macromolecules*, **21**, 2980 (1988)
27. L. A.Girifalco, R. J. Good, *J. Phys. Chem.*, **61**, 904 (1957)
28. J. M. Andreas, E. A.Hauser, W. B. Tucker, *J. Phys. Chem.*, **42**, 1001 (1938)
29. H. H. Girault, D. J. Schiffrin, B. D. V. Smith, *J.Electroanal. Chem.*, **93**, 207 (1982)
30. H. H. Girault, D. J. Schiffrin, B. D. V. Smith, *J. Colloid Interface Sci.*, **93**, 169 (1984)
31. H. C. Huh, R. L. Reed, *J. Colloid Interface Sci.*, **91**, 472 (1983)
32. Y. Rotenberg, L. Boruvka, A.W. Newman, *J. Colloid Interface Sci.*, **93**, 169 (1983)
33. A. F. Siegel Biometrica, **69**, 242 (1982)

34. A. F. Siegel, R. H. Benson, *Biometrica*, **38**, 341 (1982)
35. Y. Touhami, G. H. Neale, V. Hornof, H. Khalfalah, *Colloids Surfaces A: Physiochem. Eng. Aspects*, **112**, 31 (1996)
36. C. E. Stauffer, *J. Phys. Chem.*, **6**, 1933 (1965
37. D. O. Niederhauser, F. E. Bartell, Report of Progress - Fundamental Research on Occurrence and Recovery of Petroleum, American Petroleum Institute, Baltimore Md, 114-146, (1957)
38. S. Lin, L. Chen, J. Xyu, W. Wang, *Langmuir*, **11**, 4159 (1995)
39. S. Lin, W. Wang, L. Lin, L. Chen, *Colloids Surfaces A: Physiochem. Eng. Aspects*, **114**, 31 (1996)
40. G. T. Dee, B. B. Sauer, *Advances in Physics*, **47**, 161 (1998)
41. H. B. Callen, *Thermodynamics*, Wiley, New York (1960)
42. A. Silberberg, *J. Colloid Interface Sci.*, **125**, 14 (1988)
43. K. M. Hong, J. Noolandi, *Macromolecules*, 14, 1223 (1981)
44. Y. Rabin, *J. Polym. Sci. Lett. Edn.*, **22**, 335 (1984)
45. B. B. Sauer, G. T. Dee, *Macromolecules*, **4**, 26, (1991)
46. S. Sugden, *J. Chem. Soc.*, **125**, 32 (1924)
47. C. Jalbert, J. T. Koberstein, R. Balaji, Q. Bhatia, *Macromolecules*, **27**, 2409 (1994)
48. K. K. Chee, *J. Appl. Polym. Sci.*, **70**, 697 (1998)
49. D. G. Legrand, G. L. Gaines, *J. Colloid Interface Sci.*, **31**, 162 (1969)
50. K. S. Siow, D. Patterson, *Macromolecules*, **4**, 26 (1973)
51. S. K. Kumar, M. Vacatello, D. Y. Yoon, *Macromolecules*, **23**, 2189 (1990)
52. E. Kierlik, S. Phan, M. L. Rosenberg, *Density Functional Models in Chemistry*, American Chemical Society, New York (1996)
53. G. T. Dee, B. B. Sauer, *J. Colloid Interface Sci.*, **152**, 85 (1992)
54. P.-G. De Gennes, Scaling Concepts in Polymer Physics, Cornell University Press, Ithaca NY (1979)
55. D. Patterson, A. K. Rastogi, *J. Phys. Chem.*, **74**, 1067 (1970)
56. B. B. Sauer, G. T. Dee, *J. Colloid Interface Sci.*, **162**, 25 (1994)
57. M. R. Kamal, R. Lai-Fook, N. R. Demarquette, *Polym. Eng. Sci.*, **34**, 1834 (1994)
58. D. Broseta, G. H. Fredrickson, E. Helfand, L. Leibler, *Macromolecules*, **23**, 132 (1990)
59. K. H. Nam, W. H. Jo, *Polymer*, **36**, 3727 (1995)
60. J. Reiter, G. Ziffererer, O. F. Olaj, *Macromolecules*, **23**, 223 (1990)
61. G. T. Dee, B. B. Sauer, *Macromolecules*, **26**, 2771 (1993)
62. A. Hariharan, S. K. Kumar, *Macromolecules*, **23**, 3584 (1990)
63. R. H. Dettre, R. E. Johnson, *J. Colloid Interface Sci.*, **21**, 367 (1966)
64. G. G. Allan, A. N. Neogi, *J. Appl. Polym. Sci.*, **14**, 999 (1970)

65. J. J. Jasper M. Nakonecznyj, C. S. Swingley, H. K. Livingston, *J. Phys. Chem.*, **74**, 1535 (1970)
66. D. K. Owen, *J. Phys. Chem.*, **74**, 3305, (1970)
67. G. T. Dee, T. Ouzigawa, D. J. Walsh, *Polymer*, **33**, 3462 (1992)
68. C. J. Carriere, H.C. Silvis, *J. Appl. Polym. Sci.*, **66**, 1175 (1997)
69. G. T. Dee, B. B. Sauer, *Polymer*, **36**, 1673 (1995)
70. I. Prigogine, *The Molecular Theory of Solutions*, North-Holland Publsihing Company, Amsterdam (1957)
71. R. J. Roe, *Nat. Acad. Sci. U. S.*, **56**, 819 (1966)
72. D. Patterson, A. K. Rastogi, *J. Phys. Chem.*, **74**, 1067 (1970)
73. R. N. Haward, *J. Macromol. Sci.-Revs. Macromol. Chem.*, **C4**, 191 (1970)
74. N. R. Demarquette, *Interfacial Tension in Polymer Blends: Measurement and Analysis*, Ph. D. Thesis, Mcgill University, Montreal (1993)
75. J. P. Holman, *Experimental Methods for Engineers*, McGraw-Hill Inc., New York (1989)
76. *Kirk-Othmer Encyclopedia of Chemical Technology* (4$^{th}$ Edition), **17**, 756, John Wiley & Sons, New York (1996)
77. N. Rao, S. E. Wanke, Sundararaj U., *Canadian Chemical News*, 29, April (1998)
78. R. M. Joshi, B. J. Zwolinski, C. W. Hayes, *Macromolecules*, **1**, 31 (1968)
79. H. Schonhorn , L. H. Sharpe, *J. Polym. Sci.: Pt. A*, **3**, 569 (1965)
80. D. Patterson, *Pure Appl. Chem.*, **31**, 133 (1972)
81. H. M. Princen, I. Y. Z. Zia, S. G. Mason, *J. Colloid Interface Sci.*, **23**, 99 (1967)
82. H. T. Patterson, K. H. Hu, T. H. Grindstaff, *J. Polym. Sci., Part C*, **34**, 31 (1971)
83. D. D. Joseph, M. Arney, G. Gilberg, H. Hu, D.Hultman, C. Verdier, T. M. Vinagre, *J. Rheol.*, **36**, 623 (1992)
84. J. J. Elmendorp, G. Vos, *Polym. Eng. Sci.*, **26**, 415 (1986)
85. J. C. Hsu, R. W. Flumerfelt, *Transactions of the Society of Rheology*, **19**, 523 (1975)
86. H. H. Hu, D. D Joseph., *J. Colloid Interface Sci.*, **162**, 331 (1994)
87. G. T. Dee, B. B. Sauer, , *Macromolecules*, **24**, 2124 (1991)

# APPENDIX

## A.1) MOLECULAR STRUCTURE OF LLDPE

Linear low density polyethylene (LLDPE) is a copolymer of ethylene and α-olefin monomoers[76]. A typical LLDPE polymer molecule is generally desrcibed as:

$$\left[-\left(CH_2-CH_2\right)_n-\left(CH_2-CHR\right)-\right]_j \qquad \text{(A-1)}$$

where $n$ is the number of repeat units of the ethylene comonomer ($CH_2$-$CH_2$) within the overall repeat unit which has $j$ units and $CHR$ is the α-olefin comonomer where $R$ now corresponds to the length of the side chain or branch. The molecular structure of LLDPE is characterized by long sequences of ethylene units ($CH_2$-$CH_2$) which form the backbone of the polymer chain interuppted by single olefin units ($CH_2$-$CHR$) where $R$ corresponds to the length of the alkyl chain. For an LLDPE copolymer containing the α-olefin comonomer 1-butene, $R$ is two carbons long, for 1-pentene $R$ is three carbons long, etc.. The chain branching density, $\rho_b$, is defined as the number of branches per 1000 (or 100) carbons.

A typical LLDPE copolymer contains 2-4% of α-olefin comonomer but polymers are produced with α-olefin content ranging from 0.3-20 mol%. The most common α-olefins presently used in the production of LLDPE are 1-butene, 1-pentene, 1-hexene and 1-octene.

## A.2) EFFECT OF CATALYST ON LLDPE STRUCTURE

Catalysts are needed to incorporate the α-olefin comonomers into the ethylene chain because the ethylene comonomer has a much greater reactivity than the α-olefins, due to steric effects. Only α-olefins with the smallest alkyl groups (1-butene to 1-octene) can be easily copolymerized with ethylene due to the decrease in reactivity with increasing alkyl chain length. LLDPE resins are produced with either titanium based catalysts (Ziegler-Natta) or metallocene catalysts.

### A.2.1) ZIEGLER-NATTA CATALYSTS

All Ziegler-Natta (Z-N) catalysts contain mixtures of several different types of active centers, each of which produces polymer chains of different number average molecular weight. In addition each catalyst varies in its ability to incorporate the α-olefin comonomers into the ethylene chain, resulting in non-uniform chain branching. Usually the molecules of the smallest molecular weight have the highest degree of chain branching[76]. Thus, Z-N catalysts produce LLDPE copolymers with a broad molecular weight distribution and the α-olefin content (chain branching density) varies widely from molecule to molecule. A typical copolymer mixture produced with Z-N catalysts contains copolymer molecules with a broad range of compositions, from almost linear macromolecules, which are usually of a higher molecular weight, to short macromolecules with high α-olefin content. For example, a resin containing 3 mol% of α-olefin is in fact a mixture of of macromolecules with olefin contents ranging from below 0.3 mol% in the high molecular weight fraction of the resin, to over 20 mol% in fractions with the lowest molecular weight.

### A.2.2) METALLOCENE CATALYSTS

Metallocene catalysts contain only one type of active center. Thus, they produce ethylene α-olefin copolymers with narrow molecular weight distributions and uniform chain branching (α-olefin content).

## A.3) FREE VOLUME

The free volume is defined as follows[73]:

1) Expansion Volume

The free volume can be thought of as the volume change due to thermal expansion of initially close-packed molecules at 0° K.

$$V_f = V_T - V_o \qquad \text{(A-2)}$$

where $V_T$ is the volume at temperature T, $V_o$ is the volume occupied by the molecules at 0° K in a close-packed crystalline state and $V_f$ is the free volume.

2) Empty Volume

The free volume can also be thought of as the total volume less the Van der Waal's volume which represents the actual physical dimensions of the molecule:

$$V_f = V_T - V_w \qquad \text{(A-3)}$$

where $V_w$ is the Van der Waal's volume.

Note that there is only one type of empty space between molecules but the separate definitions allow the concept of free volume to be modelled in different ways.

## A.3.1) FREE VOLUME OF POLYMERS

The thermal expansion coefficient of polymers is considerably less than that of its corresponding monomer[80]. The difference in thermal expansion or free volume is due to differences in structure of the polymer and the monomer. As the monomer molecules are connected to form the polymer molecule, external, volume-dependent degrees of freedom of the monomer are replaced by low-amplitude vibrations internal to the polymer chain which do not affect the volume. Hence, the fraction of thermal energy which promotes liquid expansion is progressively reduced as the length of the polymer chain increases. However, a small counter-effect exists. As the monomers are joined to form the polymer, the dissapearance of the monomer ends reduces the total molecular surface available for intermolecular contacts. This decreases the total cohesive energy which resists thermal expansion. Both effects are taken into account by the Prigogine structural parameter ($c/q$) which is the ratio of the number of external degrees of freedom, $3c$ of the molecule, to the number of external contacts, $q$. The parameter $c/q$ decreases in passing from a monomeric liquid to a polymeric one. The parameter $c$ is a constant for a molecule of a given structure and it indicates the reduction in its degrees of freedom due to structural effects. For a small molecule liquid $c=1$ and for a macromolecule $c<1$. The free volume of a series of homologues decreases with increasing molecular weight through a decrease in the

structural parameter $c/q$. Furthermore, the decrease depends on the flexibility of the chain, that is the extent to which the valence bonds reduce the external degrees of freedom.

## A.4) SPINNING DROP METHOD

Vonnegut[16] was the first to suggest that the interfacial tension between two immiscible liquids could be measured by the deformation of a spinning drop of one liquid embedded in another liquid. A drop of the less dense liquid is inserted in a glass tube filled with the denser liquid. The tube is rotated at a given speed and temperature about the horizontal axis. The increase in the energy of the system, due to the centrifugal acceleration, increases the interfacial area of the drop. The drop changes from its initial spherical shape to that of a long cylindrical rod. At equilibrium, the centrifugal and interfacial forces are balanced and the drop shape remains static.

When the length of the drop is at least four times the drop diameter, the radius along the cylindrical drop can be considered constant and the curvature of the cylindrical endcaps can be ignored. The required length to diameter ($L/D$) drop ratio is achieved with high rotational speeds. Thus, the relation to determine interfacial tension is reduced to:

$$\gamma = \frac{\Delta\rho\omega^2 d^3}{32} \qquad \text{(A-5)}$$

where $\Delta\rho$ is the density difference between the liquid phases, $\omega$ is the rotational speed in radians per unit time and $d$ is the horizontal diameter of the drop. When the $L/D$ ratio is less than four, equation (A-5) may yield innaccurate estimations of the value of interfacial tension. Princen et al.[81] developed numerical solutions based on exact equations to calculate the interfacial tension for $L/D$ ratios less than four.

### A.4.1) EVOLUTION OF THE SPINNING DROP METHOD

Patterson et al.[82] were the first to use the spinning drop method to measure the interfacial tension of polymer melts. The equilibration times of the polymer systems studied were extremely long due to the high viscosity of the liquids and the low rotational

speeds of the spinning drop apparatus. However, a linear relationship was observed between the logarithm of the drop length and the reciprocal of time after a relatively short induction period. By extrapolating dynamic results to infinite time, steady state measurements could be accurately predicted after 10-20 minutes. Verdier[83] found similar results and confirmed the relationship for the drop radius, as well as drop length.

$$L(t) = L_\infty \exp\left(\frac{c}{t}\right) \qquad R(t) = R_\infty \exp\left(\frac{-d}{t}\right) \qquad \text{(A-6)}$$

$$\log[L(t)] = \log[L_\infty] + \frac{c}{t} \qquad \log[R(t)] = \log[R_\infty] - \frac{d}{t} \qquad \text{(A-7)}$$

Elmendorp et al.[84] improved the maximum rotational speed of the spinning drop apparatus while reducing vibrational effects. The higher rotational speeds reduces the time required to reach equilibrium for viscous polymer melt systems, which minimizes the effects of degradation. In addition, the use of very high rotational speeds can further reduce the equilibration times by forcing the drop to its equilibrium shape.

Joseph et al.[83] provided a comprehensive review of the spinning drop method and a detailed description of the apparatus and an experimental procedure. They also improved the relationship relating the transient behaviour of the spinning drop dimensions.

$$R(t) = R_\infty + (R_0 - R_\infty)e^{-m(t-t_0)} \qquad \text{(A-8)}$$

Joseph et al. [83] also proposed that the Hsu-Flumerfelt[85] theory of pure extension could be used to derive a relationship characterizing the equilibration time constant, $m$, of both Newtonian and visco-elastic fluids.

$$m = \left(\frac{\gamma^2 \Delta\rho}{4\omega}\right)^{\frac{1}{3}} \frac{1}{(\Delta\mu)} \qquad \text{(A-9)}$$

In a subsequent study, Hu et al.[86] improved the expression which characterized the equilibrium time constant. Numerical simulations indicated that the equilibration time depended on a complex function of the two polymer viscosities rather than a simple

viscosity difference. The results also indicated that the time constant was affected by the dimensions of the glass tube in addition to the other parameters from equation (A-9).

## A.5) DROP PROFILE ANALYSIS PROGRAM

The program is inititiated in MS-DOS by typing the command line [resto 1 "filename" 170 1] in the tape-e directory.

The edge detection program reduces the image of the drop to a contour by comparing colors of adjacent pixels. The drop refracts incoming light away from the camera lens so it appears as a black object on a white background. The contour is defined as the region where the black pixels change in color to white. If the drop is not adequately illuminated, the camera will not detect a transition in the pixel color at the drop interface and the program will not be able to establish the drop contour.

The program prompts the user to select a portion of the drop profile to analyze allowing the elimination of the syringe contour.

Next, the program smooths the drop contour. An error in the smoothing algorithm prevents certain drop images from being analyzed. If this problem is encountered re-record the drop image until the program can analyze it. Moving the camera so the image of the drop profile shifts on the screen can help.

The next stage of the program is the shape comparison routine. The program asks the user to specify a range of values of B. The program generates a profile from each value of B which it compares to the experimental drop profile and determines the sum of the residuals between the two curves. The optimum fit corresponds to the value of B which generates a profile that minimizes the sum of the residuals. The computer determines the residuals by three different methods, sr, srr and ten, thus generating three optimum fits.

The program requires the user to input the range of B values to be tested but the experimental value of B is unknown. Initially, the user must try a wide range of B (0.5-1.1) with a large step size (.01-.005) and 20-30 steps to determine an approximate value

of B, then, increase the precision by narrowing the step size (.002). If the correct value of B is outside the range of values tested, the optimum fit will usually correspond to a value close to either the upper or lower limit tested.

The optimum fit generated by the program to match the experimental profile can be visually inspected. Usually, the optimum fit does not match the experimental profile, exposing another serious flaw in the program. The user must rerun the program varying the percentage of the curve analyzed until the optimum fit visually matches the experimental profile perfectly.

When the program queries "do you want to cut the syringe?", answer yes and select the entire drop profile just below the syringe. The fit will most likely be poor as explained above. Rerun the program, this time choosing a smaller portion of the drop profile, perhaps 5-10 pixels below the previous point, which eliminated the syringe from the drop contour. The fit should improve as small portions of the drop profile are successively eliminated. This procedure is repeated until the profile generated by the program matches the experimental profile **perfectly**. If the profiles do not match, then the value of B provided by the program is meaningless as it does not represent the experimental drop profile shape.

The influence of the syringe body causes the closest points to deviate from the Bashforth & Adams equation, requiring their elimination to obtain a proper fit to the remaining experimental profile. Note, that only a small portion of the drop profile closest to the syringe should be eliminated to obtain a proper fit. If a large portion of the drop profile is eliminated, the fit generated by the B&A equn will not be representative of the true drop shape.

## A.6) RADIUS OF CURVATURE

Technically, the shape comparison program should provide the radius of curvature at the drop apex, as it is one of the adjustable parameters used to fit the Bashforth and Adams equation to the experimental drop profile. Once again, the program has an error, which calculates the radius of curvature incorrectly. It assumes the radius of curvature at

the drop apex, a, is the distance between the two furthest points on the curve which is incorrect.

The correct radius of curvature is calculated by fitting the equation of a circle to the drop profile. Because the drop profile is ellipsoidal and not a perfect circle, the radius of curvature is not a constant and increases, progressing along the drop profile from the apex to the equatorial diameter. The correct radius of curvature is determined by fitting a circle to an unknown portion of the drop profile which has an average residual of 1% of the radius of curvature itself.

In MS-DOS under tape-e, files are generated, each representing a different percentage of the drop profile, with the command line: [redtheo filename.ext newfilename.ext %]. The filename.ext is generated by visually inspecting the optimum fit to the experimental curve in the shape comparison program. Thus, there should be three files each with the same image filename, but a different extension: sr, srr or ten. The newfilename is the new filename denoted by the user. The extension can be any 3 characters but should be labeled .sr for reasons that will become clear later. The % is a number from 0-50 which indicates the percentage of the drop profile added to the new file. Files are generated with percentages varying from 35 to 45% of the drop.

Returning to windows, open SigmaPlot and press F5 then open cir.fit and then press F10 and open resid.xfm. Both programs are in the tape-e directory. The first file fits the drop profile to a circle and the second calculates the average residual between the profile and the fitted circle. Then execute a program called RofC10, (icon in Programs window) which is a winbatch file that automates the calculations within SigmaPlot. The program only works with an extension .sr which is why all files generated with the redtheo program must use this particular extension. After the program is completed a column with two numbers should be visible, the top number is the radius of curvature in pixels and the bottom number is the average residual. Try different percentages of the curve until obtaining a residual which is 1% of the radius of curvature.

## A.7) AUTOMATED RECORDING OF PENDANT DROP IMAGES

Open the TCPro imaging software and focus the digital camera on the drop. In the Windows group "Programs" is an owl icon labelled TimeRev6. Once executed, the program asks the user to enter a filename no more than 5 digits. I usually incorporate the data into the filename like "k0621": k for kevin, 06 is month, 21 is day. The program then asks a for the time in minutes between pictures. The program then makes an image labelled k0621sXX.tif every specified time interval. The s stands for sample number which is indicated by a two digit number the program assigns to each image 1-99. If the number of images exceeds 99, the program starts over using a different first letter specified within the program code, ie j0621s1-99 and then l0621s1-99. This allows a total of 300 images to be independently taken during any individual unmonitored experiment.

## A.8) PROGRAM CODE

Both programs use the Winbatch scripting language and are macro programs that run over the Microsoft Windows operating system.

### A.8.1) AUTOMATED RECORDING OF PENDANT DROP IMAGES

```
Sample = Askline("Filename","Input filename","")
n=AskLine("Enter the number of last picture to be taken","Iterations","99")
m=AskLine("Enter the number of minutes between pictures","Minutes (between 1-
60)","30")
s=m*60
j=AskLine("Enter the starting sample number","Initial Sample Number","1")
Display(3,"Time delay between images","%s% seconds")

For b=1 to 3 by 1
 If b==1
  d="s"
 EndIf
 If b==2
  d="k"
 EndIf

 If b==3
```

```
  d="l"
 EndIf

 For i = j to n by 1
  WinActivate("TCPro")
  SendKeysTo("TCPro","g") ;disable screensaver if present
  WinActivate("TCPro")
  SendKeysTo("TCPro","!ag")
  WinActivate("TCPro")
  SendKeysTo("TCPro","!af!fs~")
  WinWaitExist("Save", 10)
  SendKeysTo("Save","%Sample%%d%%i%.tif~~")
  TimeDelay(s)
 Next

 j=1
Next
```

## A.8.2) RADIUS OF CURVATURE PROGRAM

```
WinActivate("SigmaPlot")
File = AskLine("Filename","filename in CAPITAL LETTERS","")
ext= "SR"

 SendKeysTo("SigmaPlot","!fn!fi%file%.%ext%{TAB}~")


 WinActivate("Import Text - %File%.%ext%")
 WinWaitClose("Analyzing")

WinActivate("SigmaPlot")
WinActivate("Import Text - %File%.%ext%")
SendKeysTo("Import Text - %File%.%ext%","{TAB}w{TAB 6}~")
 WinWaitClose("Importing")

 SendKeysTo("SigmaPlot","{f5}{TAB}r")
 WinWaitClose("Regression")

 SendKeysTo("Curve Fit Results - CIR.FIT","k")

 SendKeysTo("Keep Regression Results - CIR.FIT","p{TAB}f{TAB}r{TAB}~")
 SendKeysTo("Curve Fit Results - CIR.FIT","d")
```

```
SendKeysTo("SigmaPlot","{F10}")
SendKeysTo("User-Defined Transform - RESID.XFM","{TAB}x")
WinWaitClose("User-Defined Transform - RESID.XFM")
```